*A SHORT INTRODUCTION TO FRACTURE MECHANICS

Professor Roberto Ballarini
University of Houston

*Dedicated to ”my brother from another mother”, and to our sister.

My students have been my teachers.

Introduction to the Mechanics of Fracture and Fatigue:
It is a beautiful topic!

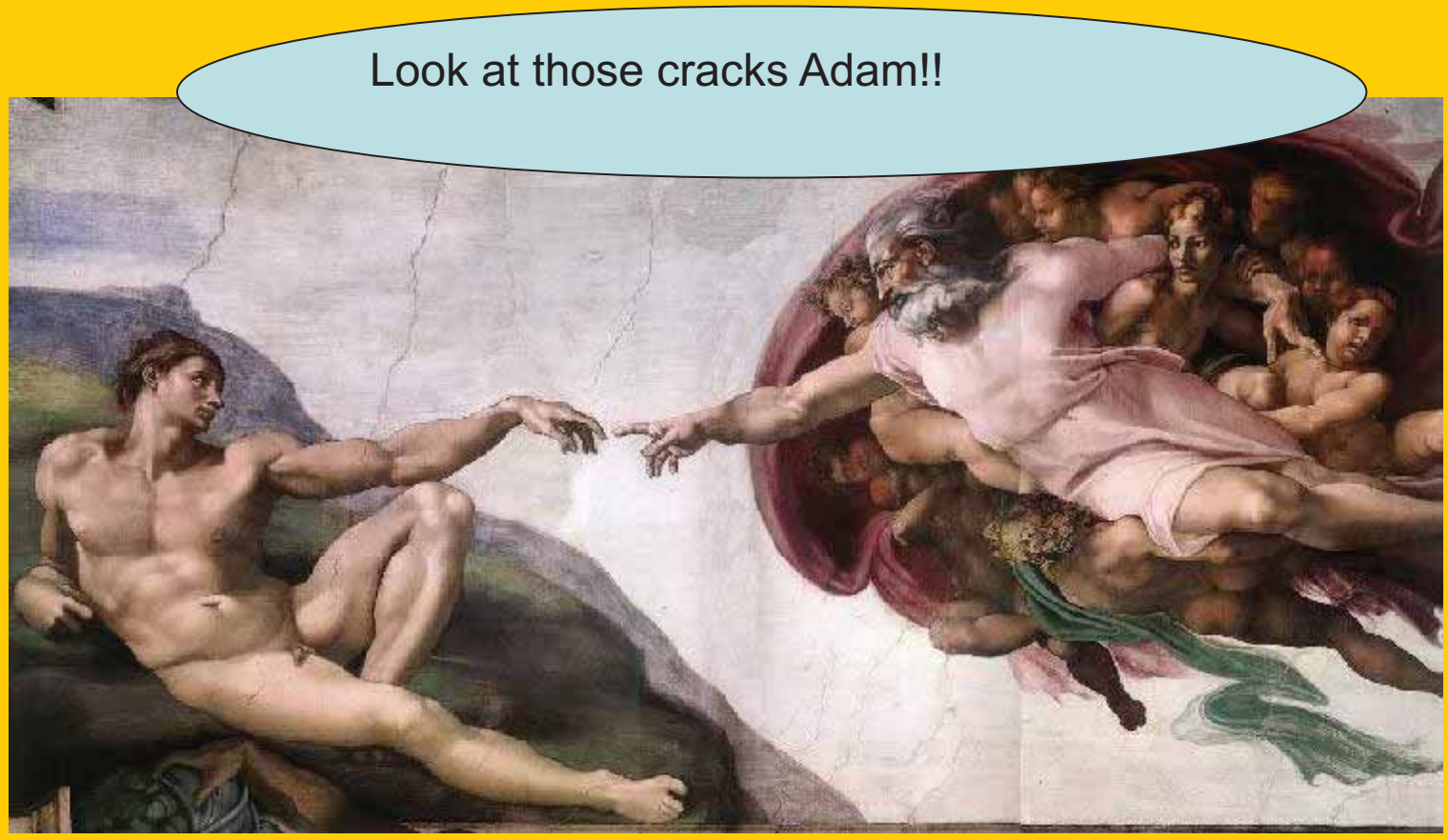

Outline

- Introduction to the role of fracture and fatigue in numerous fields.
- Strength theories versus fracture mechanics theories.
- Linear elastic fracture mechanics using the stress intensity factor approach; small-scale-yielding arguments.
- Scale effects introduced by the presence of a crack; failure by progressive collapse versus by crack propagation.
- Crack propagation under mixed-mode conditions.
- Two examples of fracture mechanics-based design.

Fracture is with me even when I am on vacation; Vancouver Island

Strathcona Park

Tofino

Cedar, by Hilary Stewart,
U. of Washington Press, 1984.

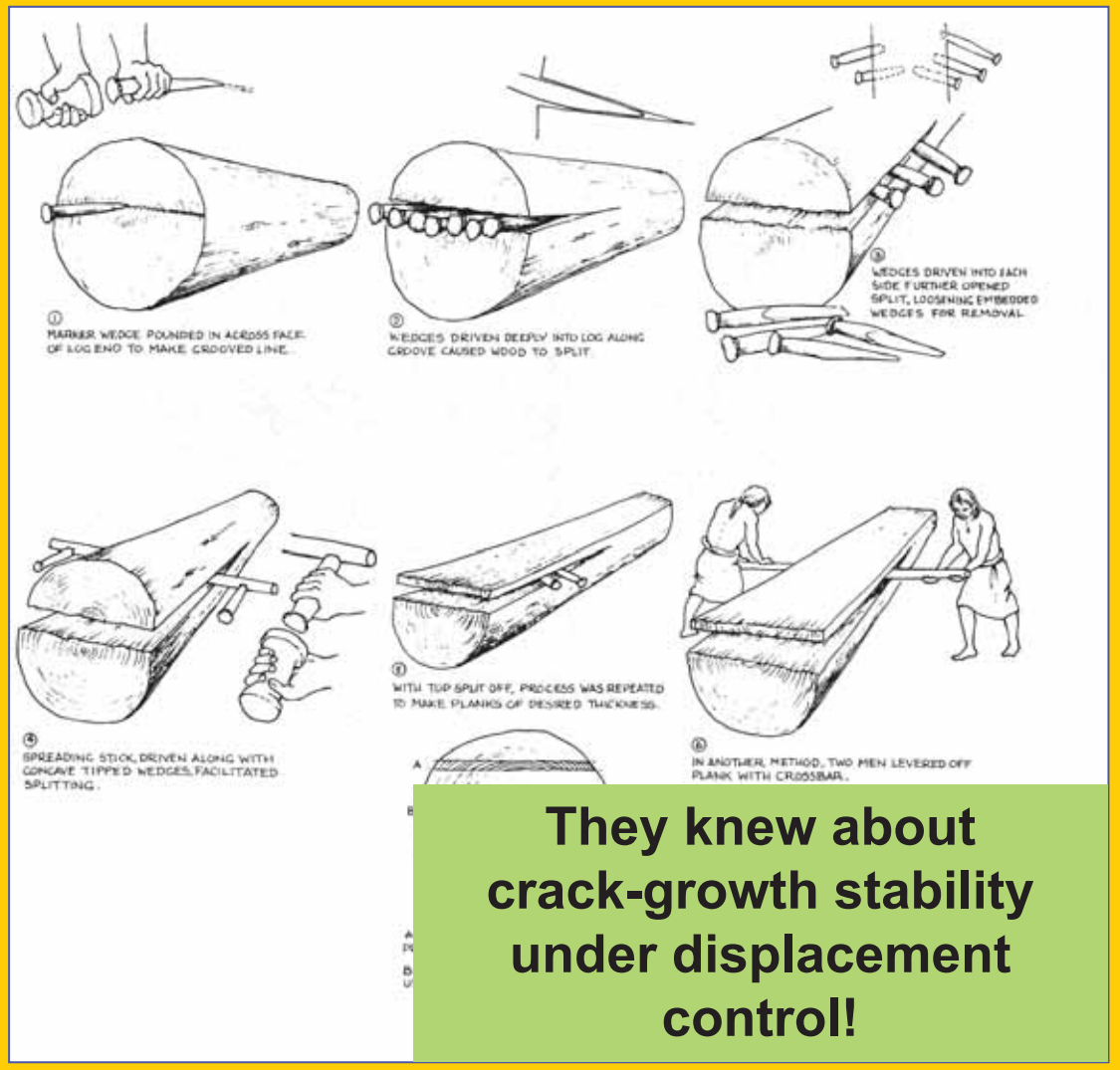

They knew about crack-growth stability under displacement control!

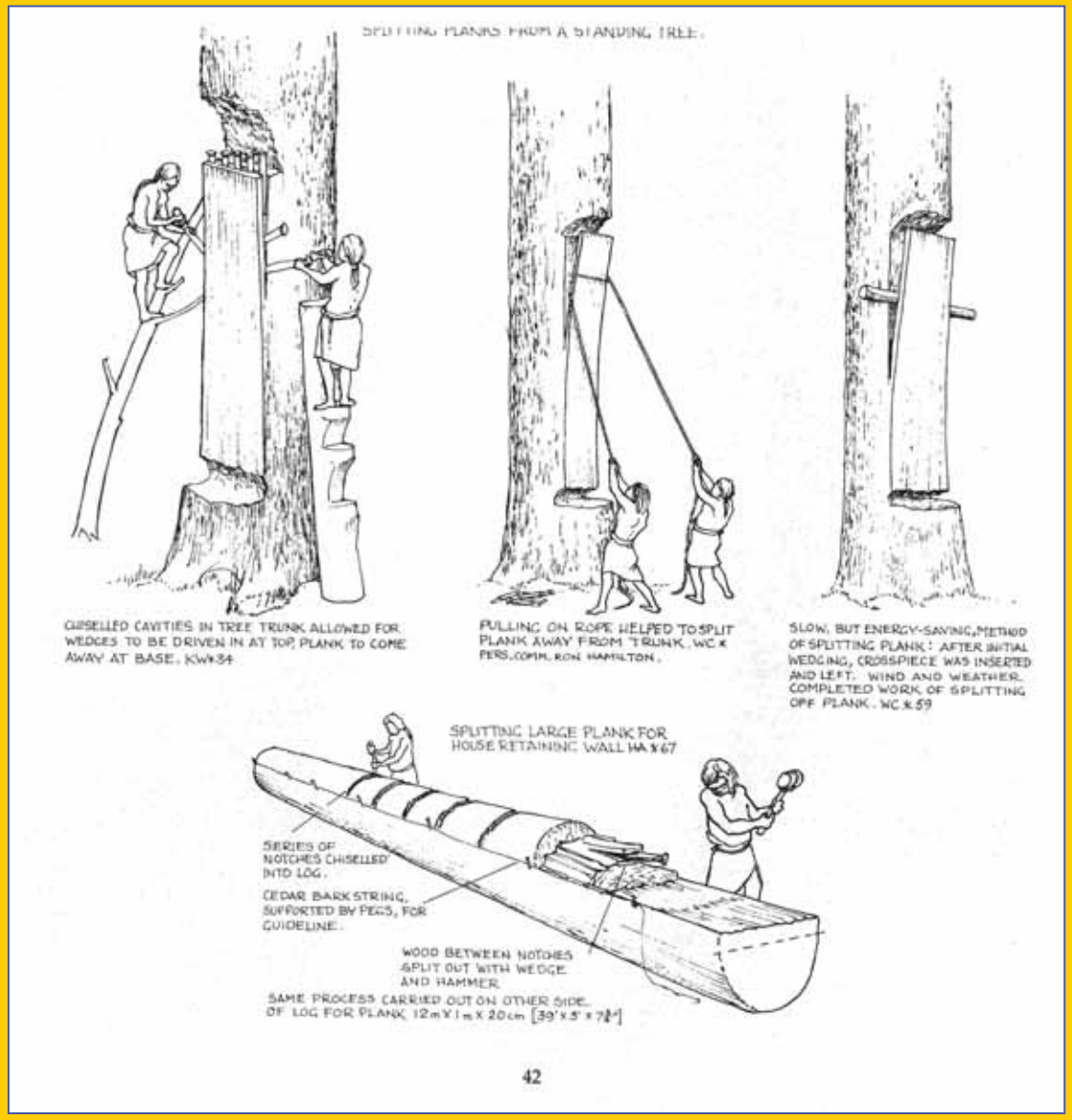

They knew about static fatigue!

Examples of failures in various fields

One of the Liberty Ships
S.S. Schenectady

January 16, 1943
Fractured soon after its sea trials in 4°C water and -3°C air temperatures

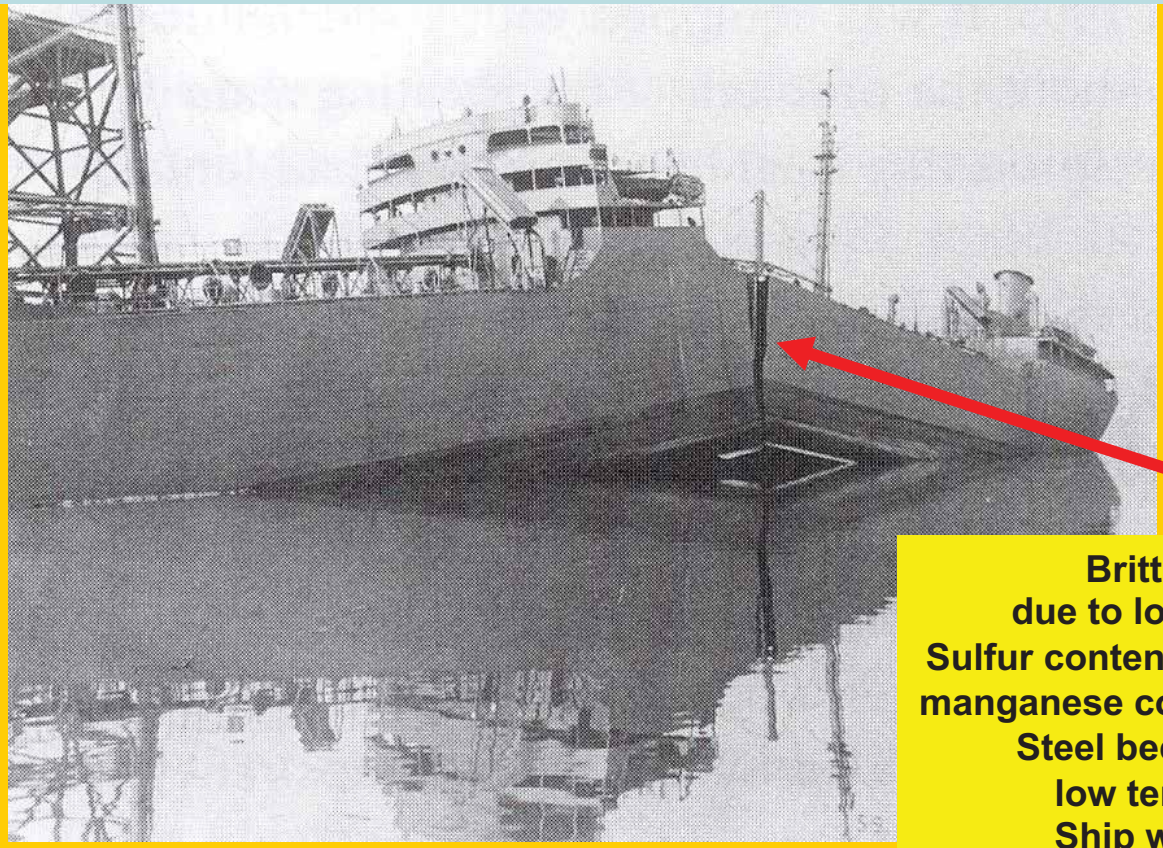

Brittle fracture
due to low-grade steel;
Sulfur content was too high and
manganese content was tool low.
Steel became brittle at
low temperatures.
Ship was repaired
and returned to service.

Aging Aircraft Problem

Aloha Airlines Flight 243, 1988

One fatality, 58 year old flight attendant Clarabelle Lansing

DOT/FAA/AM-
DOT-VNTSC-FAA-93-10

FAA Tech Center
Atlantic City
NJ 08405

Full Scale Testing and Analysis of Curved Aircraft Fuselage Panels

G. Samavedam
D. Hoadley
D. Thomson

Foster-Miller, Inc.
350 Second Avenue
Waltham, MA 02154-1196

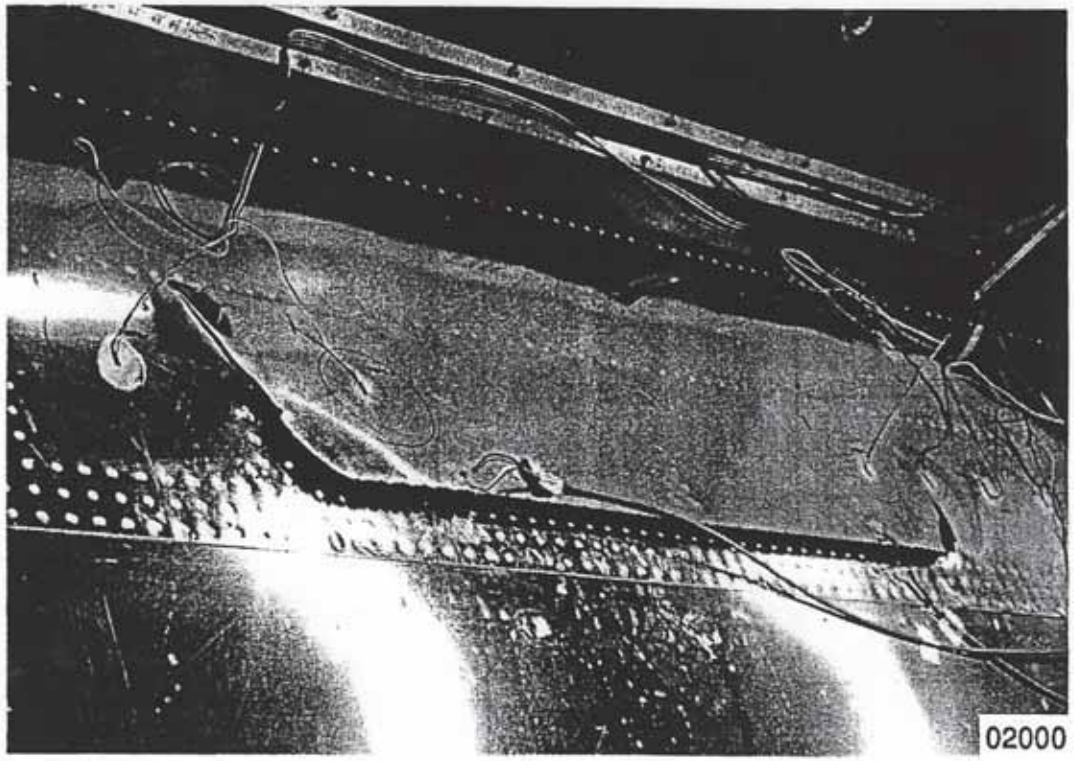

Small cracks start at each rivet hole...

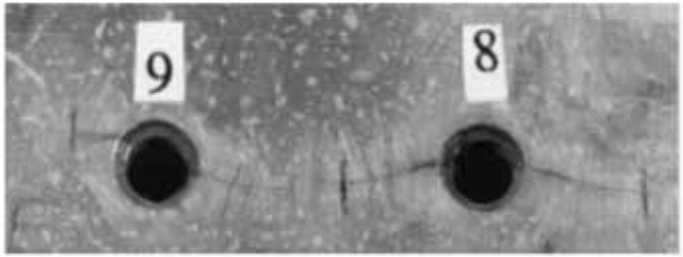

25 mm

...then link to form a lead crack

Bone Fractures

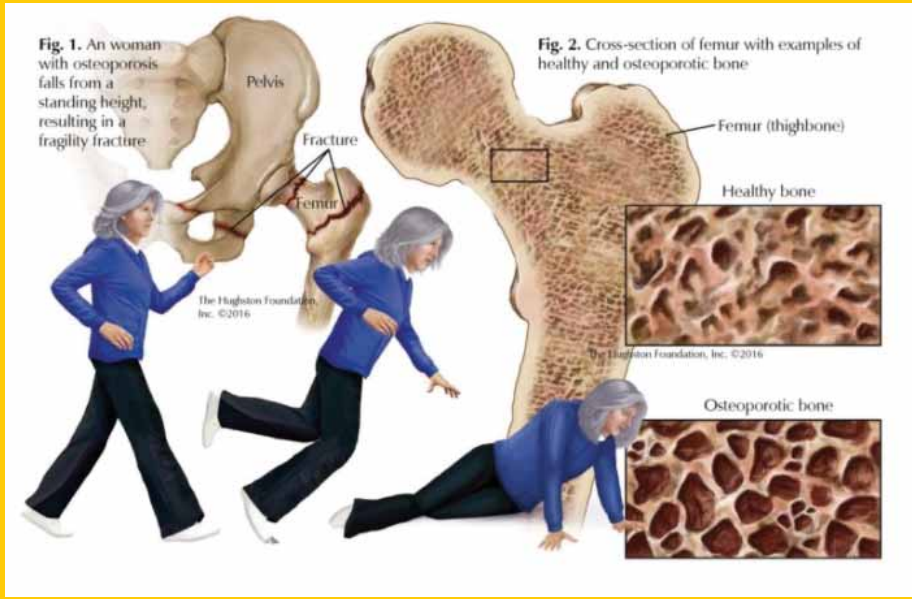

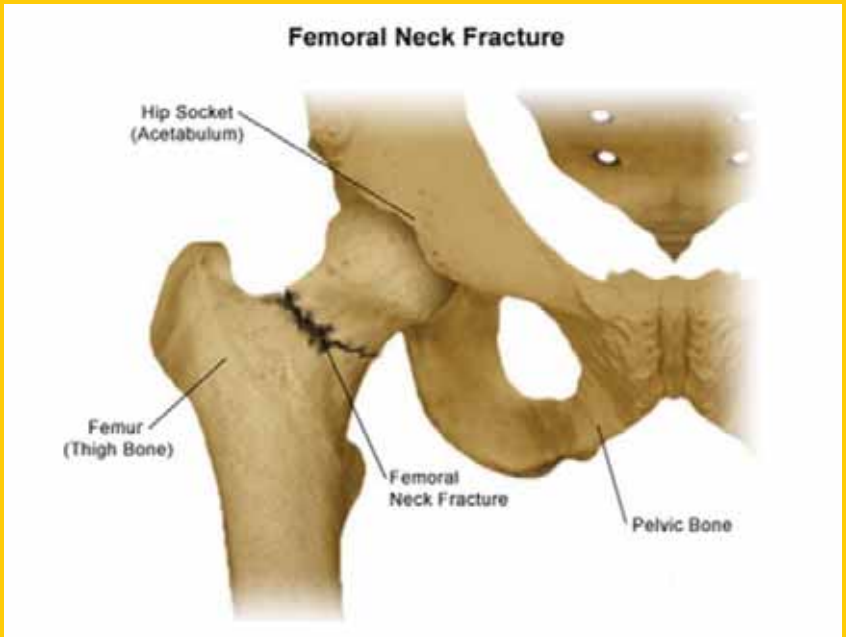

Fracture of Medical Stents

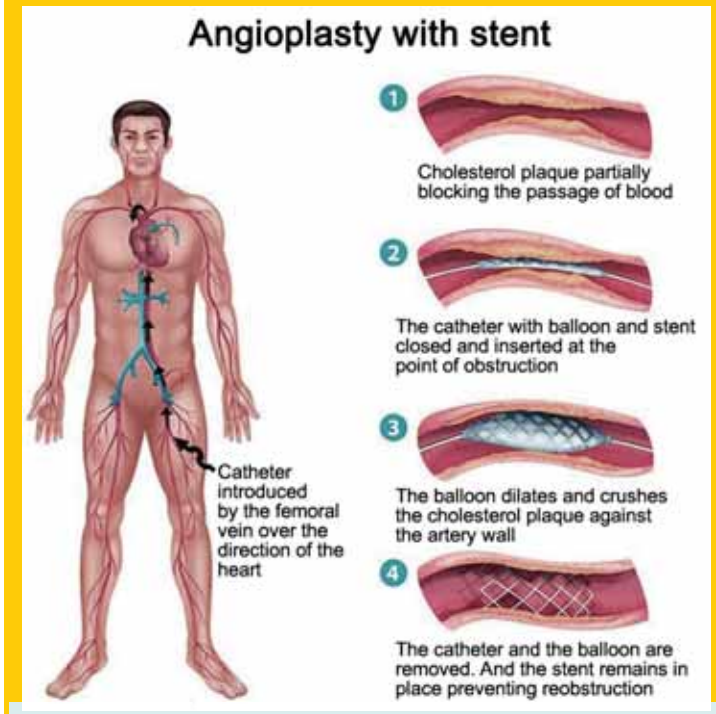

http://www.tabletsmanual.com/wiki/read/cardiac_catheterization

https://www.hindawi.com/journals/crp/2011/320983/

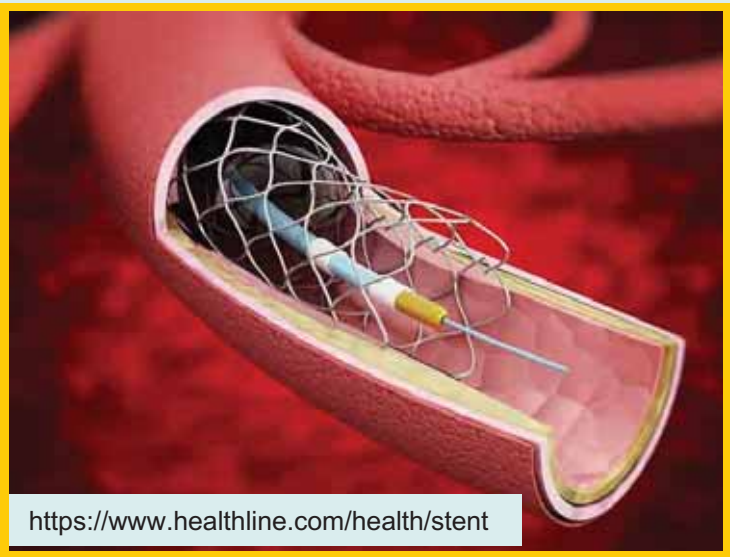

https://www.healthline.com/health/stent

https://jksronline.org/ViewImage.php?Type=F&aid=509594&id=F3&afn=2016_JKSR_63_6_513&fn=jksr-63-513-g003_2016JKSR

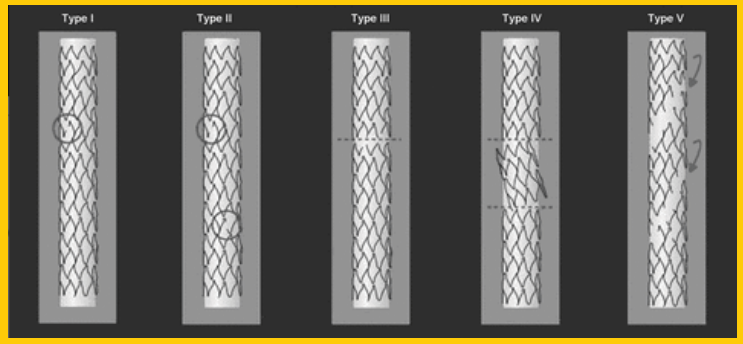

https://onlinelibrary.wiley.com/doi/full/10.1111/j.1540-8183.2010.00567.x

Cracking in concrete dams

Engineering Fracture Mechanics Vol. 35, No. 1/2/3, pp. 553–564, 1990
Printed in Great Britain.

0013-7944/90 $3.00 + 0.00
Pergamon Press plc.

CASE STUDIES OF SIMULATION OF FRACTURE IN CONCRETE DAMS

A. R. INGRAFFEA
Department of Structural Engineering and Program of Computer Graphics, Cornell University, Ithaca, NY 14853, U.S.A.

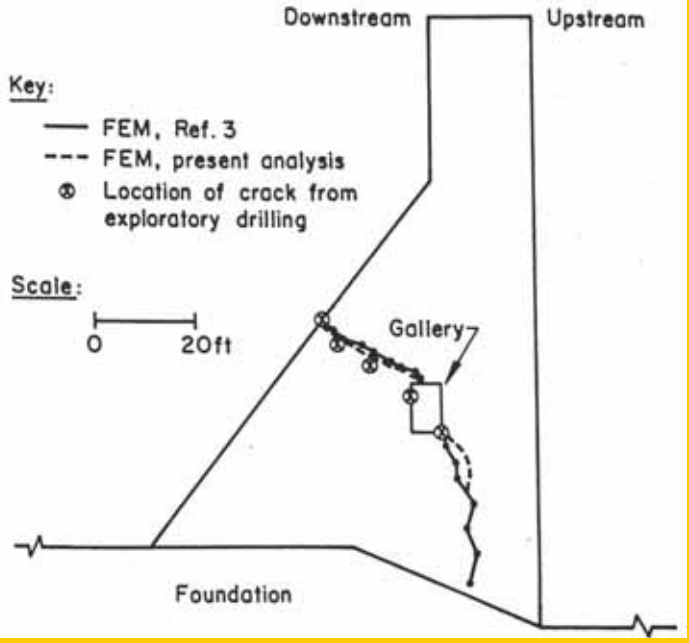

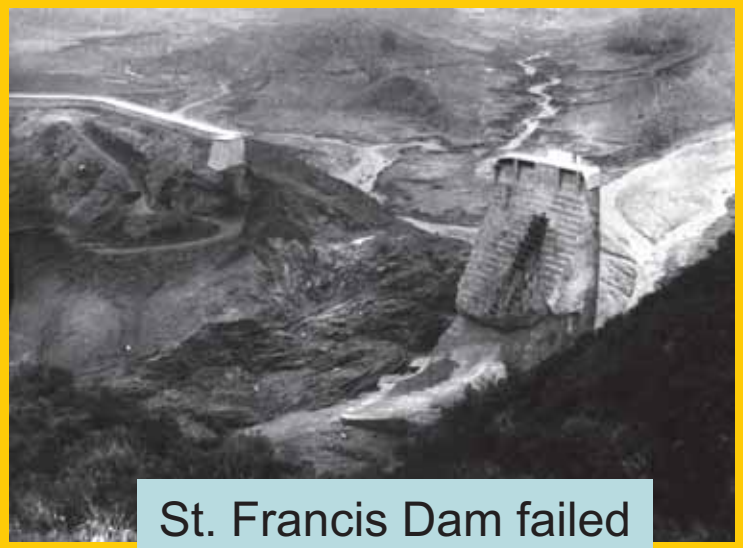

St. Francis Dam failed on March 12, 1928

Potential Collapse of Historic structures

Engineering Fracture Mechanics Vol. 35, No. 1/2/3, pp. 493–499, 1990
Printed in Great Britain.
0013-7944/90 $3.00 + 0.00
Pergamon Press plc.

OBSERVATIONS DURING STABILIZATION OF
OLD BELL TOWERS DAMAGED BY CRACKS

J. MAJER and G. NIEDERWANGER
Institut für Festigkeitslehre und Flächentragwerke, Universität Innsbruck, Innsbruck, Austria

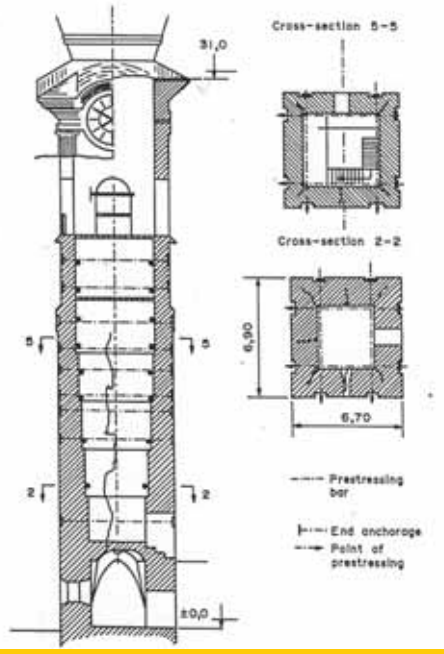

Venice
San Marco Belltower
1902 Collapse

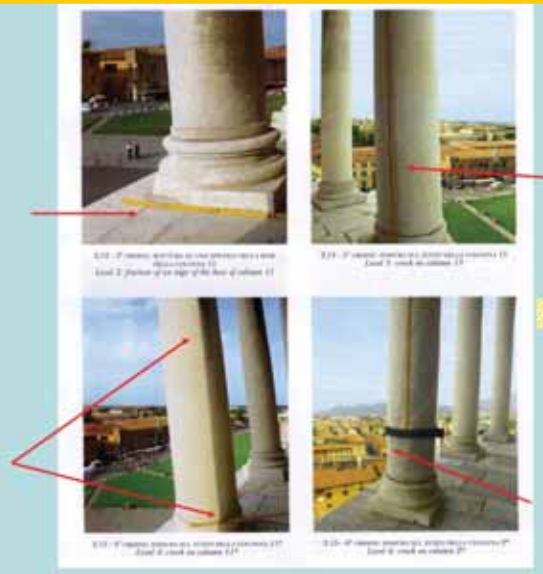

Cracks in columns

Offshore structures

Shell Oil Bullwinkle Platform

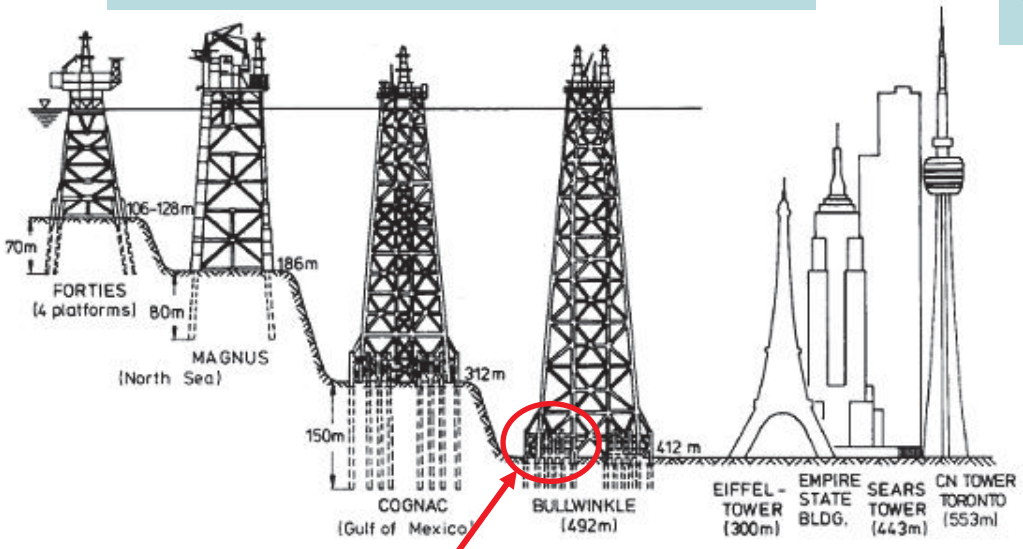

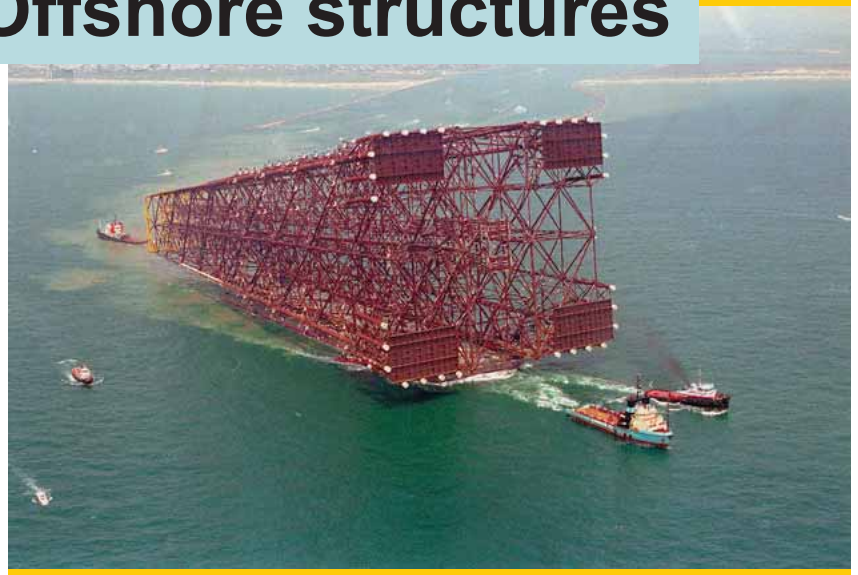

Design against fatigue crack initiation and propagation from the weld that connects the tubes that make up the structure.

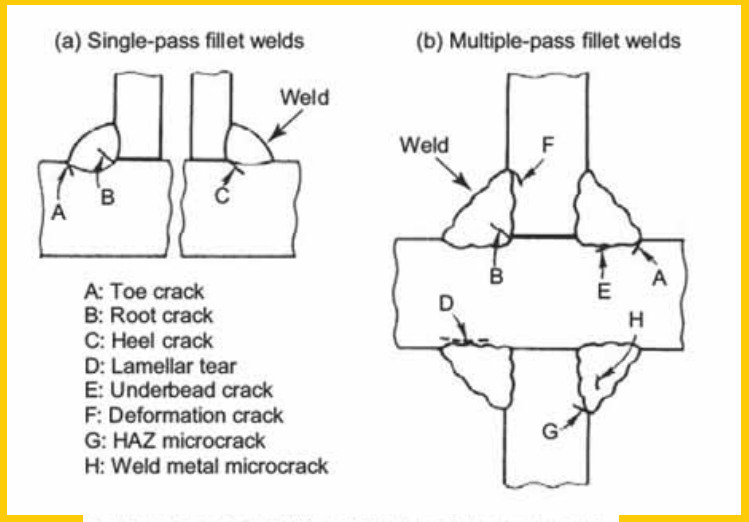

The Japan Welding Engineering Society, MAG/MIG Welding Defects and Preventive Measures, Sanpo Publications Inc.

Hydraulic Fracturing Technology

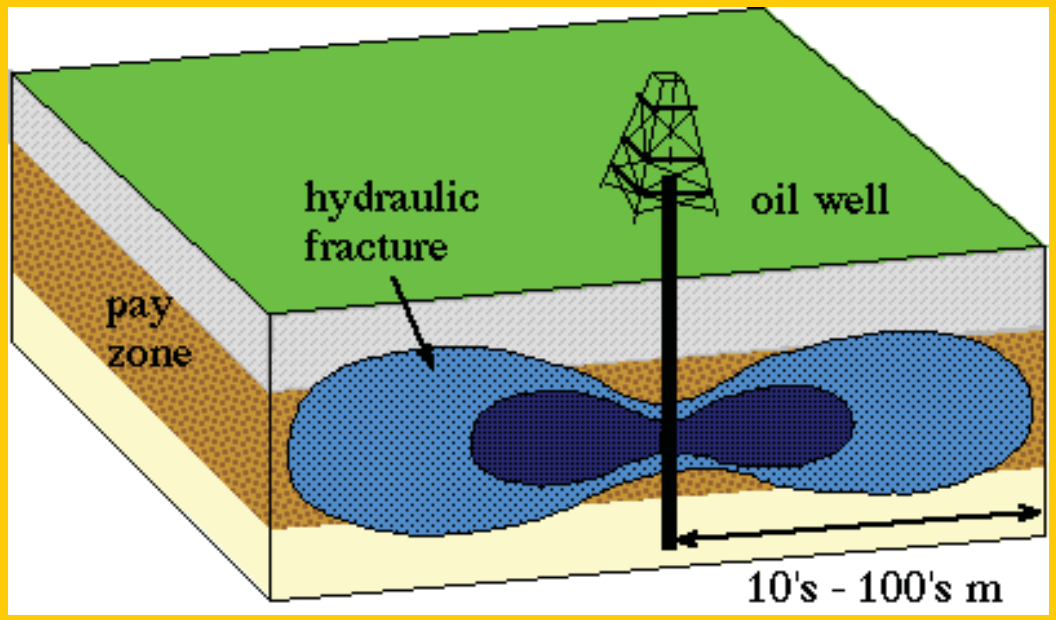

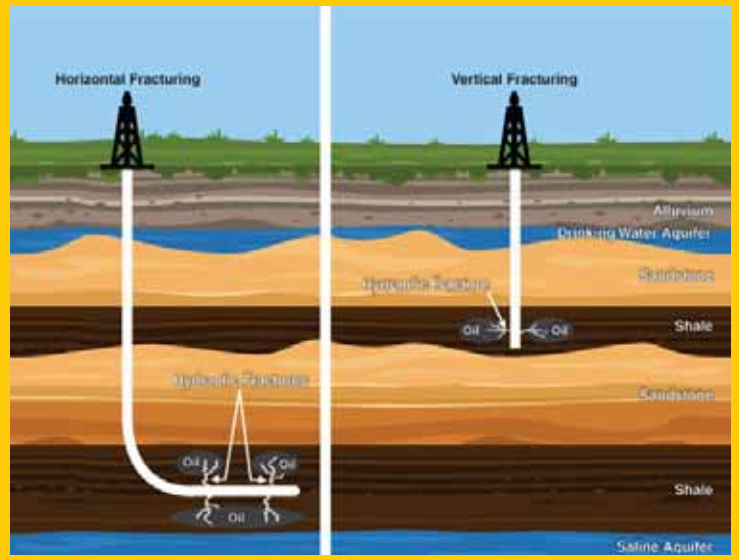

Creation of Materials with Superior Properties

What is an ideal composite?

It should be comprised of readily available and inexpensive materials.

It should be strong, tough and light.

It should be capable of self-healing.

It should not require prohibitive manufacturing processes.

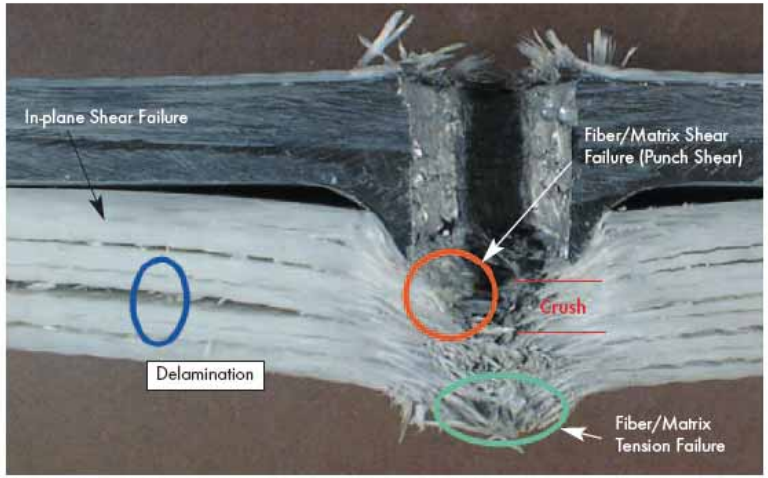

Figure 6. Damage Mechanisms Observed During the Impact and Penetration of a Composite.

Let's turn to *Nature* for inspiration.

Example: Bioinspired design of ceramic composites with high toughness (reverse-engineering)

STROMBUS GIGAS: WHY IS IT SO TOUGH?

CROSSED-LAMELLAR MICROARCHITECTURE

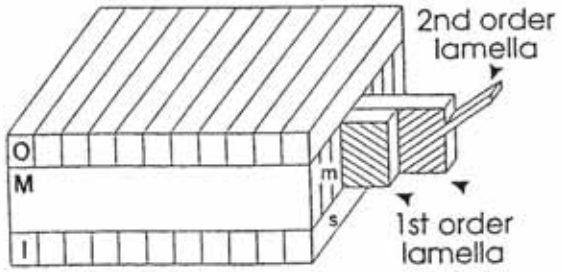

Layers 0.5-2 mm thick

First order lamellae
5-60 μm thick; many μm wide

Second-order lamella

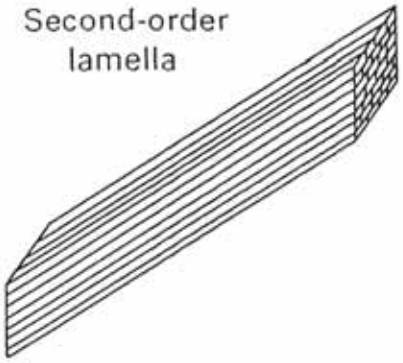

5-30 μm thick;
5-60 μm wide

Third-order lamella

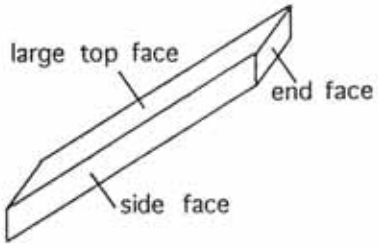

60-130 nm thick;
100-380 nm wide

Twinning in third-order lamella

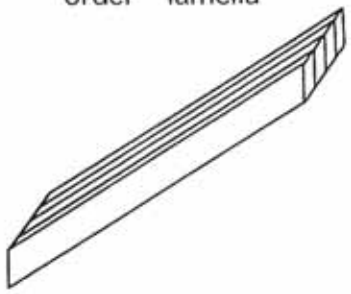

1-20 nm wide

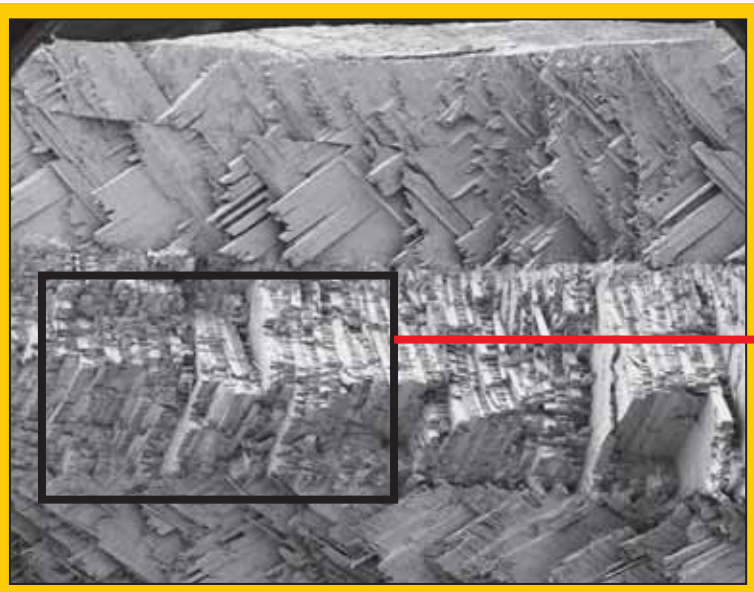

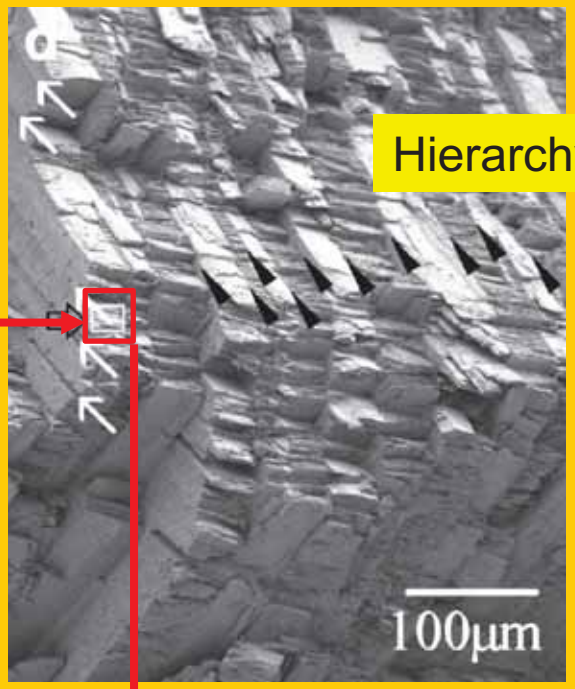

Hierarchy!!

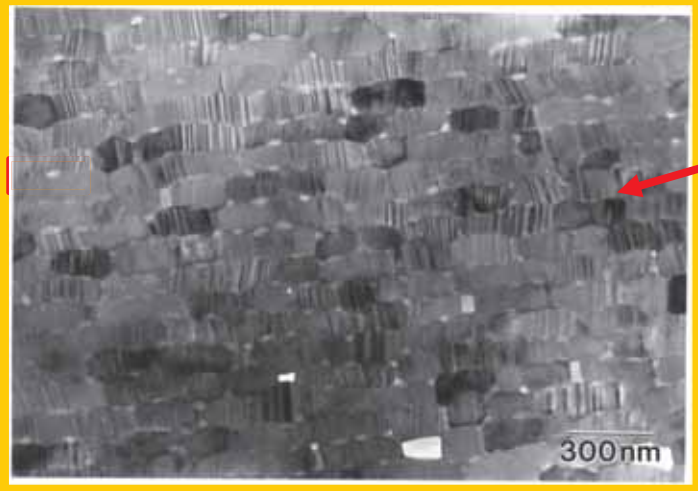

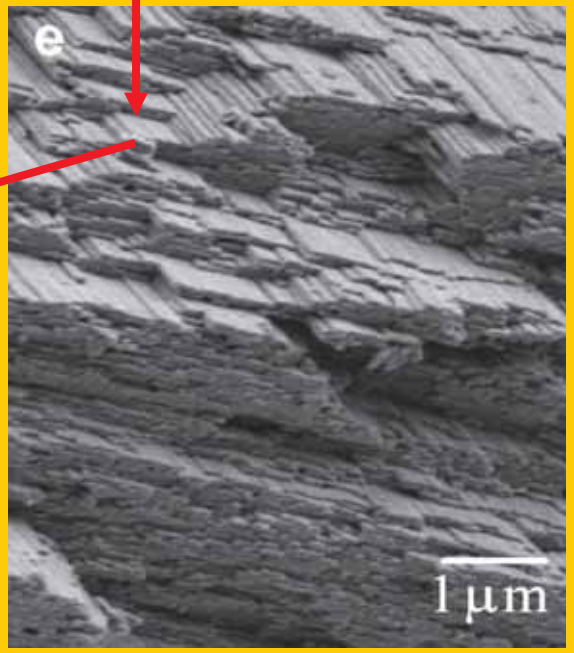

Fracture surface showing crossed lamellar microstructure

REVERSE ENGINEERING

Microstructure

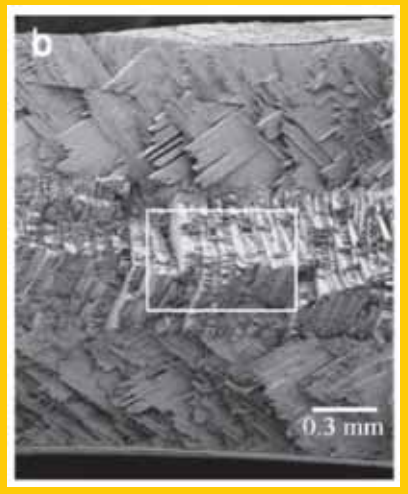

Dominant fracture mechanisms

Tunnel cracking

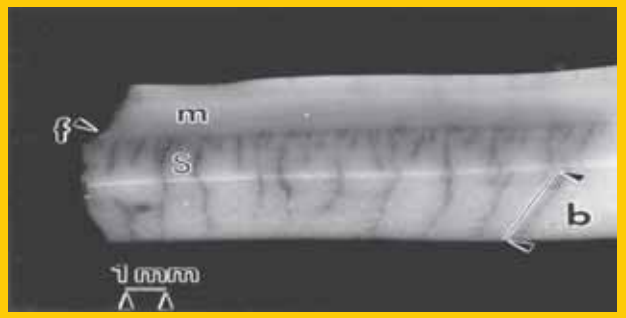

Crack bridging

Modeling

Steady-state tunneling

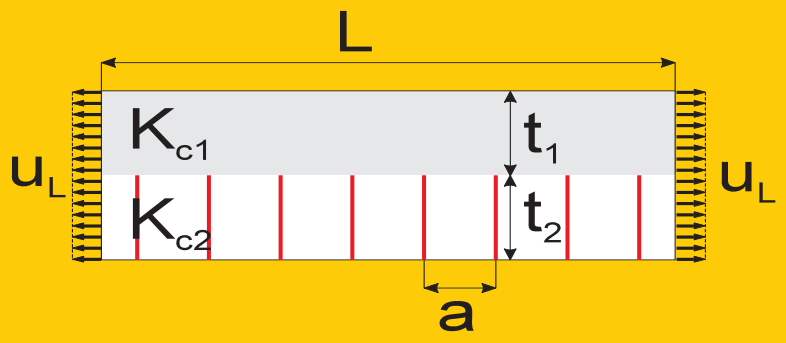

Crack bridging

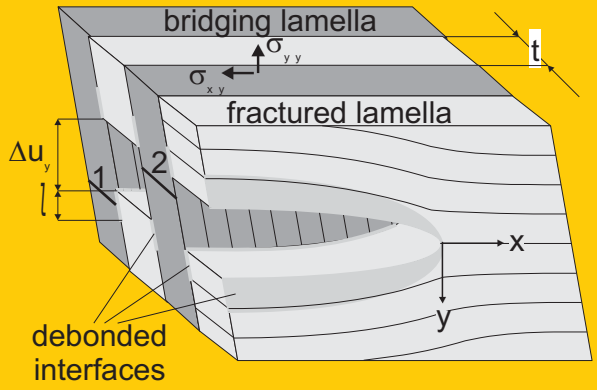

http://www.gereports.com/post/110549411475/ceramic-matrix-composites-allow-ge-jet-engines-to/

GE CMC Engine

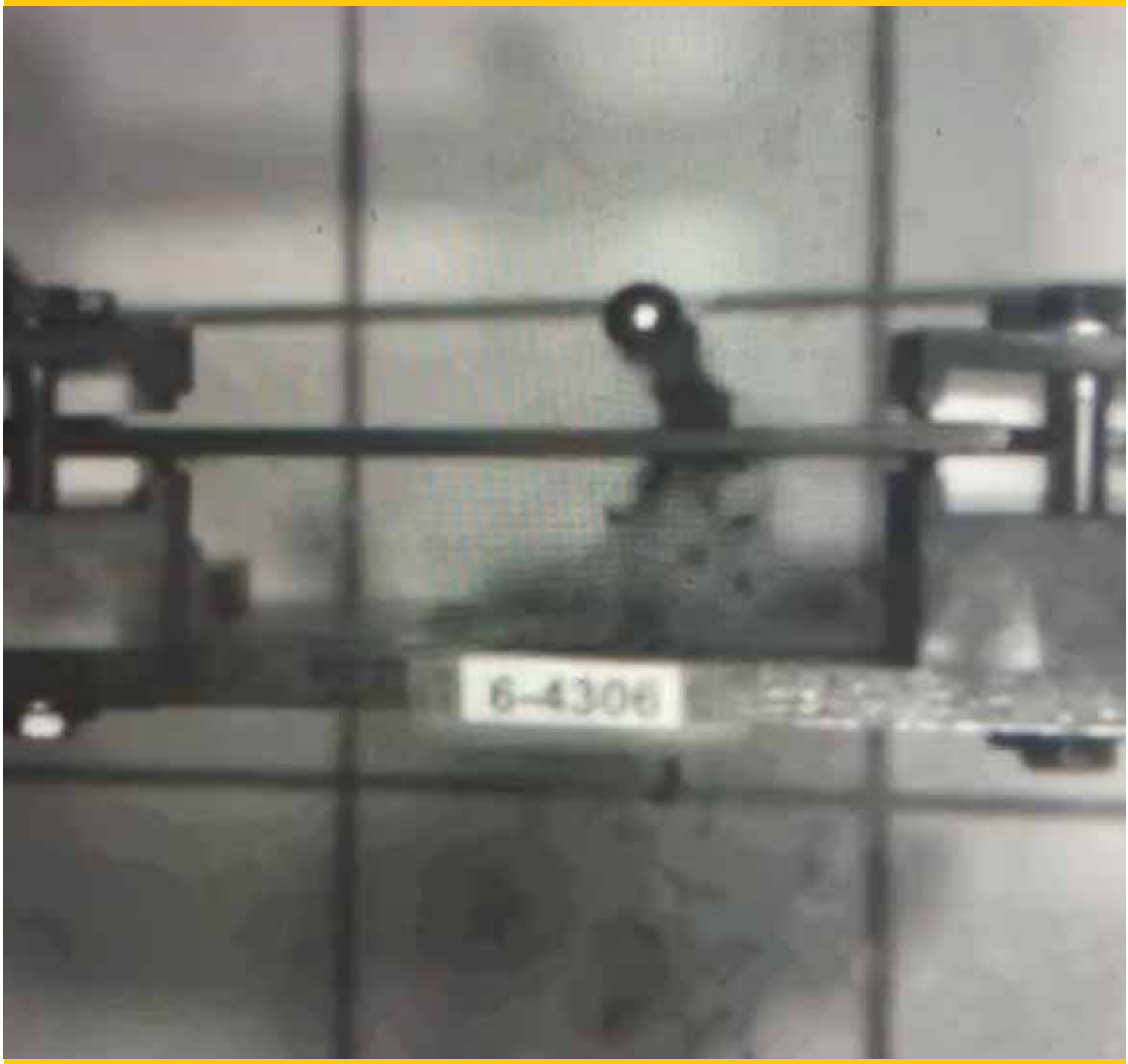
6-4306

Gears Used in Rotorcraft Transmission and Drive Systems

David Lewicki

Backup ratio = 3.3

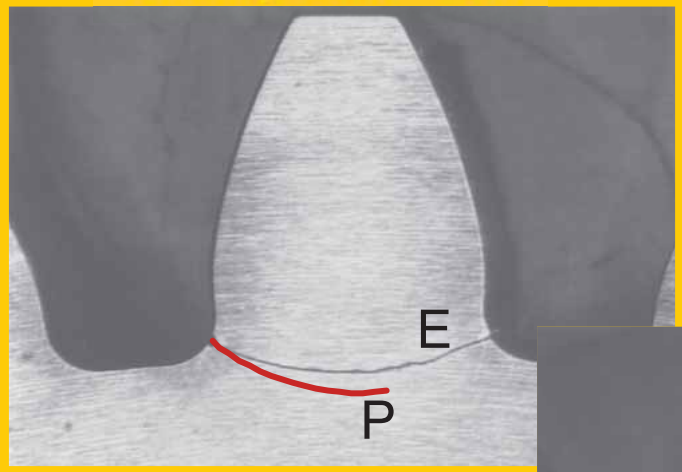

E = Experiment
P = Predicted

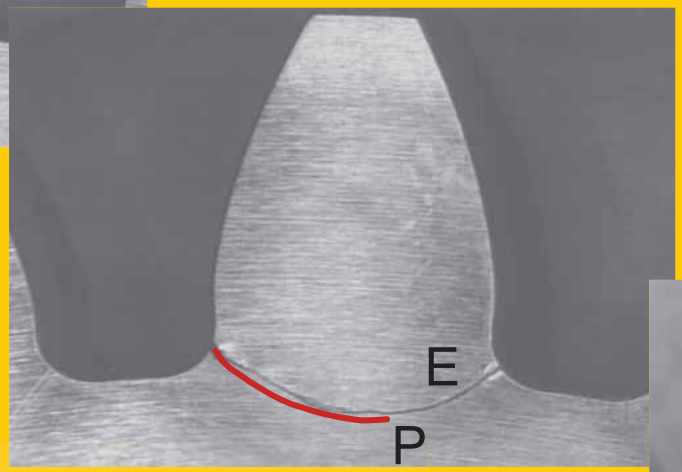

Backup ratio = 1.0

Backup ratio = 0.5

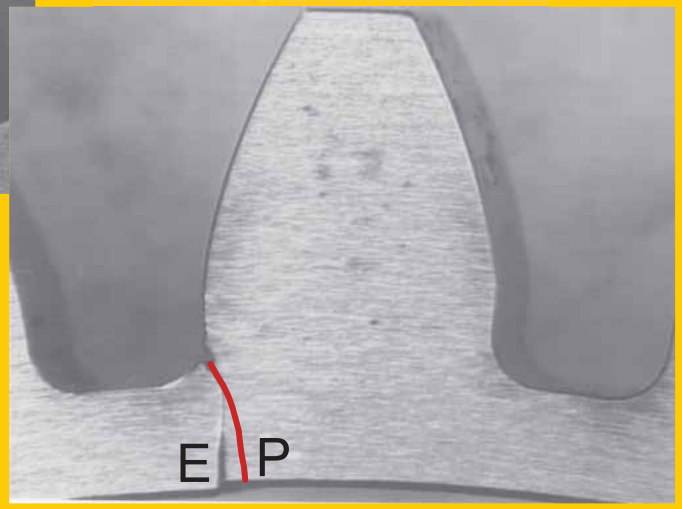

Cracking in Semiconductor Devices

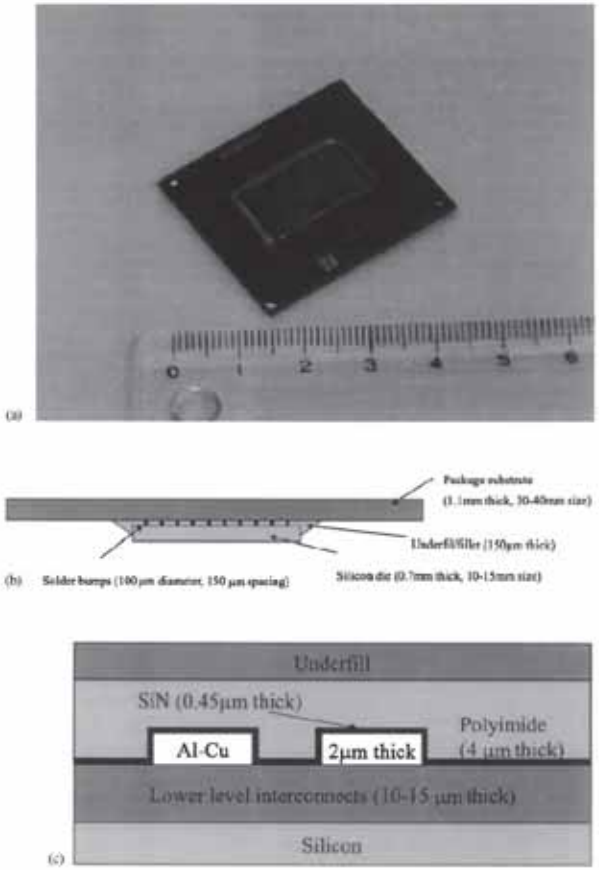

Figure 25 (a) A photo of a flip-chip package. (b) A schematic of cross-section of the package. (c) Magnified view of the interconnect structure.

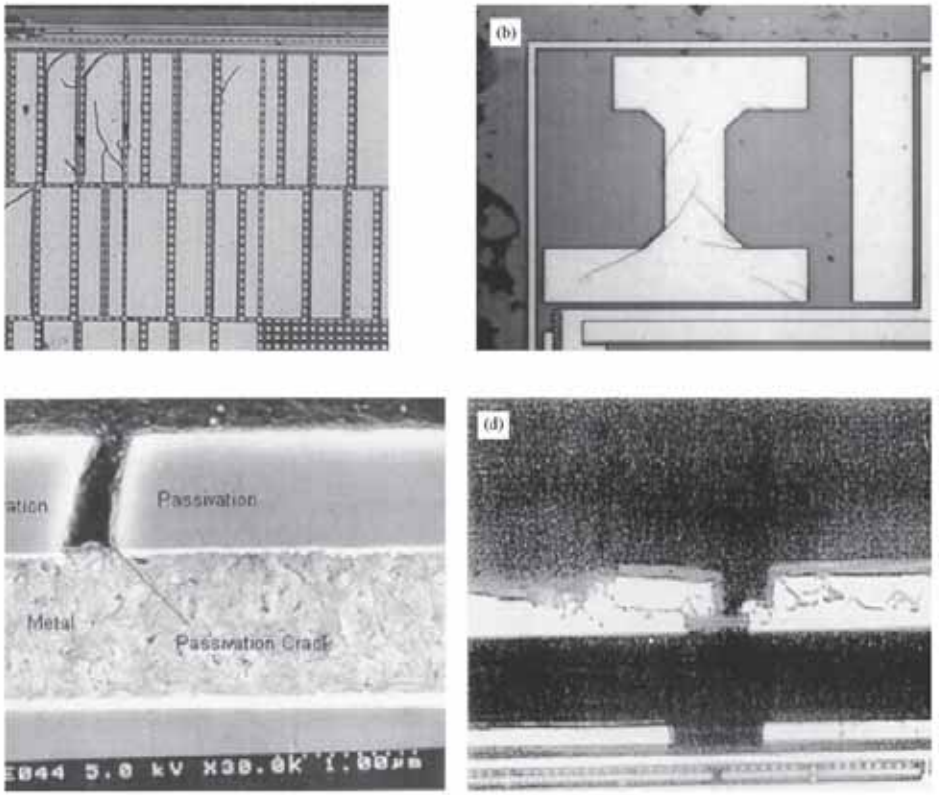

Figure 26 (a) The plan view of the surface of a die, near a die corner (source bib57 Huang *et al.*, 2000). (b) Patterned aluminum pads. Cracks form in SiN over aluminum, but not in SiN over silica (source bib56 Huang *et al.*, 2002). (c) A cross-section shows a crack in SiN (courtesy of Dr. J. B. Han). (d) A cross-section shows shifted aluminum pads (source bib55 Huang *et al.*, 2001).

Fracture, fatigue and strength of MEMS materials

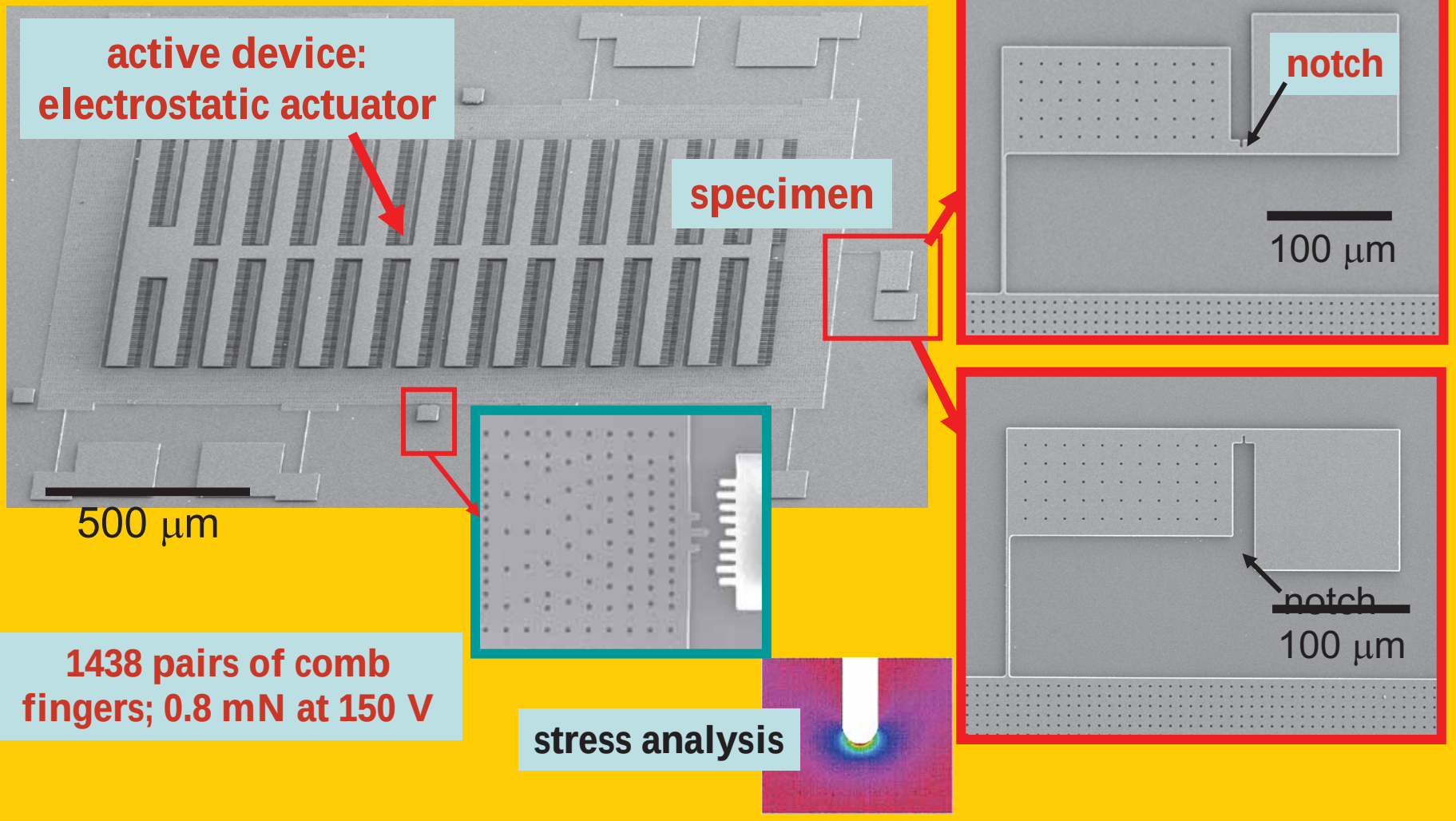

1438 pairs of comb fingers; 0.8 mN at 150 V

R. Ballarini and A.H. Heuer Research Group

Developing models and experimental techniques for fracture and fatigue at small scales

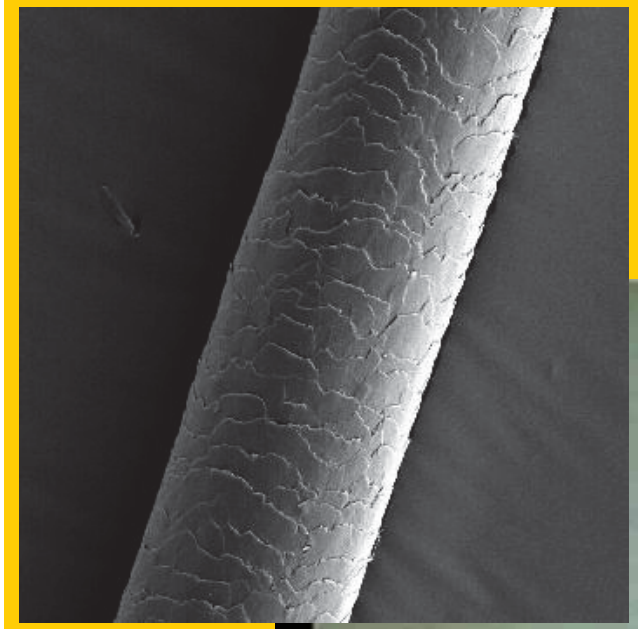

Fatigue of polycrystalline silicon for MEMS

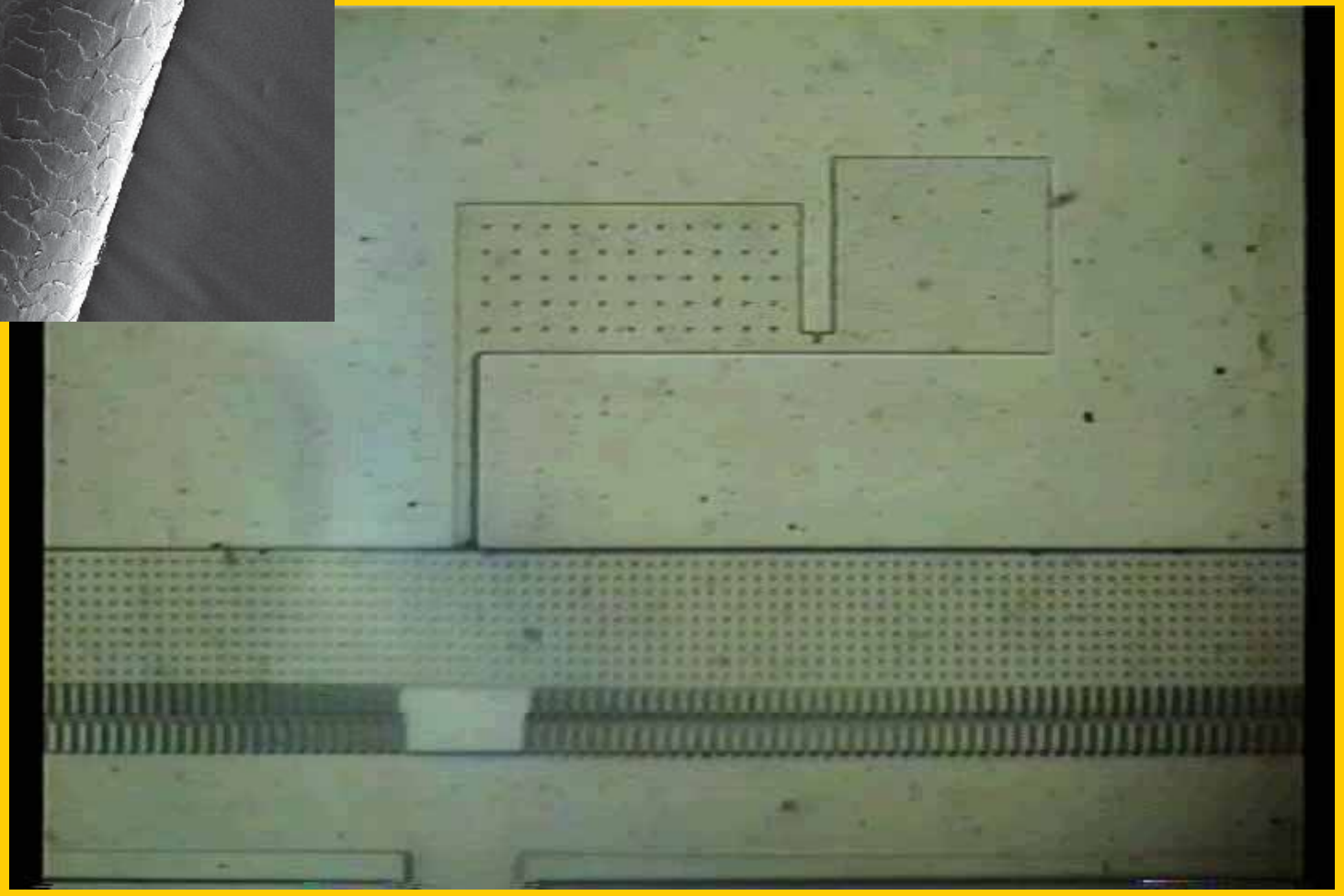

Developing models and experimental techniques for fracture and fatigue at small scales

Submicrometer high-temperature fracture experiments on silicon.

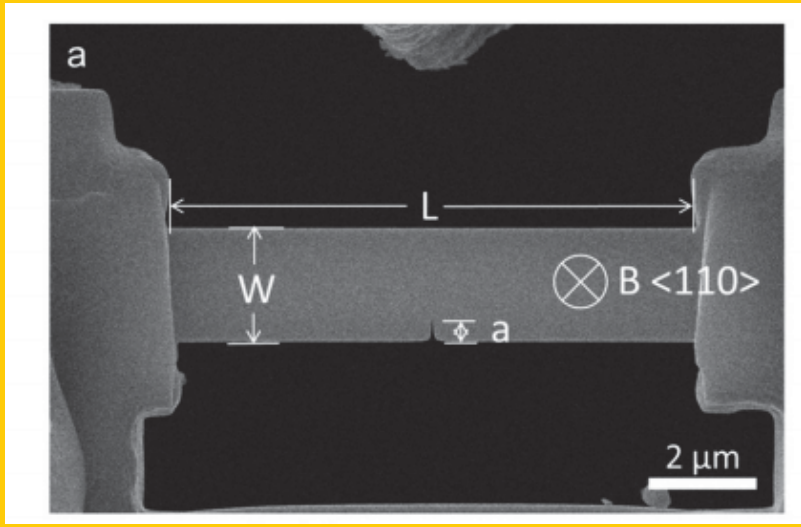

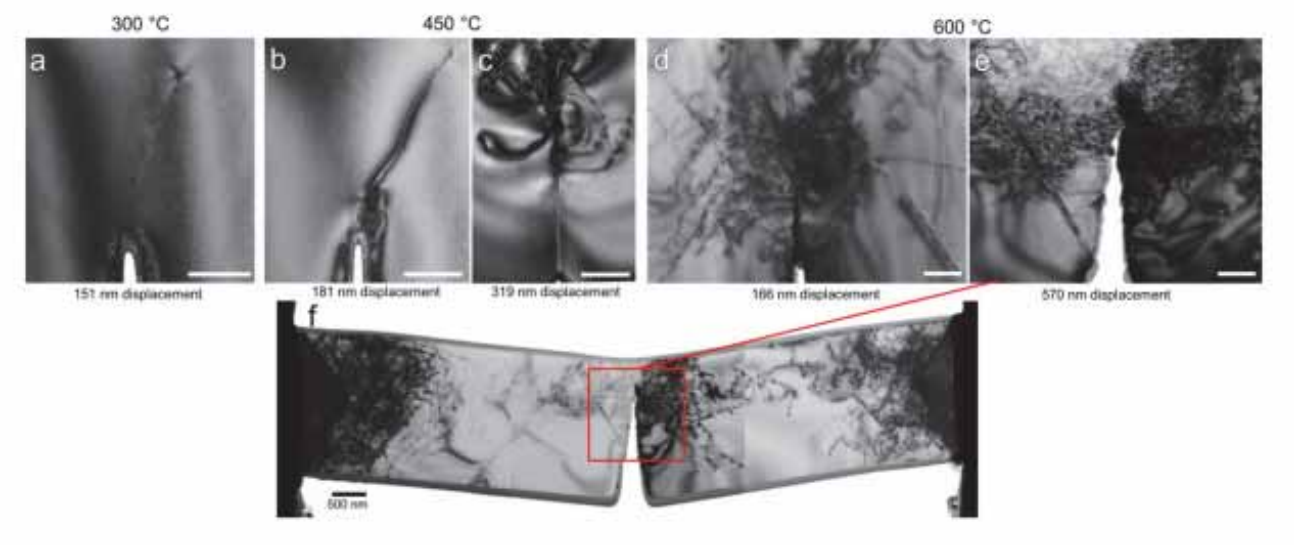

Why?

1. What are the origins of the toughness of bone and other tissues?

2. Development of multiscale models

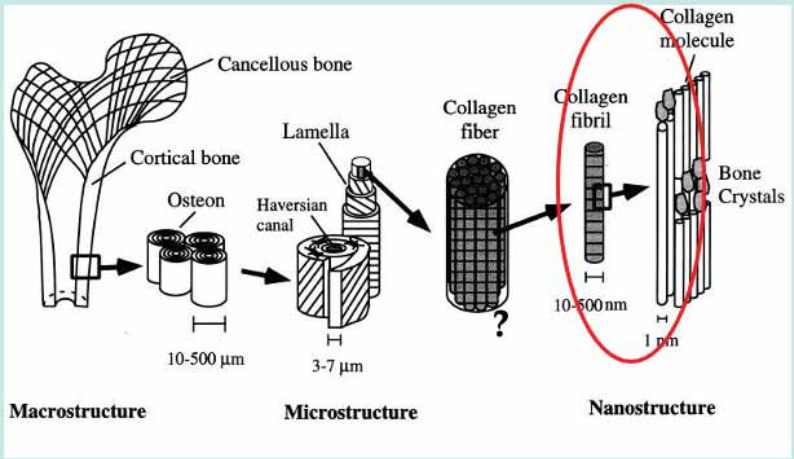

Fracture of Individual Collagen Fibrils

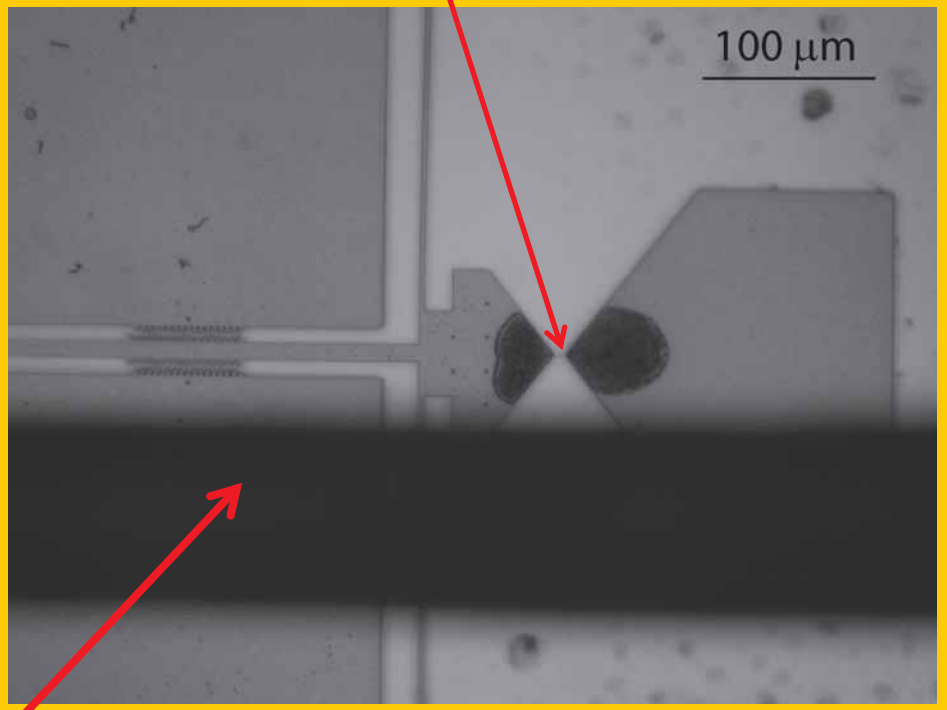

Human hair

Strength Theories vs. Fracture Theories

Strength:

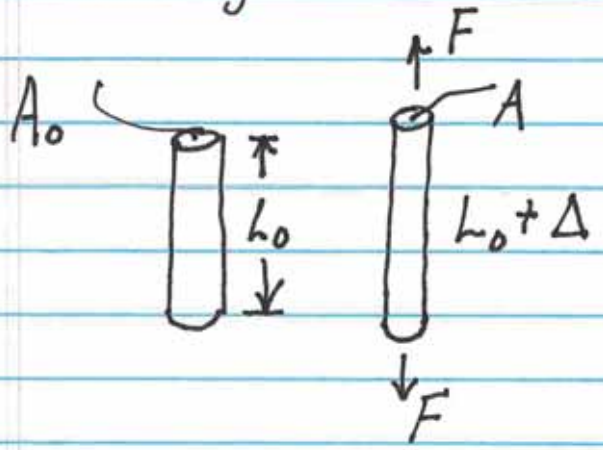

$$\sigma_N \equiv F/A_o$$

$$\epsilon_N \equiv \Delta/L_o$$

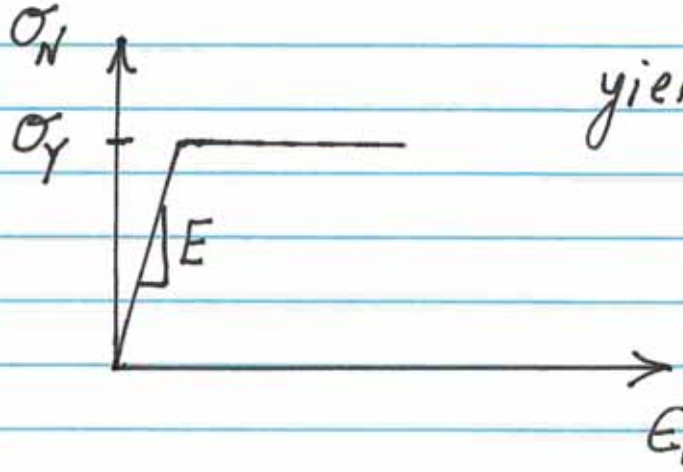

yielding at $\sigma_N = \sigma_Y$

or

$$\boxed{\frac{\sigma_N}{\sigma_Y} = 1}$$

To prevent yielding:

$$F_{MAX} = \sigma_Y A_o / S_f$$

(S_f: safety factor)

We can generalize one-dimensional plasticity initiation using a yield criterion such as von Mises:

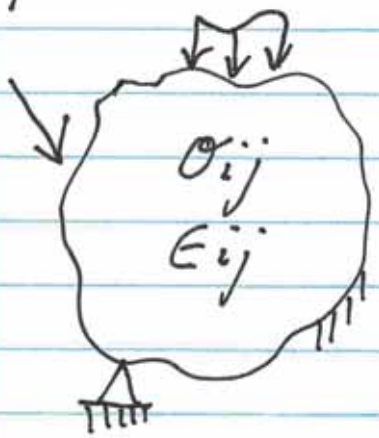

$$F(\sigma_{ij}) - K = 0$$

$$\sigma_Y^2$$

$$(\sigma_1-\sigma_2)^2+(\sigma_3-\sigma_1)^2+(\sigma_2-\sigma_3)^2$$

The important result for our discussion is that in plasticity theories, the stress level required to initiate yielding (the failure stress) is <u>independent</u> of the scale of the structure!!

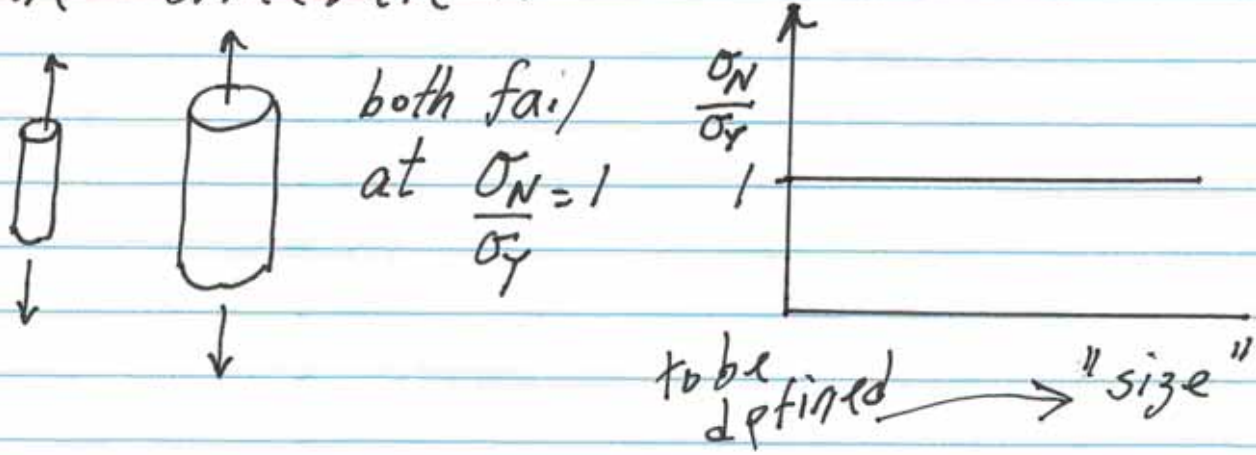

Consider how plasticity would deal with a <u>cracked</u> structure:

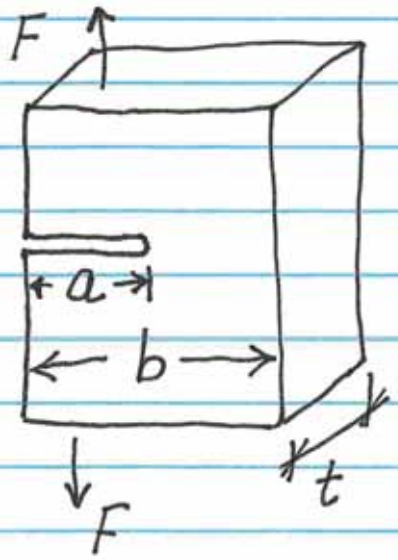

as loading is increased:

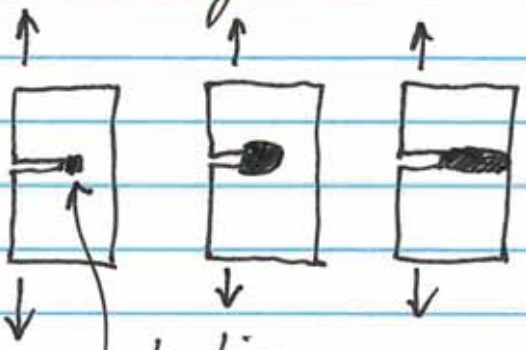

plastic deformation increases with load

The "limit" load according to a statically admissable solution is:

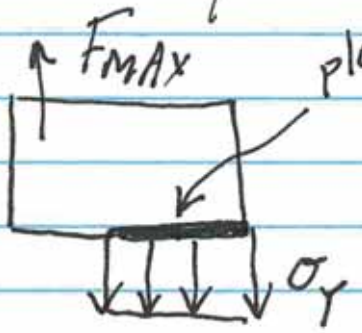

$$F_{MAX} = \sigma_Y t (b-a)$$

$$\frac{F_{MAX}}{\sigma_Y t b} = 1 - a/b \equiv \frac{\sigma_N}{\sigma_Y}$$

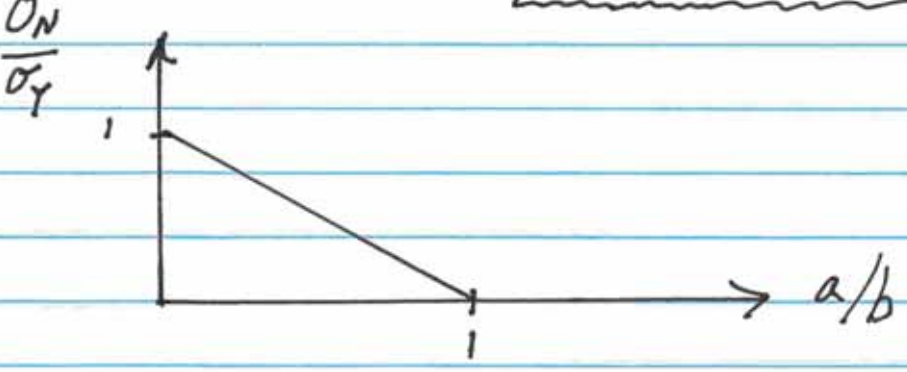

Influence of a Crack

We will limit our discussion to linear, elastic, isotropic materials experiencing small strains.

unKnowns:

$$\sigma_{ij},\ \epsilon_{ij},\ u_i$$

equilibrium: $\dfrac{\partial \sigma_{ji}}{\partial x_j} + f_i = 0, \quad \sigma_{ij} = \sigma_{ji}$

strain-displacement: $\epsilon_{ij} = \dfrac{1}{2}\left(\dfrac{\partial u_i}{\partial x_j} + \dfrac{\partial u_j}{\partial x_i}\right)$

Hooke's law: $\sigma_{ij} = 2G\left(\epsilon_{ij} + \dfrac{\nu}{1-2\nu}\epsilon_{kk}\delta_{ij}\right)$

Compatibility: $R_{ij} \equiv \epsilon_{ipq}\epsilon_{jrs}\epsilon_{qs,pr} = 0$

\+ Boundary conditions

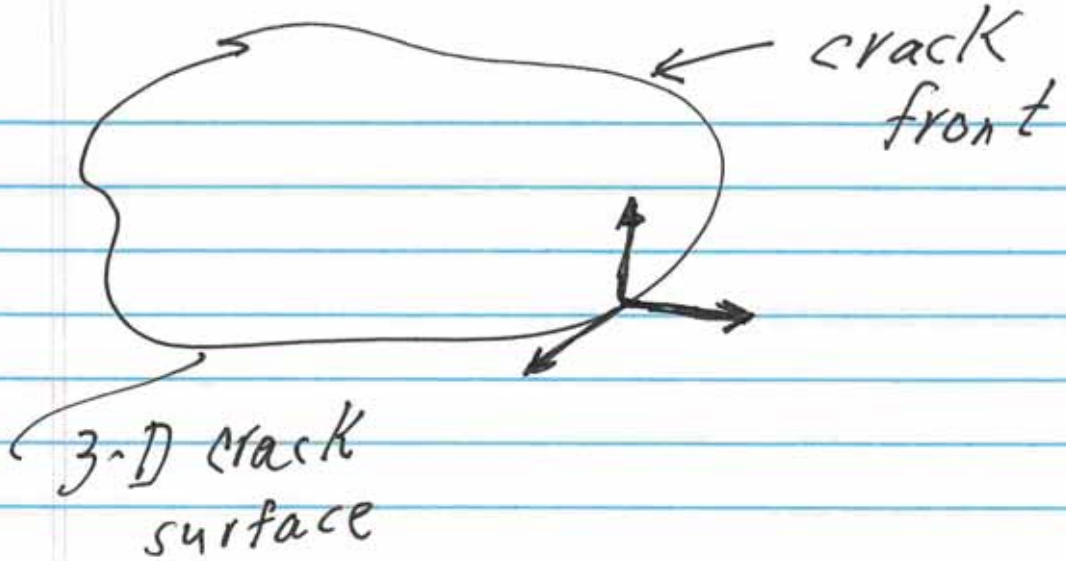

It can be shown that near the front, the elastic fields are a combination of three independent modes:

Mode I - "opening" or "tension"

Mode II - "sliding" or "in-plane shear"

Mode III - "tearing" or "anti-plane shear"

However, experimental data shows that the validity of strength theories as applied to cracked structures is severely limited. Plasticity does not account for "flaw sensitivity." In general the nominal strength of a cracked structure depends on the combination of characteristic dimensions of the structure, and a material length scale.

We will show that the strength plot looks like this:

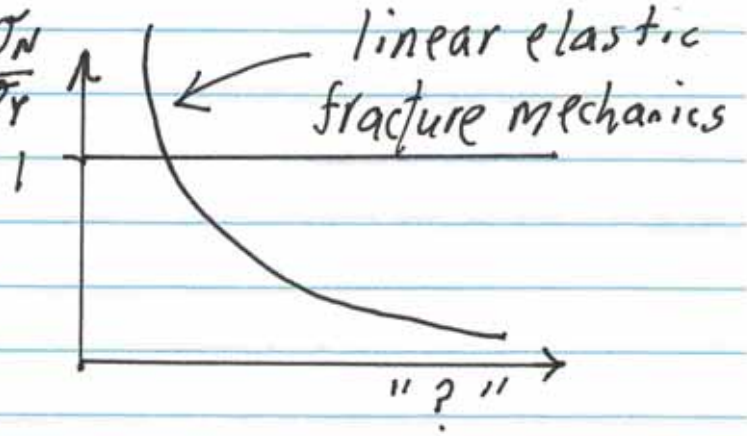

Let us consider plane strain/stress

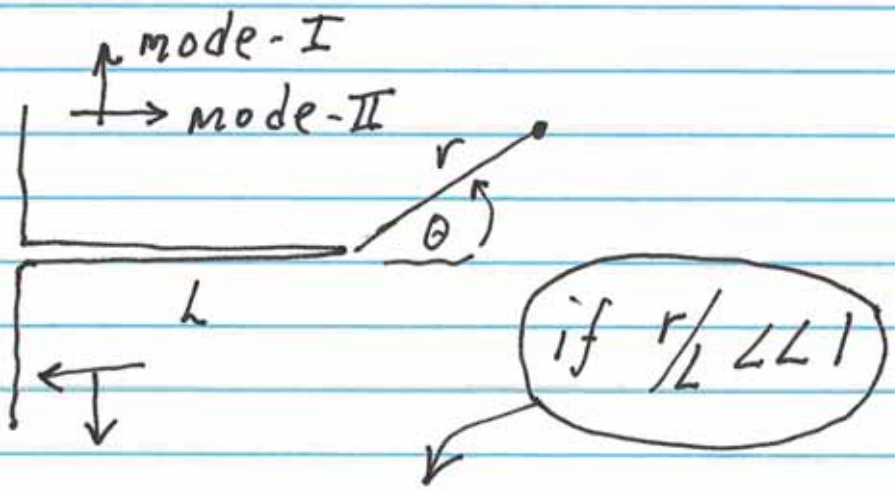

$$\sigma_{ij} = \frac{K_I}{\sqrt{2\pi r}} f_{ij}(\theta) + \text{Bounded terms}$$

$$+ \frac{K_{II}}{\sqrt{2\pi r}} g_{ij}(\theta) + \text{Bounded terms}$$

f_{ij} & g_{ij} are universal functions

K_I, K_{II} depend on geometry of the structure and the boundary conditions. Note $K_{I,II} = \left[\frac{F}{L^{3/2}}\right]$

Since $\sigma_{ij} \to \infty$ as $r \to 0$, we must abandon the idea that failure initiates at a critical stress level.

Examples of K_I:

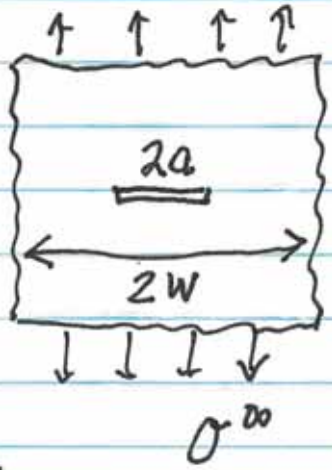

$\frac{a}{W} \to 0$

$$K_I = \sigma^\infty \sqrt{\pi a}$$

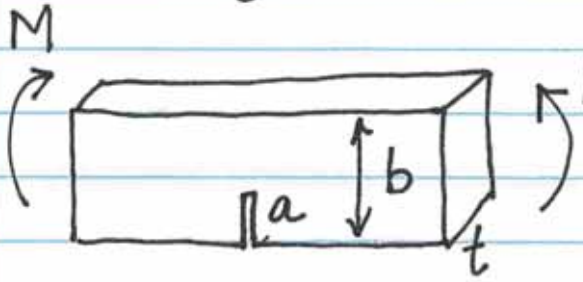

$$\sigma^N \equiv \frac{M\frac{b}{2}}{t\frac{b^3}{12}} = \frac{6M}{tb^2}$$

$$K_I = \frac{6M}{tb^2}\sqrt{\pi a}\, F(a/b)$$

How can we use the elastic singular fields to predict crack extension?

First, we note that the stress concentration produces a damage zone (process zone):

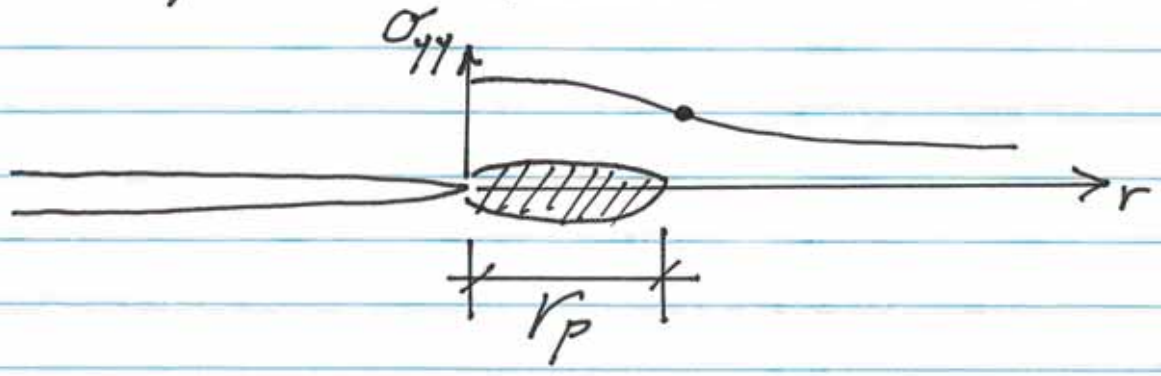

"Quick and dirty estimate" of r_p

$$\sigma_{yy}(r=r_p) = \sigma_y = K_I / \sqrt{2\pi r_p}$$

$$r_p \sim \left(\frac{K_I}{\sigma_y}\right)^2$$

An example of the “process zone” that develops at crack tips

Moreover, it has been determined theoretically, computationally, and experimentally that if $\frac{r_p}{L} \ll 1$, there exists a K_I-dominated zone

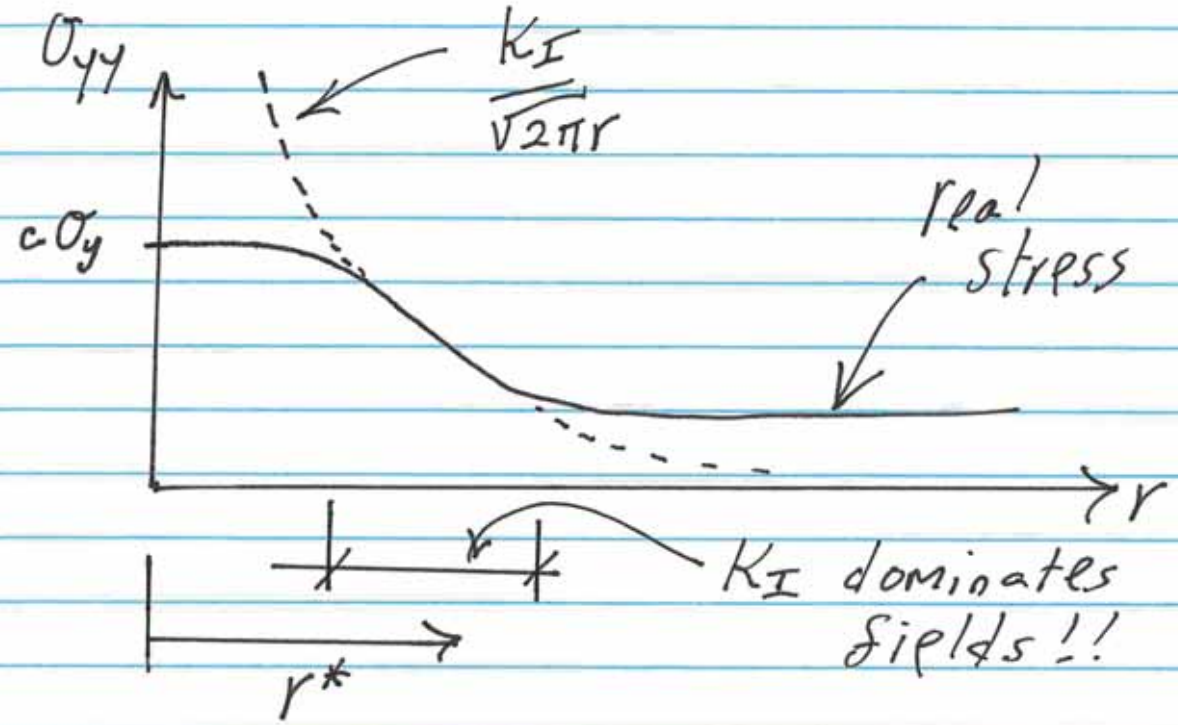

Let's visualize the K_I dominated zone through a free body diagram.

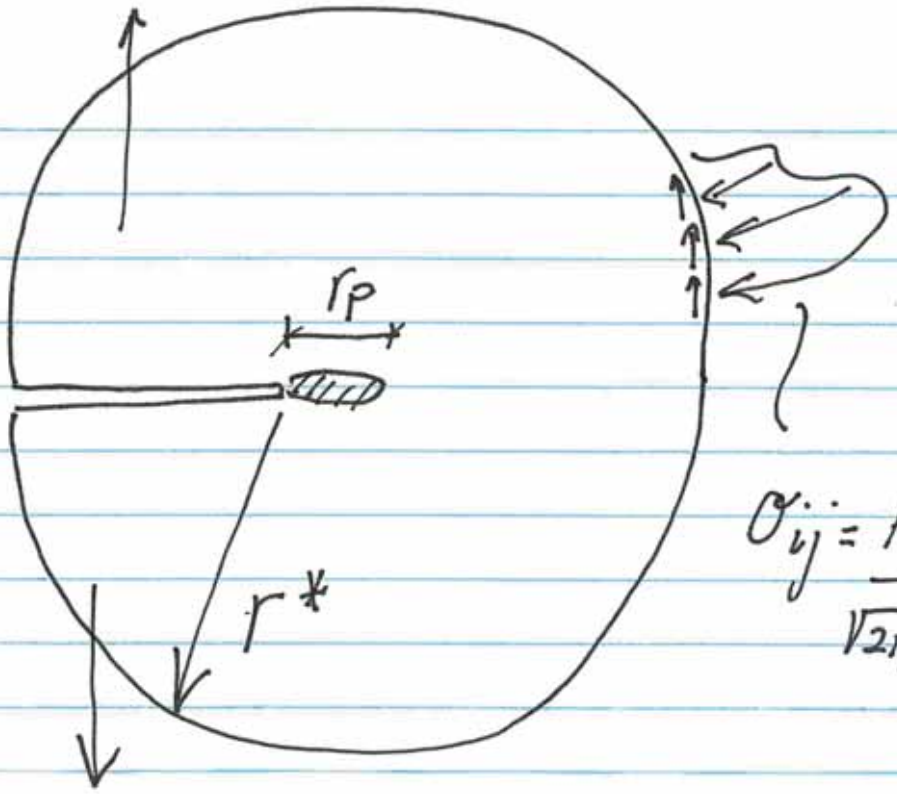

K_I is the only parameter required to characterize how the near-tip region responds to the applied loads and specimen geometry!!

Therefore we postulate:

$K_I = K_I^{CRITICAL}$ as the crack extension criterion

$$K_I = K_I^{CRITICAL}$$

instead of $f(\sigma_{ij}) = f^{CRITICAL}$

If $\frac{r_p}{L}$ is relatively large:

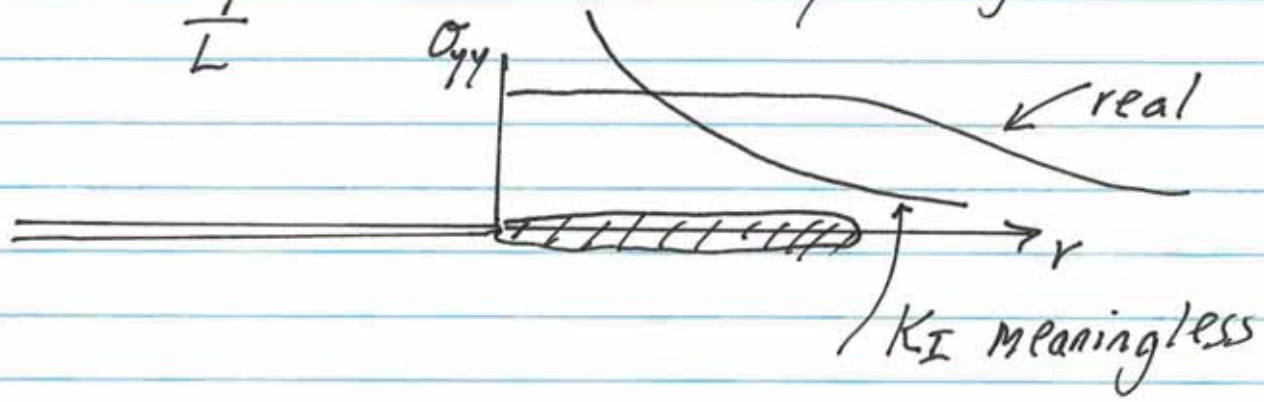

Illustrative values of r_p:

Material	K_{IC}	σ_y	$r_p = \frac{1}{2\pi}\left(\frac{K_{IC}}{\sigma_Y}\right)^2$
7075-T6 Al	25 Ksi$\sqrt{in}$	75 Ksi	0.02 in
PMMA	750 psi$\sqrt{in}$	7500 psi	0.002 in
A533B ↑ pressure vessel steel	170 Ksi$\sqrt{in}$	100 Ksi	0.5 in

Note that $K_I^{CRITICAL}$ is dependant on specimen thickness, temperature, and other things:

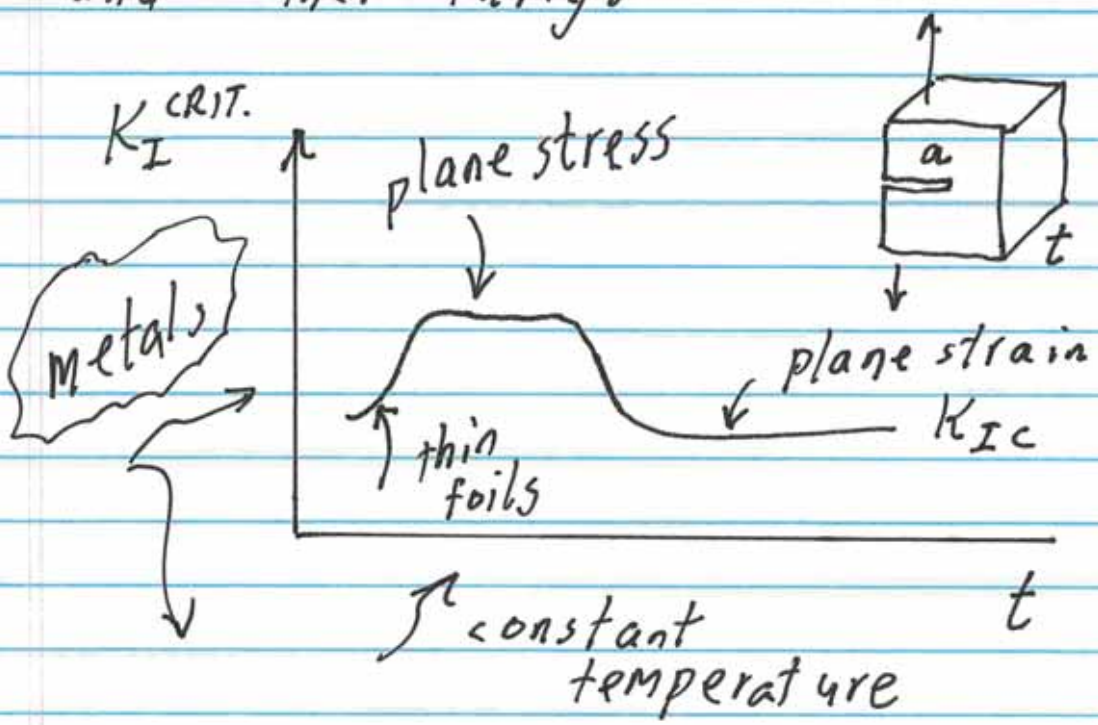

when $a, t > 2.5\left(\frac{K_{Ic}}{\sigma_y}\right)^2$, plane strain prevails

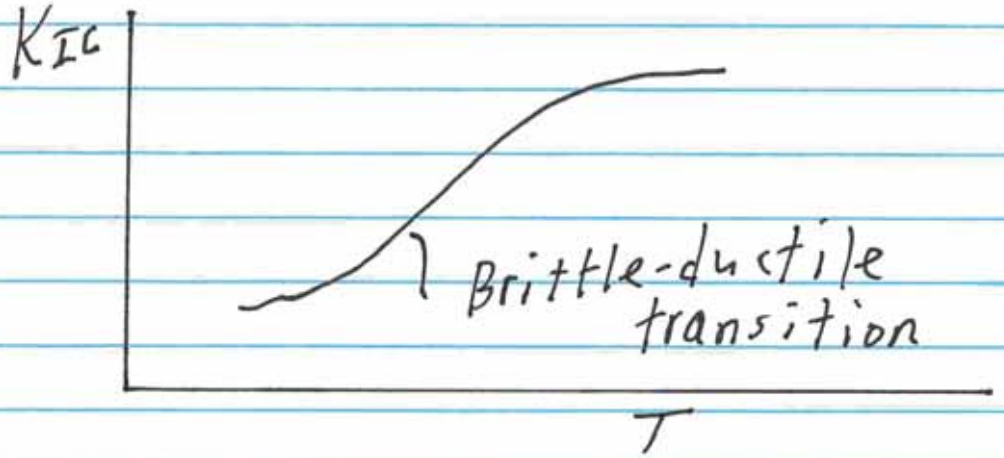

Let's complete the strength-"size" plot:

$$\sigma_{CRIT} \sim \frac{K_{Ic}}{\sqrt{a}} \qquad r_p \sim \left(\frac{K_{Ic}}{\sigma_y}\right)^2$$

$$\frac{\sigma_{CRIT}}{\sigma_y} \sim \frac{1}{\sqrt{a/r_p}}$$

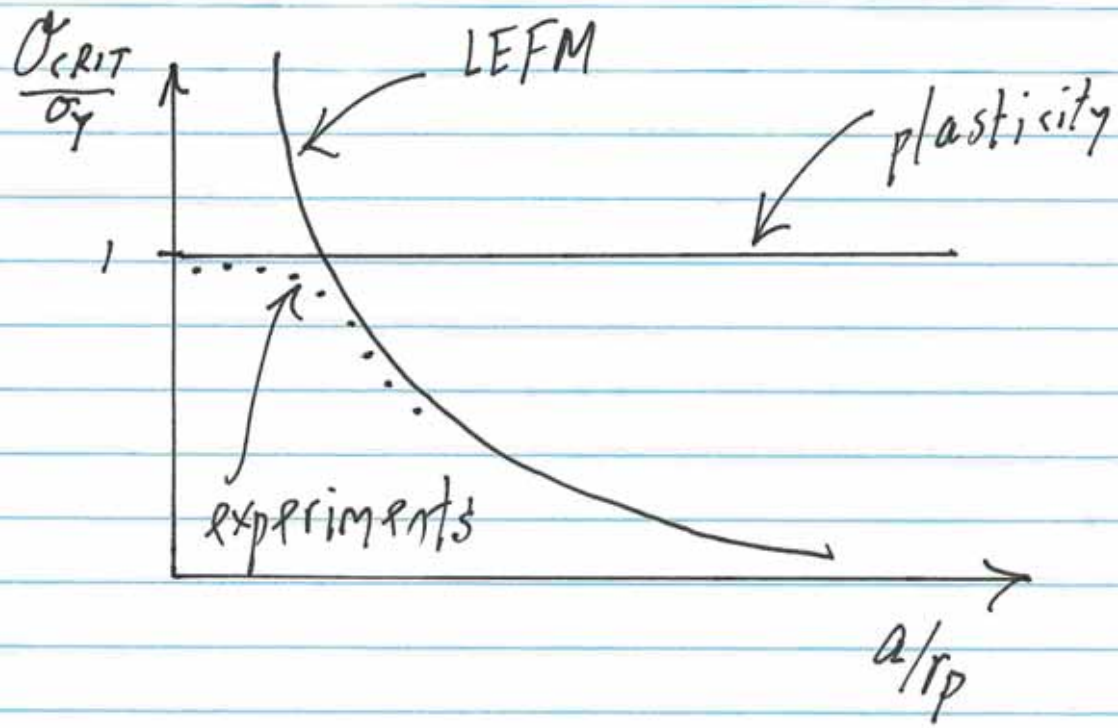

Let's return to the cracked beam

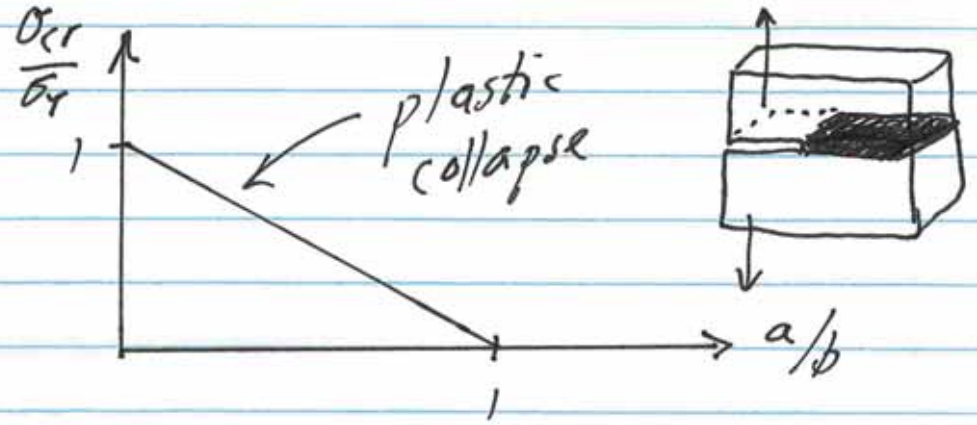

$$\frac{\sigma_{cr}}{\sigma_Y}^{LEFM} = \frac{K_{Ic}}{\sqrt{\pi a}\, F\left(\frac{a}{b}\right)\sigma_Y} = \frac{K_{Ic}}{\sigma_Y\sqrt{b}}\,\frac{1}{\sqrt{\pi\, a/b}\; F}$$

$$\boxed{\frac{\sigma_{cr}}{\sigma_Y}^{LEFM} \equiv \frac{1}{B\, G(a/b)}}$$

$$B \equiv \frac{\sigma_Y\sqrt{b}}{K_{Ic}}$$

$$G \equiv \sqrt{\pi\, a/b}\; F$$

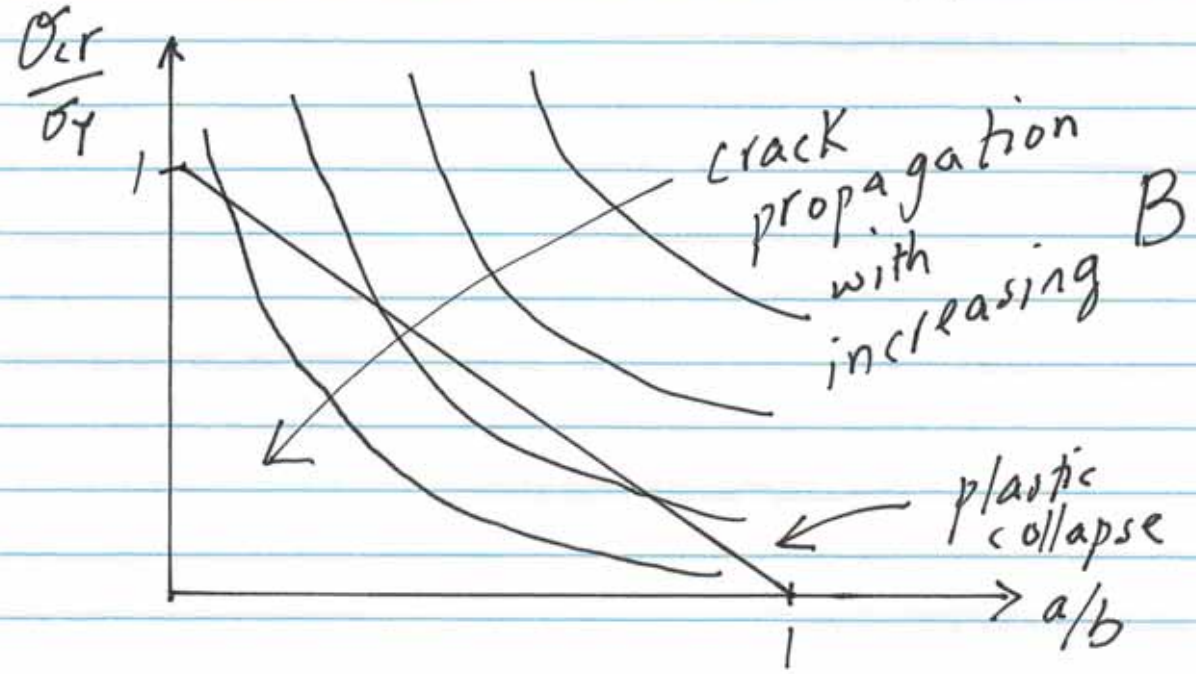

Mixed-mode Propagation in Tension-weak (brittle) solids

We want to predict the load required to extend the crack, and the direction of extension.

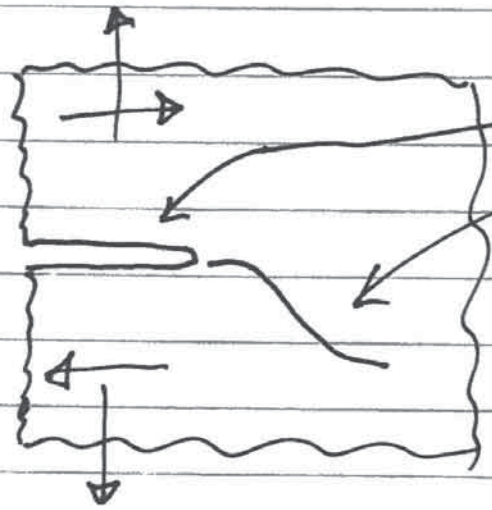

Let's start with pure Mode-II ($K_I = 0$)

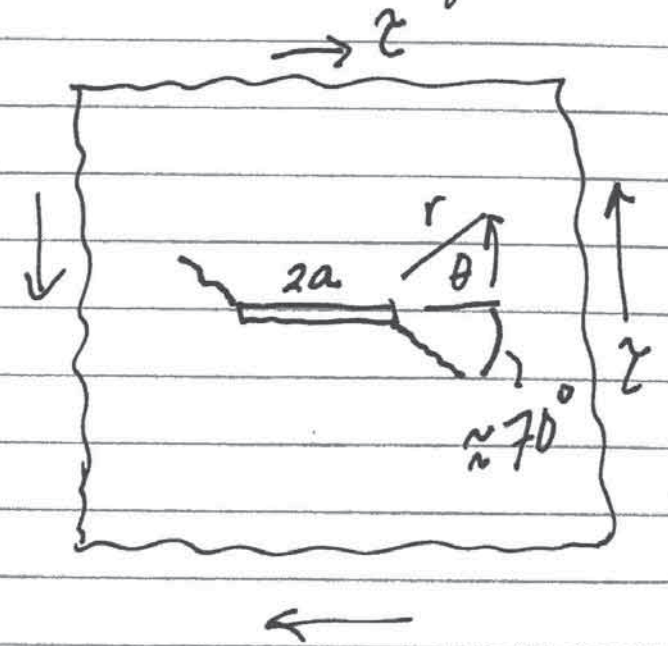

$$K_{II} = +\tau\sqrt{\pi a}$$

why does crack choose $-70°$?

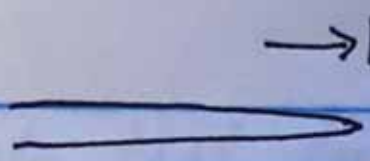

$$\sigma_{\theta\theta} = \frac{K_{II}}{\sqrt{2\pi r}} f_{\theta\theta}(\theta)$$ ← Known

$$\sigma_{\theta\theta} = -\frac{K_{II}}{\sqrt{2\pi r}} \frac{3}{4}\left(\sin\frac{\theta}{2} + \sin\frac{3\theta}{2}\right)$$

$$\sigma_{r\theta} = \frac{K_{II}}{\sqrt{2\pi r}} \frac{1}{4}\left(\cos\frac{\theta}{2} + 3\cos\frac{3\theta}{2}\right)$$

Assume crack extends in the direction perpendicular to maximum tension.

$$\frac{d\sigma_{\theta\theta}}{d\theta} = 0 \quad (\sigma_{r\theta} = 0)$$

$$\hookrightarrow \theta = \pm 70.6^\circ$$

(choose -70.6° for tension)

<< 70.6° is compression >>

Note that for $\theta = -70.6°$

$$\sigma_{\theta\theta} \cong \frac{2}{\sqrt{3}} \frac{K_{II}}{\sqrt{2\pi r}}$$

it looks like the stress field ahead of a Mode-I crack with $K_I \equiv \frac{2}{\sqrt{3}} K_{II}$

Therefore $\boxed{K_{II}^{CRITICAL} = \frac{\sqrt{3}}{2} K_I^{CRITICAL}}$

Generalizing to K_I & K_{II}

$$\sigma_{\theta\theta} = \frac{1}{\sqrt{2\pi r}} \left\{ K_I f_1(\theta) + K_{II} f_2(\theta) \right\}$$

$$\sigma_{r\theta} = \frac{1}{\sqrt{2\pi r}} \left\{ K_I f_3(\theta) + K_{II} f_4(\theta) \right\}$$

set $\sigma_{r\theta} = 0$: $\Rightarrow \theta_m$

$$\boxed{\tan\left(\frac{\theta_m}{2}\right) = \frac{1}{4}\left\{ \frac{K_I}{K_{II}} \pm \sqrt{\left(\frac{K_I}{K_{II}}\right)^2 + 8} \right\}}$$

set $\sigma_1 = \dfrac{K_{Ic}}{\sqrt{2\pi r}}$

↑ DIRECTION

$$\boxed{\frac{K_I}{K_{Ic}} \cos^3\frac{\theta_m}{2} - 3\frac{K_{II}}{K_{Ic}} \cos^2\frac{\theta_m}{2} \sin\frac{\theta_m}{2} = 1}$$

↑ EXTENSION LOAD

Examples of
Fracture Mechanics-Based Design:

1. **Break-out strength of anchors embedded in concrete.**

2. **Design of gears in rotorcraft transmission and drive systems.**

Roberto Ballarini
Thomas and Laura Hsu Professor
University of Houston

Tongji University

Fracture Mechanics Model of Anchor Group Breakout: A Classroom Example

or

ACI/RILEM have learned a lot, but not enough

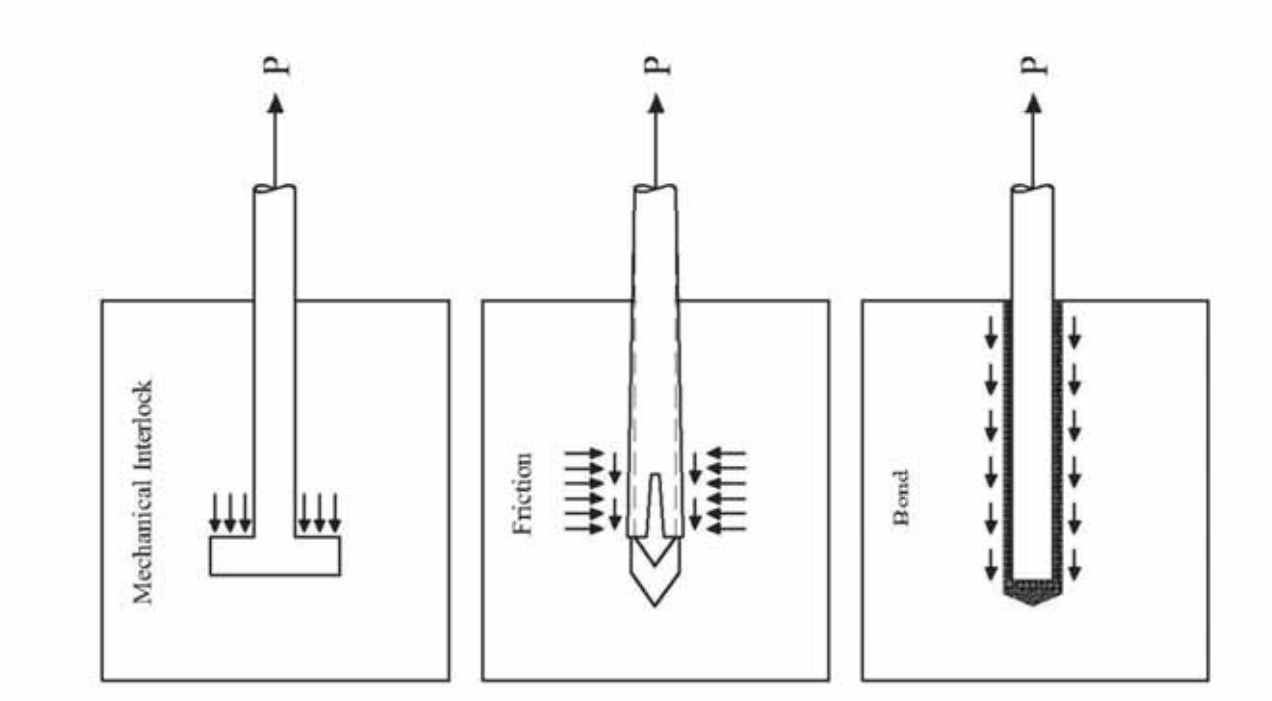

The codes up to the early 1990's

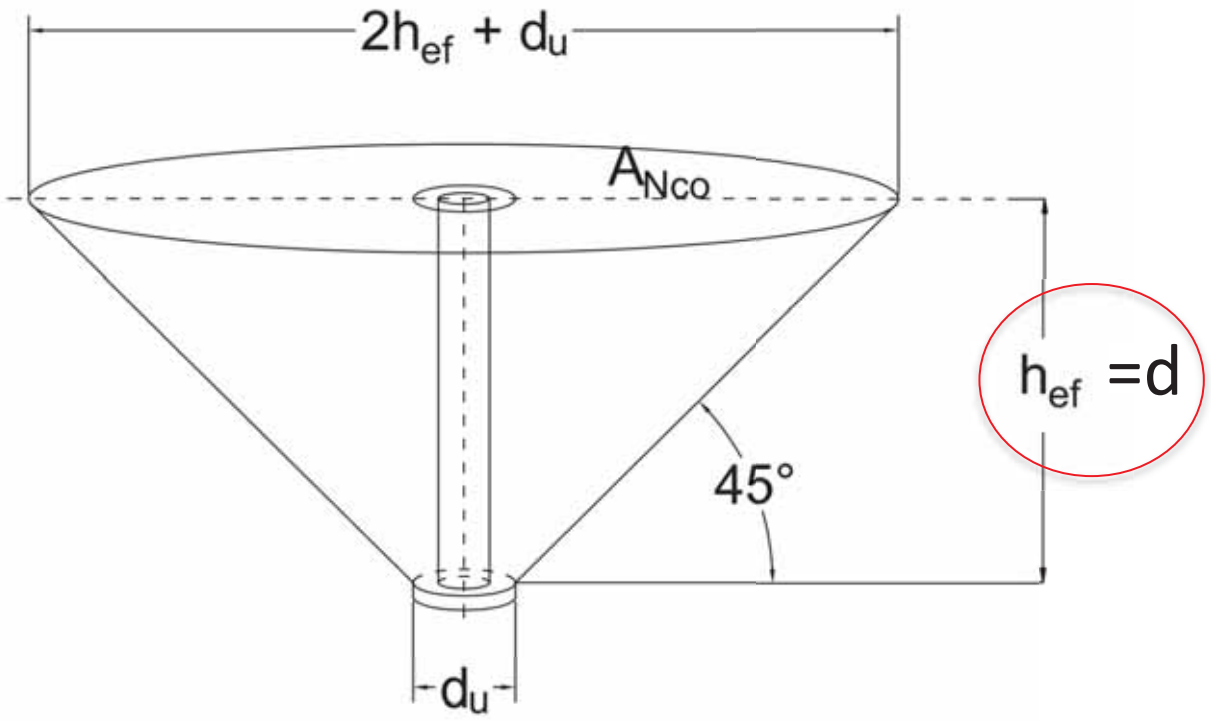

$$P_{u,ACI} = f_t \pi d^2 \left(1 + \frac{c}{d}\right) = 4\phi\sqrt{f_c'}\pi d^2 \left(1 + \frac{c}{d}\right) \approx f_t d^2$$

$$\phi \ (f_t = 4\phi\sqrt{f_c'}).$$

Does not agree with experimental data!
Overpredicts capacity!

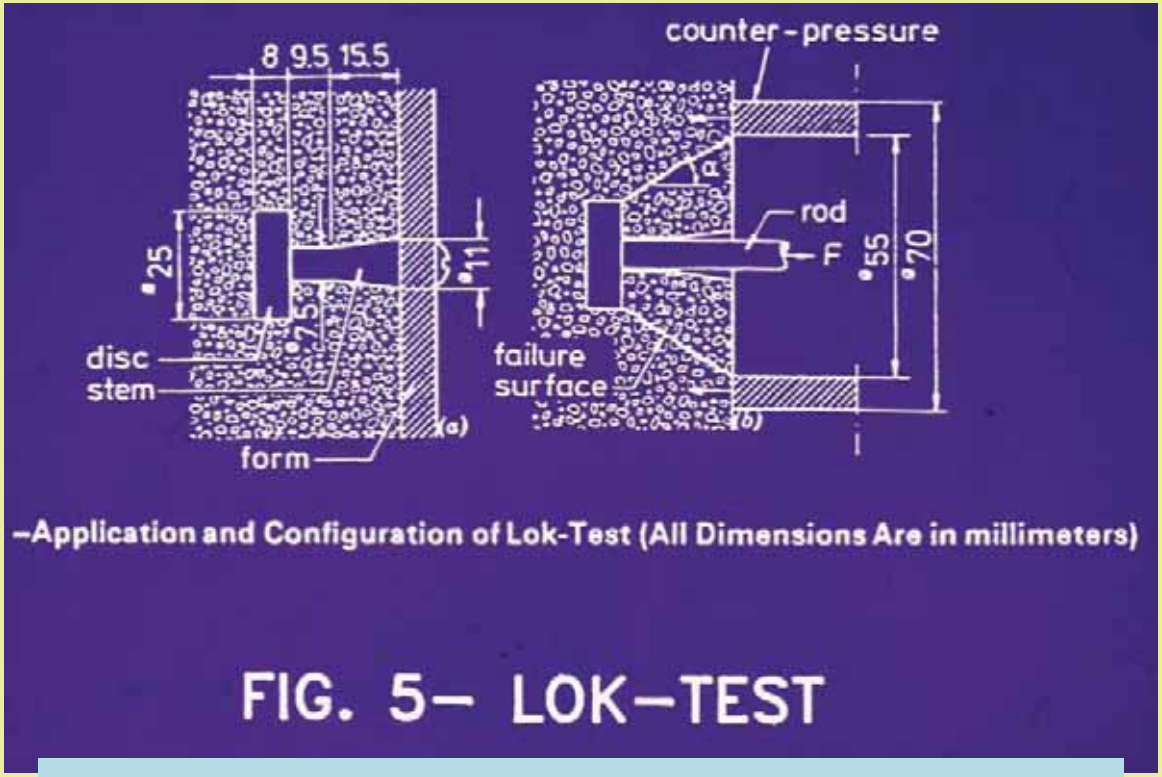

–Application and Configuration of Lok-Test (All Dimensions Are in millimeters)

FIG. 5– LOK–TEST

What material property is this test measuring?
The compressive strength is correlated with the force required to pull out the anchor.

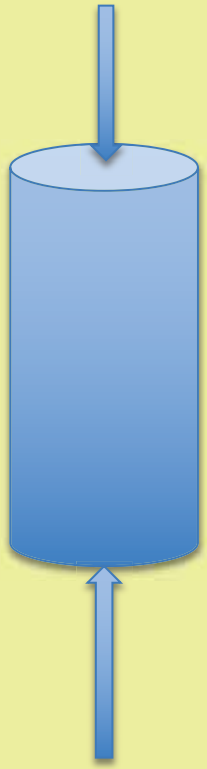

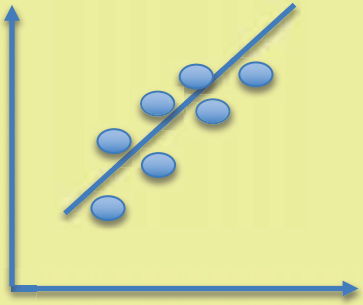

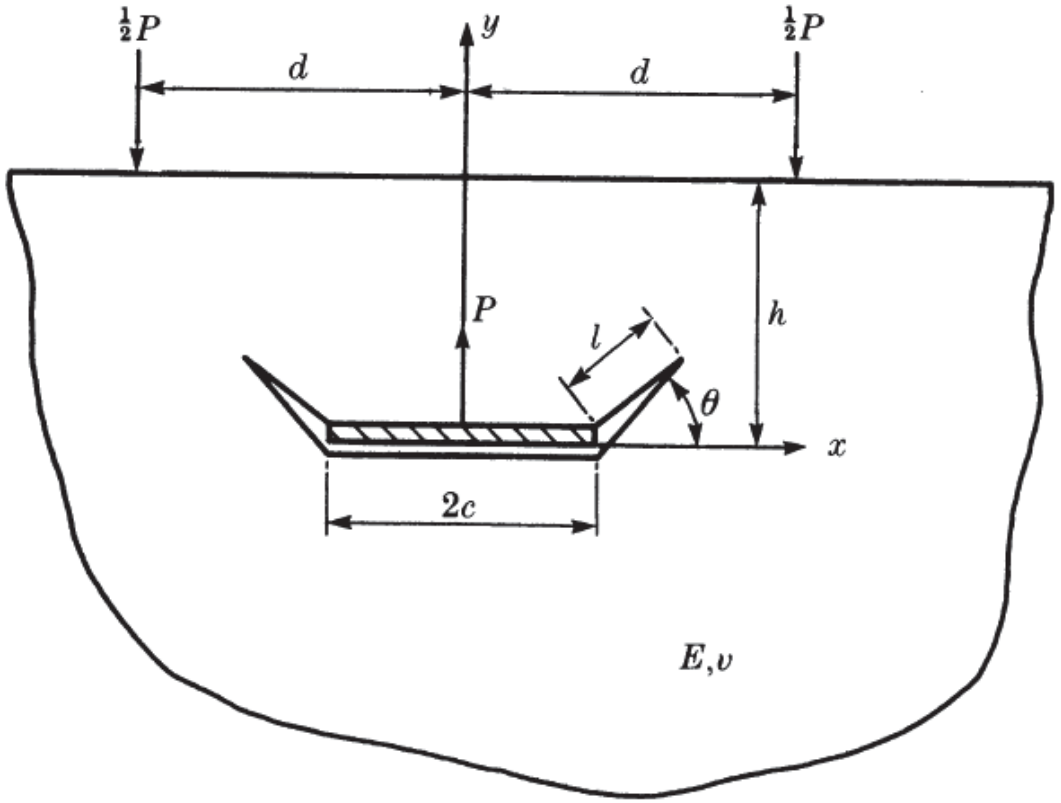

- **Failure of headed anchors reflects a progressive crack propagation process; (Ballarini *et al.*, 1985) Two-dimensional configuration**

- **Experimental and analytical investigation of LOK test and pullout problem by changing the position of the support reactions;**

Stress Intensity Factors

K_I = mode I stress intensity factor

K_{II} = mode II stress intensity factor

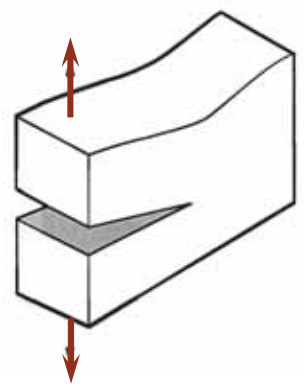

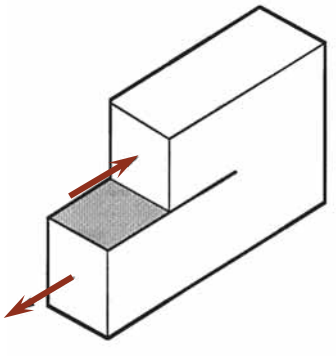

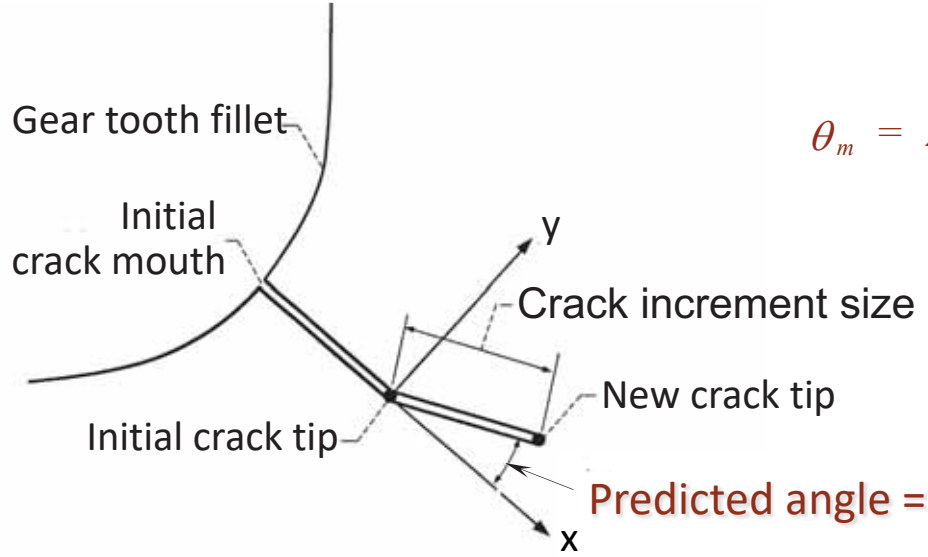

$$\theta_m = 2\tan^{-1}\left[\frac{\frac{K_I}{K_{II}} \pm \sqrt{\left(\frac{K_I}{K_{II}}\right)^2 + 8}}{4}\right]$$

Predicted angle = $f(K_{II}/K_I)$

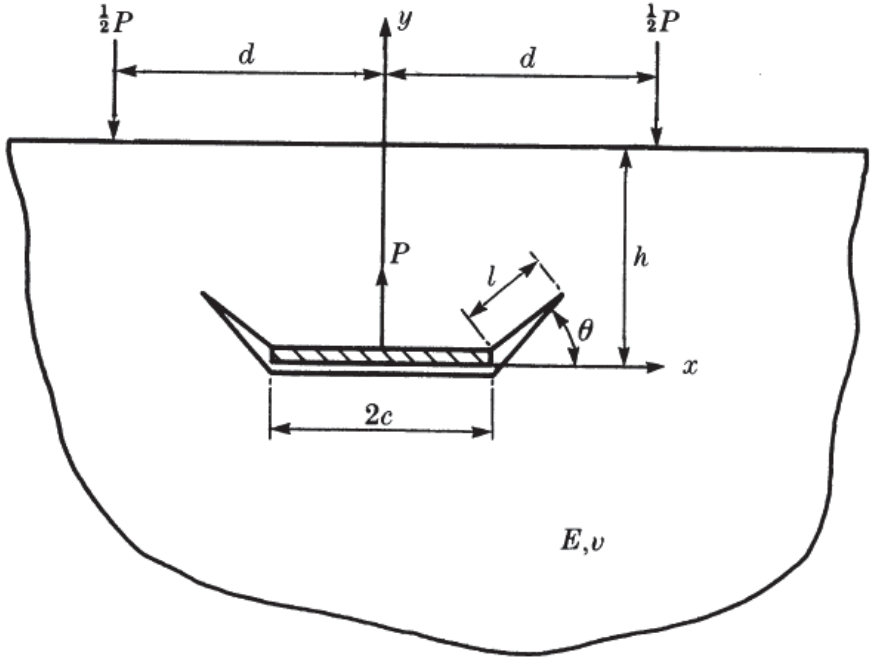

$$2\mu\left(\frac{\partial u}{\partial x} + i\,\frac{\partial v}{\partial x}\right)^{+} = 0 \qquad \text{(bonded upper portion)}$$

$$(\sigma_{yy} - i\sigma_{xy})^{-} = 0 \qquad \text{(unbonded lower portion)}$$

$$\sigma_{\phi\phi} - i\sigma_{\rho\phi} = 0 \qquad \text{(stress free crack surface)}$$

$$\alpha(\xi) = \frac{-1}{2\pi(\kappa+1)} \frac{\partial}{\partial \xi} (F_x + \mathrm{i}F_y),$$

$$\beta(\xi) = \frac{\mu \mathrm{e}^{\mathrm{i}\theta}}{\pi \mathrm{i}(\kappa+1)} \frac{\partial}{\partial \xi} \{[u_r] + \mathrm{i}[v_\theta]\},$$

$$\psi(\tau) = \frac{\mu \mathrm{e}^{\mathrm{i}\theta}}{\pi \mathrm{i}(\kappa+1)} \frac{\partial}{\partial \tau} \{[u_r] + \mathrm{i}[v_\theta]\},$$

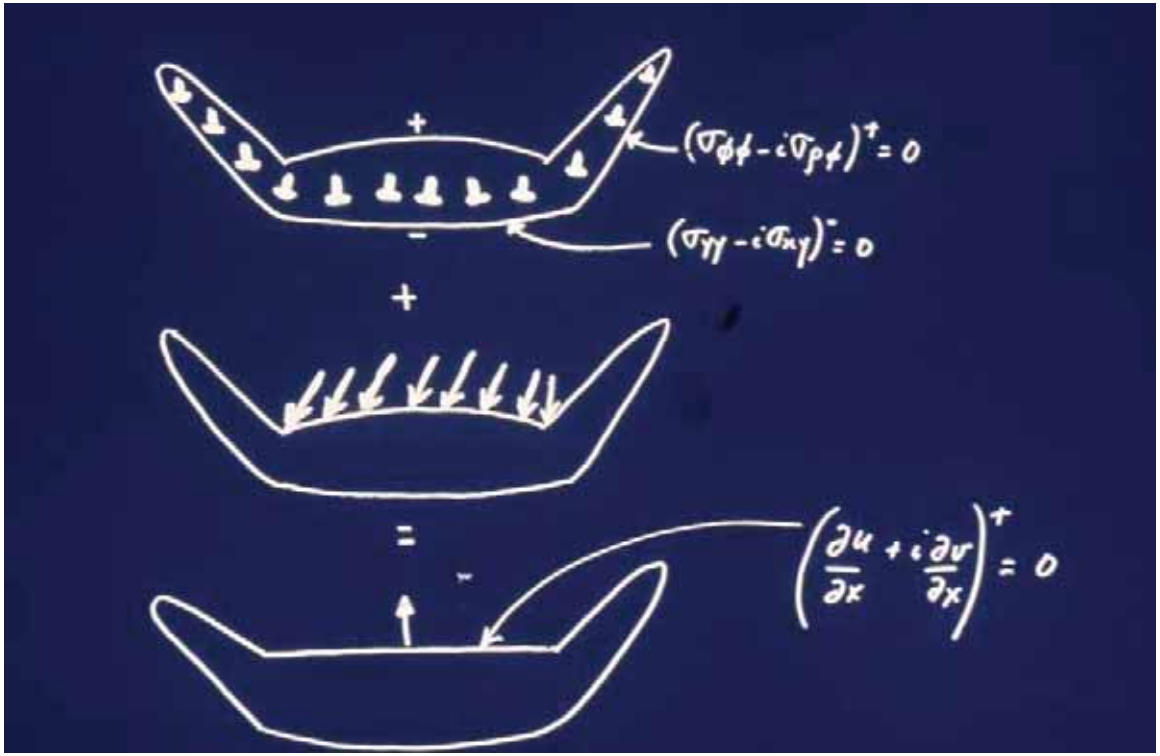
+
$(\sigma_{\phi\phi} - i\sigma_{r\phi})^+ = 0$
−
$(\sigma_{rr} - i\sigma_{xy})^- = 0$
+
=
$\left(\frac{\partial u}{\partial x} + i\frac{\partial v}{\partial x}\right)^+ = 0$

$$\int_0^c \alpha(\xi)\left\{\frac{\kappa-1}{\xi-x} + K_1(x,\xi) - K_2(x,-\xi)\right\} d\xi + \int_0^c \overline{\alpha(\xi)}\left\{K_2(x,\xi) - K_1(x,-\xi)\right\} d\xi$$

$$+ \pi i\,(\kappa+1)\,\alpha(x) + \int_0^c \beta(\rho)\left\{\frac{-2}{\rho-x} + K_3(x,\rho) - K_4(x,-\rho)\right\} d\rho$$

$$+ \int_0^c \overline{\beta(\rho)}\left\{K_4(x,\rho) - K_3(x,-\rho)\right\} d\rho$$

$$+ \int_0^\ell \psi(\tau)\,K_9(x,\tau)\,d\tau + \int_0^\ell \overline{\psi(\tau)}\,K_{10}(x,\tau)\,d\tau + f_1(x) = 0 \qquad -c \le x \le c$$

$$\int_0^c \left[\alpha(\xi) - \overline{\alpha(\xi)}\right] d\xi = \frac{P}{2\pi i(\kappa+1)}$$

$$\int_0^c \left[\beta(\xi) - \overline{\beta(\xi)}\right] d\xi + \int_0^\ell \left[\psi(\tau) - \overline{\psi(\tau)}\right] d\tau = 0$$

All physical quantities can be obtained after solving numerically the equations (3.4)–(3.8). In particular, the stress intensity factor, defined by

$$K_{\mathrm{I}} - \mathrm{i}K_{\mathrm{II}} = \lim_{r \to l^+} \sqrt{[2\pi(r-l)]}\,(\sigma_{\phi\phi} - \mathrm{i}\sigma_{r\phi}) \tag{3.10}$$

can be directly related to the dislocation density $\psi(r)$ by taking the asymptotic form of (3.6). In terms of dimensionless quantities arising from the numerical scheme, the result is

$$(K_{\mathrm{I}} - \mathrm{i}K_{\mathrm{II}})\,(c^{\frac{1}{2}}/P) = 2^{\frac{1}{2}}\pi^{\frac{1}{2}}\mathrm{e}^{-\mathrm{i}\theta}\sqrt{(l/c)}\overset{*}{\psi}(1), \tag{3.11}$$

where

$$\psi(r) = \frac{\overset{*}{\psi}(s)}{(1-s^2)^{\frac{1}{2}}}\frac{P}{c}; \quad s = \frac{2r}{l} - 1. \tag{3.12}$$

FIG. 13– MINIMUM PRINCIPAL STRESSES

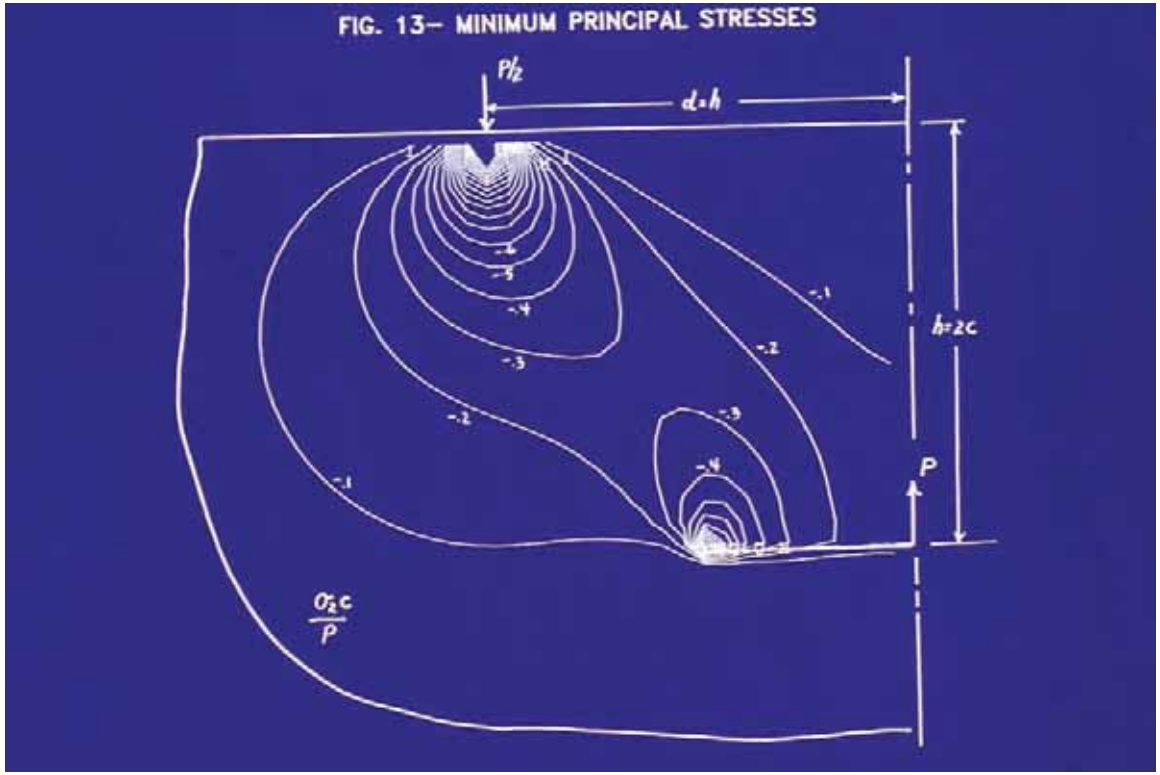

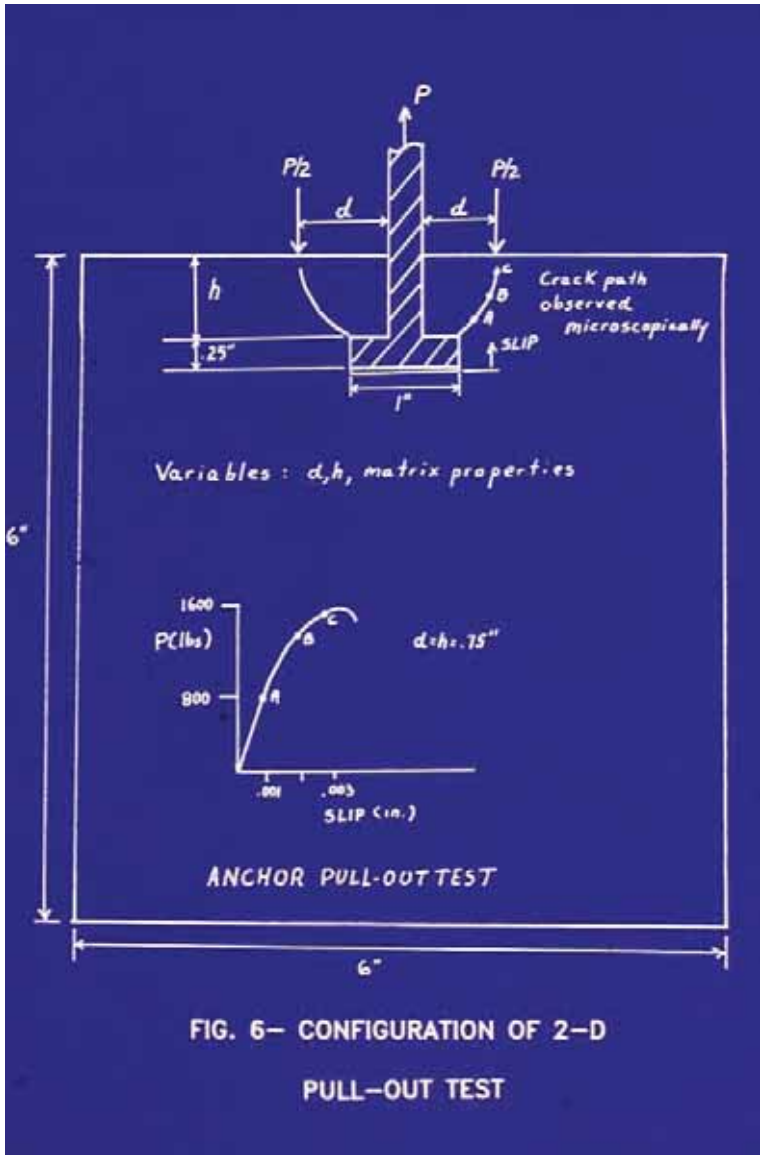

FIG. 6– CONFIGURATION OF 2–D PULL–OUT TEST

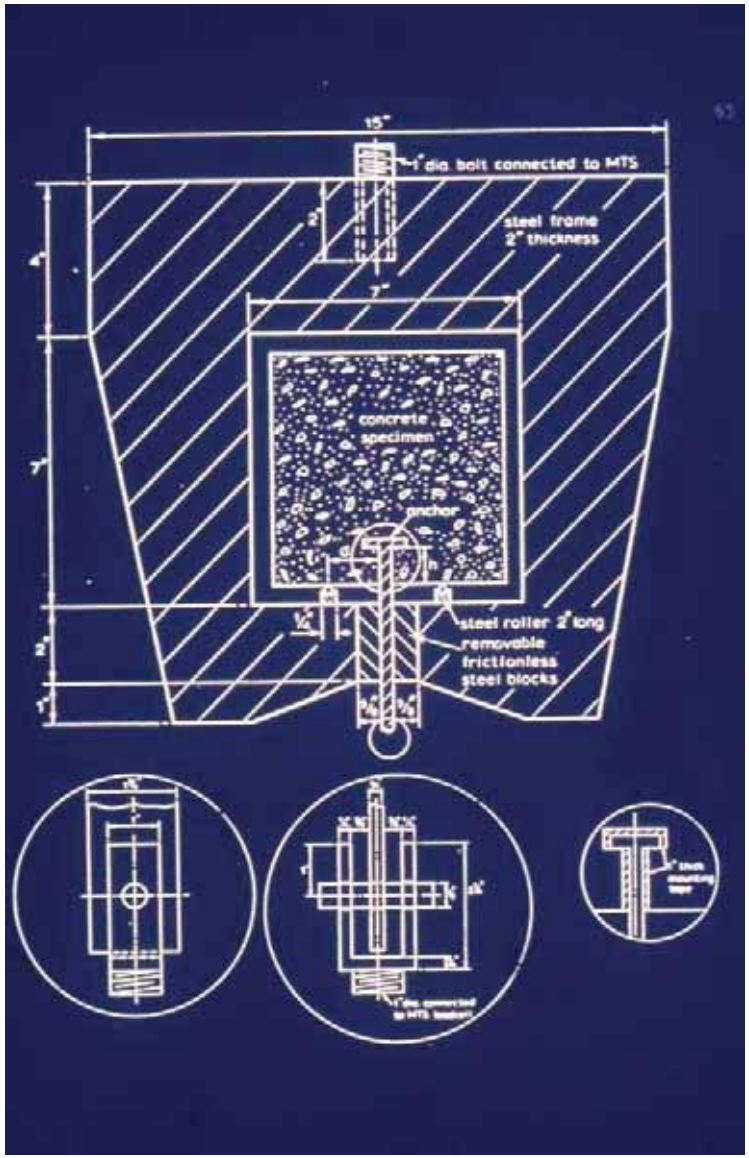
15"
1" dia. bolt connected to MTS
steel frame
2" thickness
7"
concrete
specimen
anchor
steel roller 2" long
removable
frictionless
steel blocks

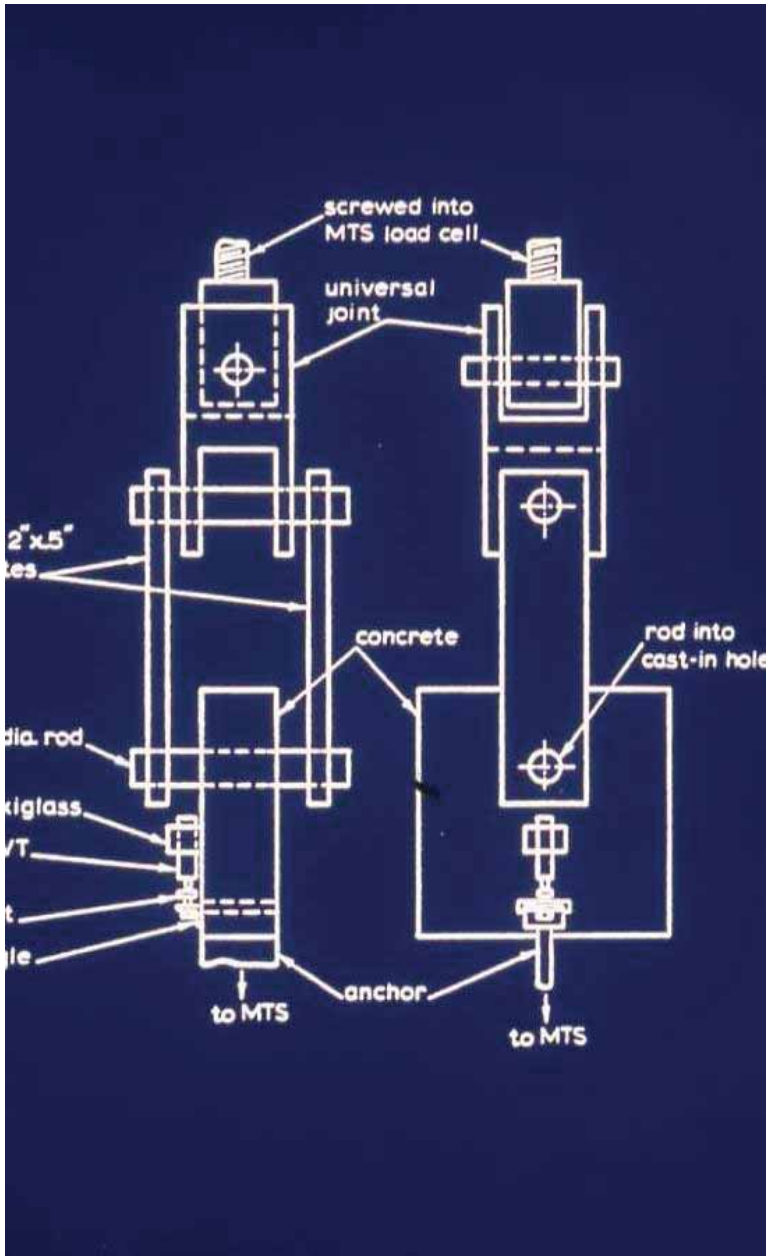
screwed into
MTS load cell
universal
joint
2"x.5"
concrete
rod into
cast-in hole
anchor
to MTS
to MTS

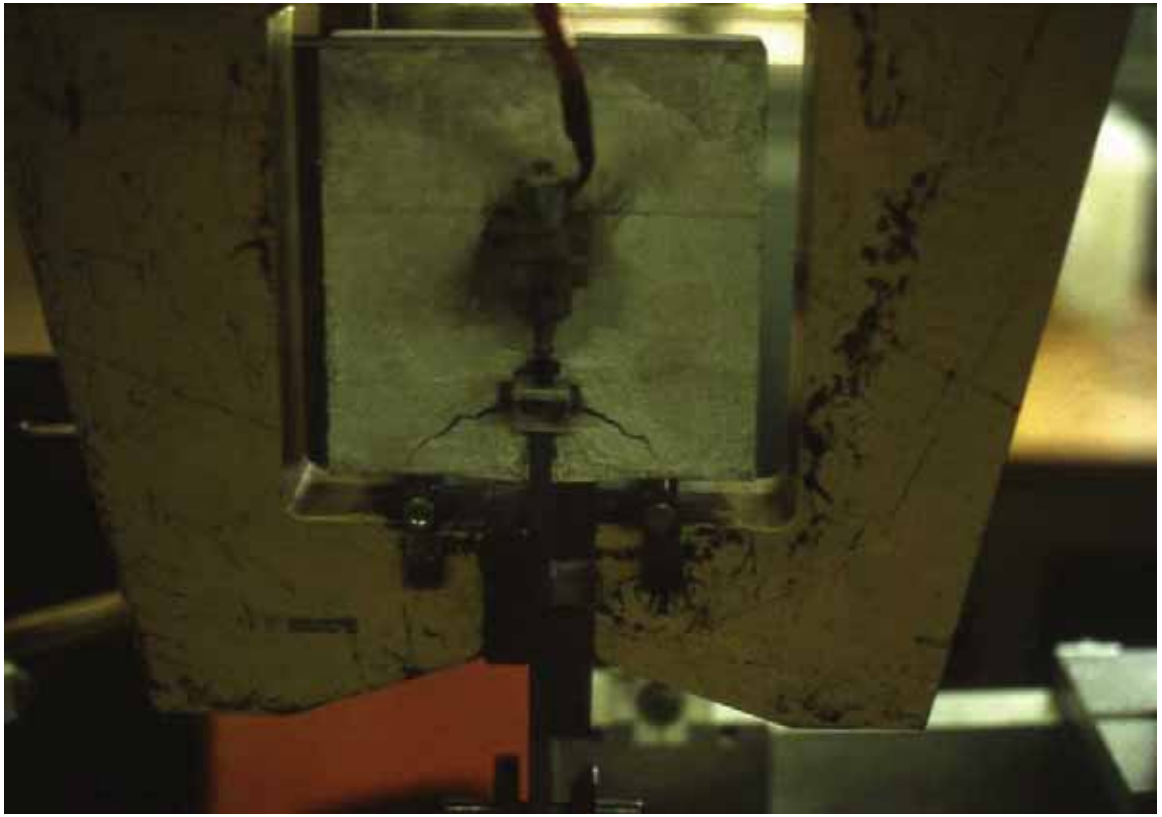

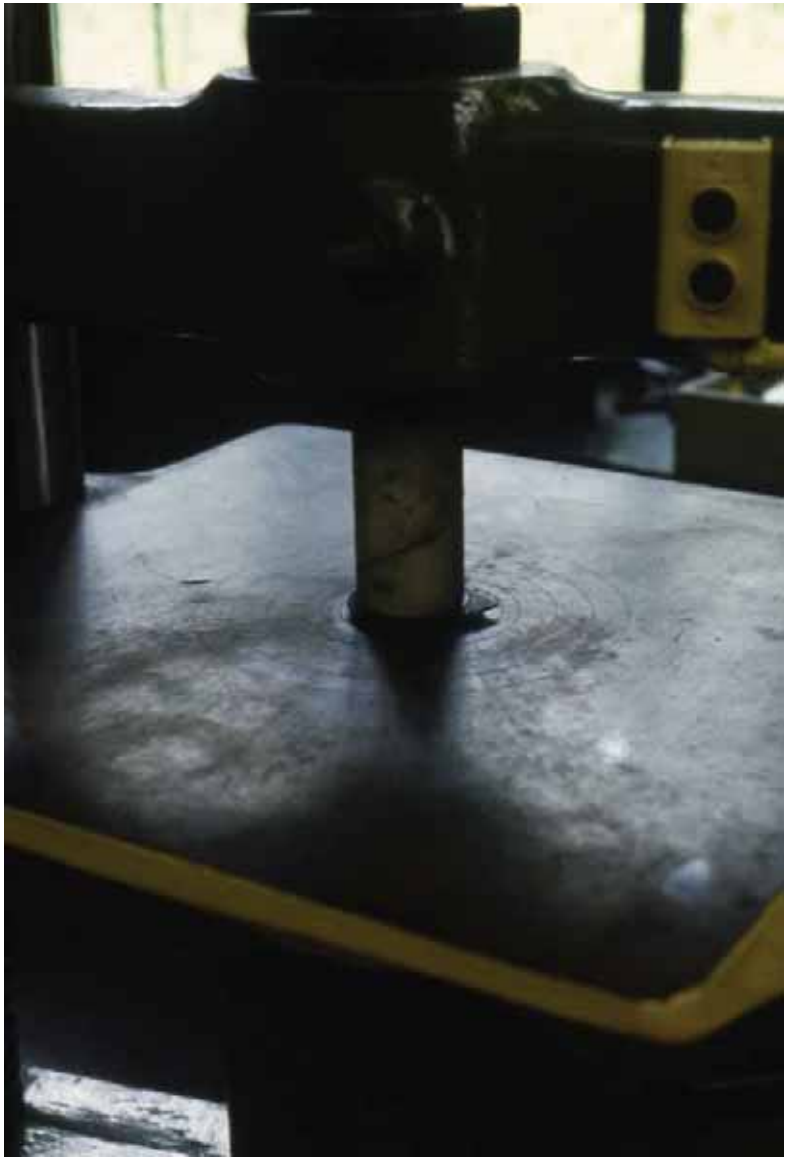

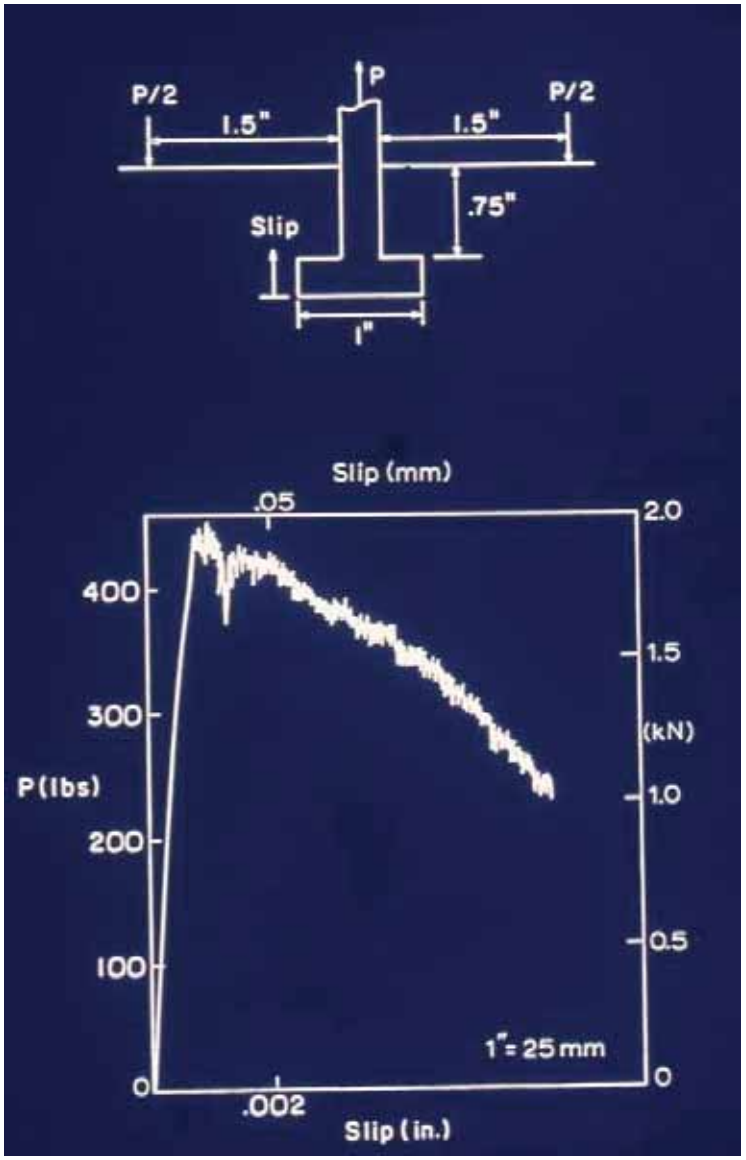
P/2
P
P/2
1.5"
1.5"
.75"
Slip
1"
Slip (mm)
.05
2.0
400
1.5
300
(kN)
P (lbs)
1.0
200
0.5
100
1"=25 mm
0
0
.002
Slip (in.)

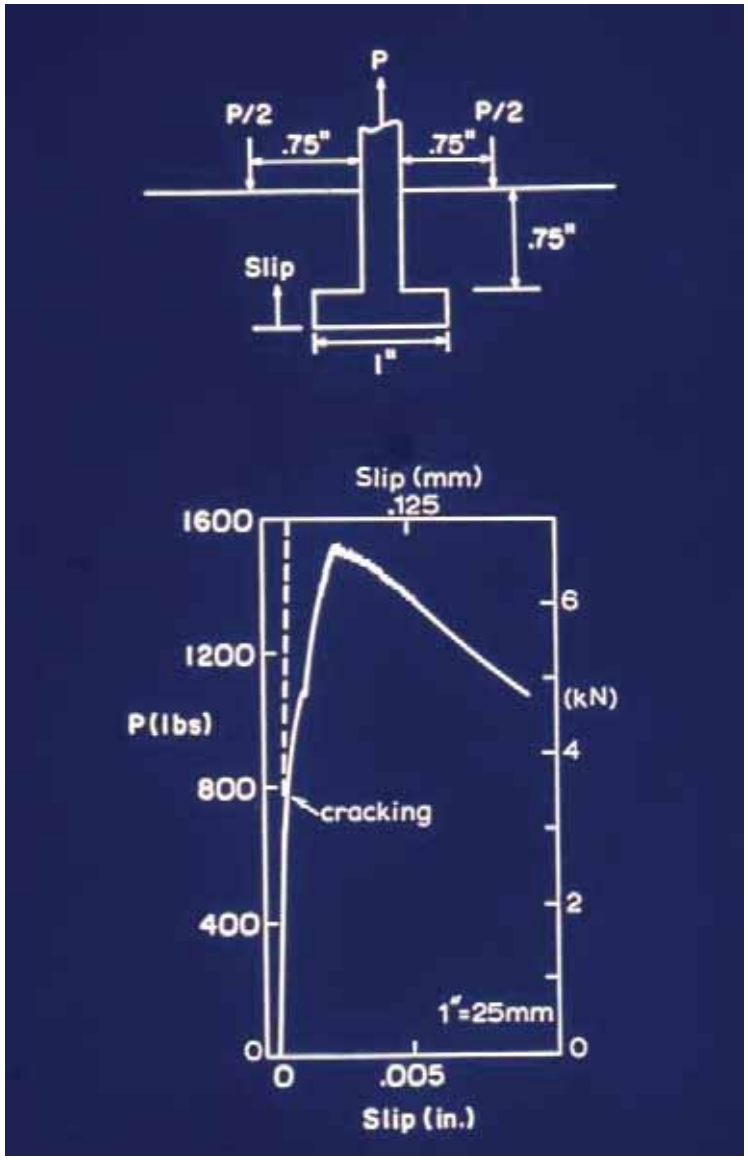
P
P/2
P/2
.75"
.75"
.75"
Slip
1"
Slip (mm)
.125
1600
6
1200
(kN)
P (lbs)
4
800
cracking
400
2
1"=25mm
0
0
0
.005
Slip (in.)

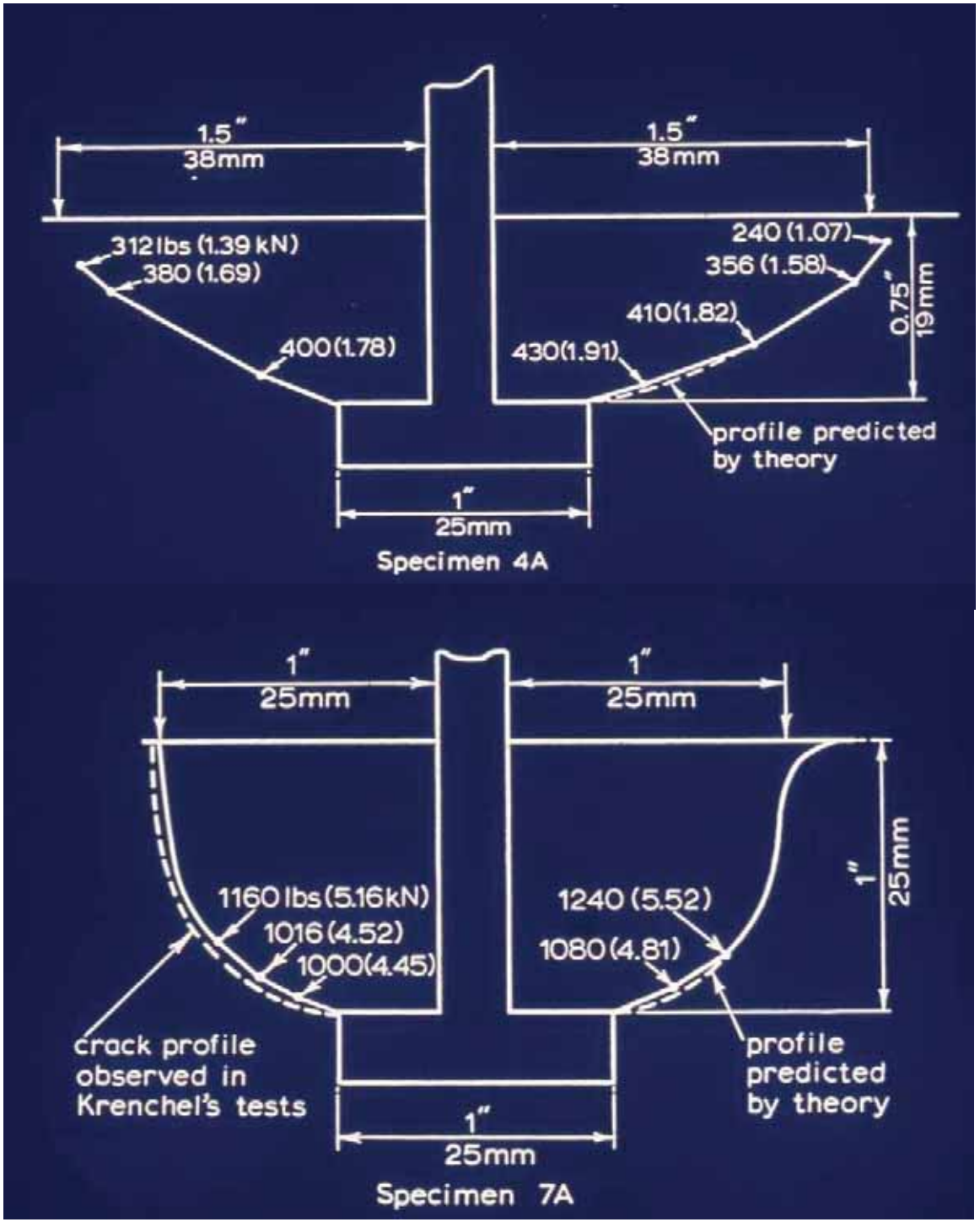
1.5"
38mm
1.5"
38mm
312 lbs (1.39 kN)
380 (1.69)
400(1.78)
240 (1.07)
356 (1.58)
410(1.82)
430(1.91)
0.75"
19mm
profile predicted
by theory
1"
25mm
Specimen 4A
1"
25mm
1"
25mm
1160 lbs (5.16kN)
1016 (4.52)
1000(4.45)
1240 (5.52)
1080 (4.81)
1"
25mm
crack profile
observed in
Krenchel's tests
profile
predicted
by theory
1"
25mm
Specimen 7A

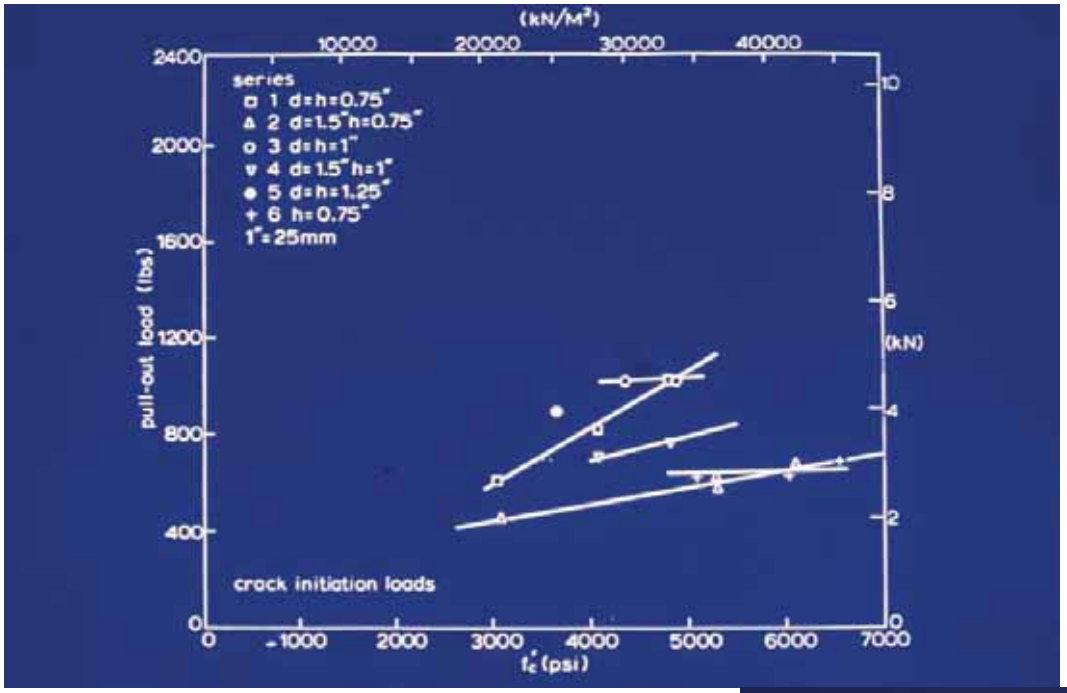
(kN/M²)
10000
20000
30000
40000
2400
2000
1600
1200
800
400
0
series
1 d=h=0.75"
2 d=1.5" h=0.75"
3 d=h=1"
4 d=1.5" h=1"
5 d=h=1.25"
6 h=0.75"
1"=25mm
pull-out load (lbs.)
(kN)
10
8
6
4
2
0
crack initiation loads
0
1000
2000
3000
4000
5000
6000
7000
f'c (psi)

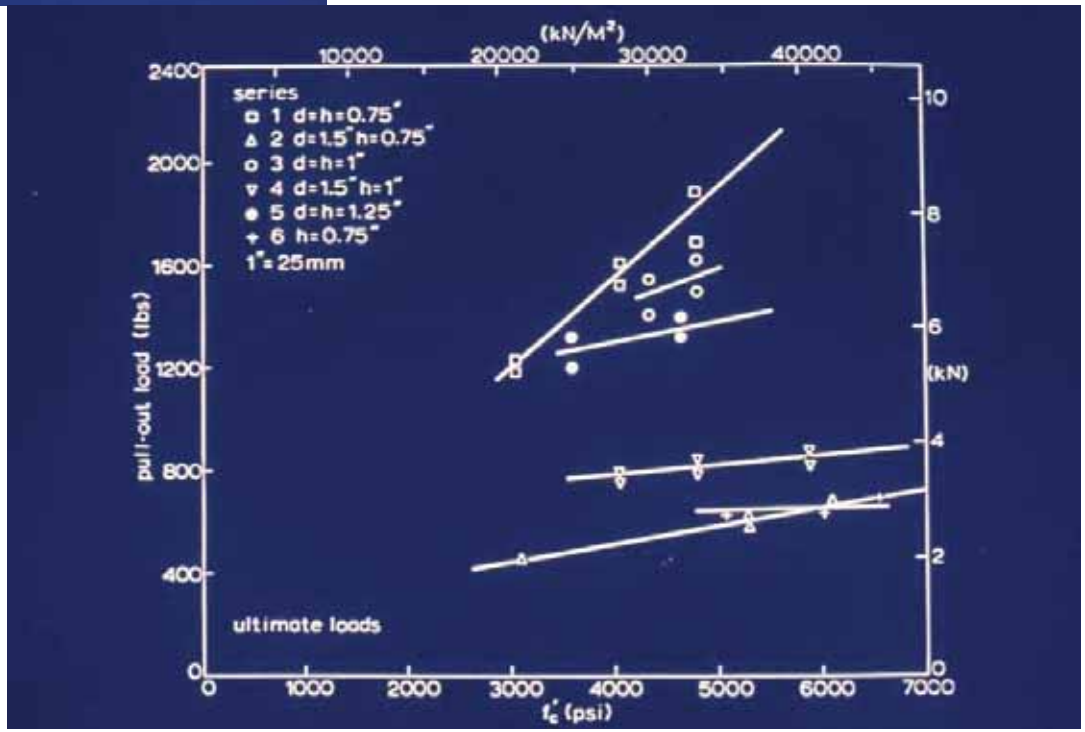
(kN/M²)
10000
20000
30000
40000
2400
2000
1600
1200
800
400
0
series
1 d=h=0.75"
2 d=1.5" h=0.75"
3 d=h=1"
4 d=1.5" h=1"
5 d=h=1.25"
6 h=0.75"
1"=25mm
pull-out load (lbs.)
(kN)
10
8
6
4
2
0
ultimate loads
0
1000
2000
3000
4000
5000
6000
7000
f'c (psi)

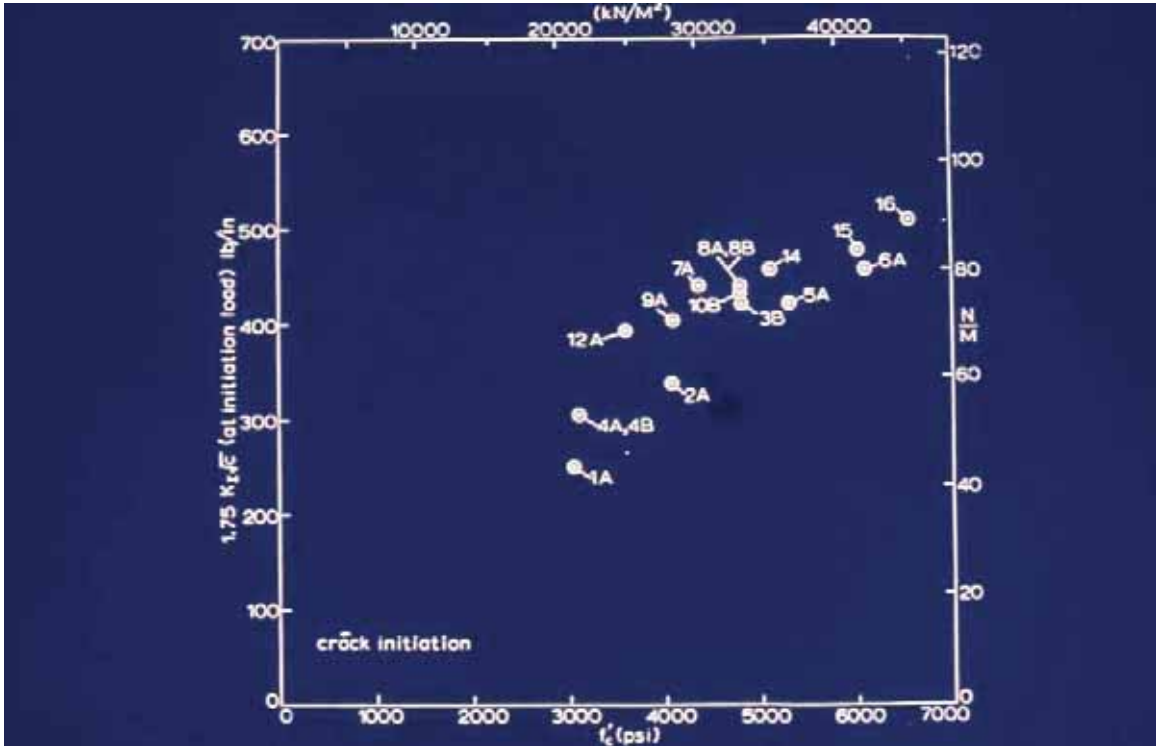
(kN/M²)
10000
20000
30000
40000
700
600
500
400
300
200
100
0
120
100
80
60
40
20
0
N/M
1.75 K_IC (at initiation load) lb/in
16
15
6A
8A,8B
14
7A
5A
9A
10B
3B
12A
2A
4A,4B
1A
crack initiation
0
1000
2000
3000
4000
5000
6000
7000
f'c (psi)

The new code formulas are based on LEFM

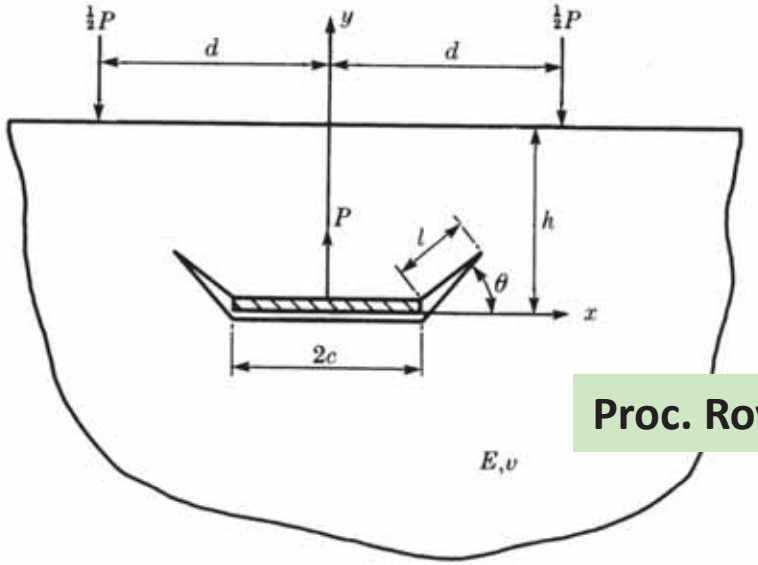

Proc. Royal Society of London, 1986

$$P_{LEFM} \approx K_c d^{3/2} \approx k_c \sqrt{f_c'} d^{3/2}$$

Ballarini *et al.* 1986,1987; Elfgren 1998; Elfgren and Ohlsoon 1992; Eligehausen and Sawade 1989; Eligehausen and Balogh 1995; Eligehausen *et al*. 2006; Fuchs *et al*. 1995; Karihaloo 1996; Krenchel and Shah 1985; Ozbolt et al. 1992,1999; Vogel and Ballarini 1999; Piccinin *et al*. 2010,2012

The pullout test is basically a fracture toughness test; it obeys The strongest size effect (-1/2)

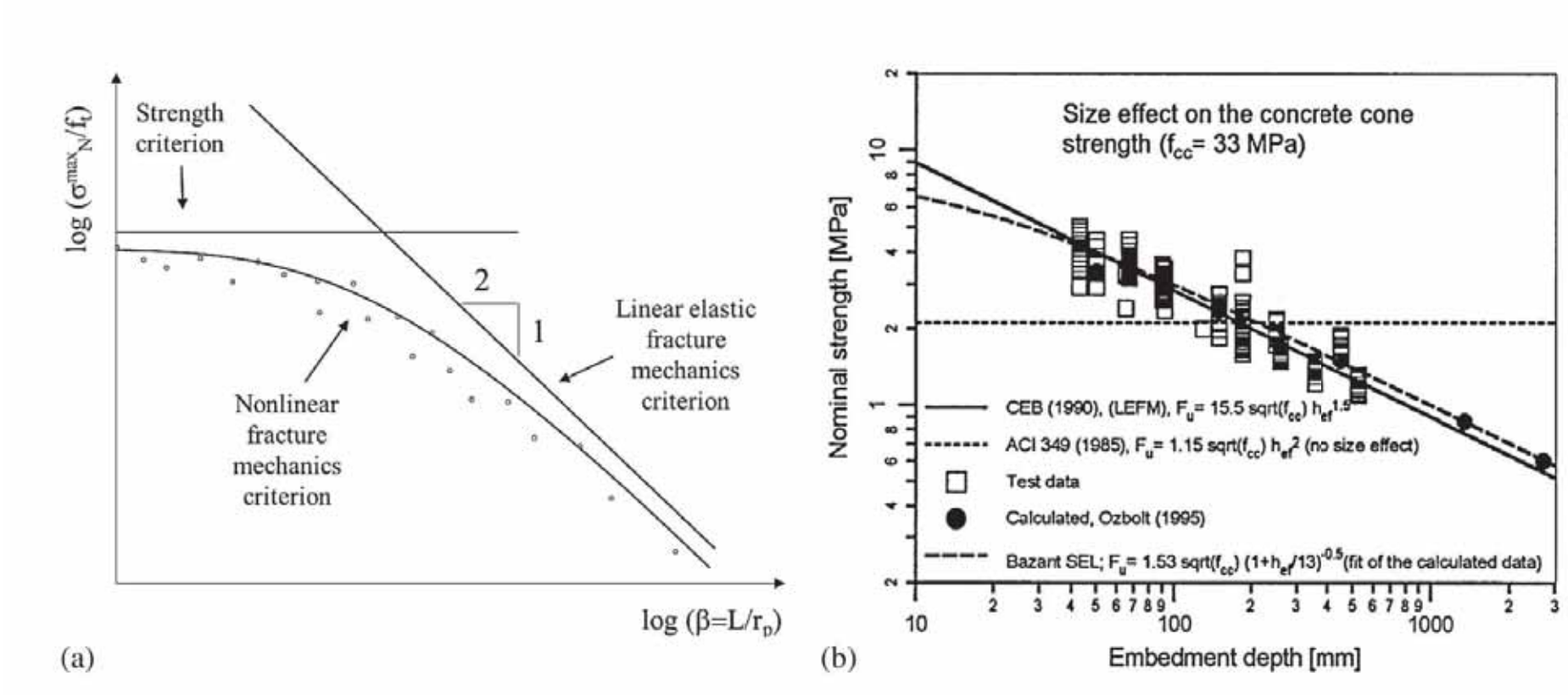


Roberto Piccinin
Now at Hilti, Liechtenstein

Very shallow embedments and with prestress

Experiments

Crack Profiles: *d/c=2*

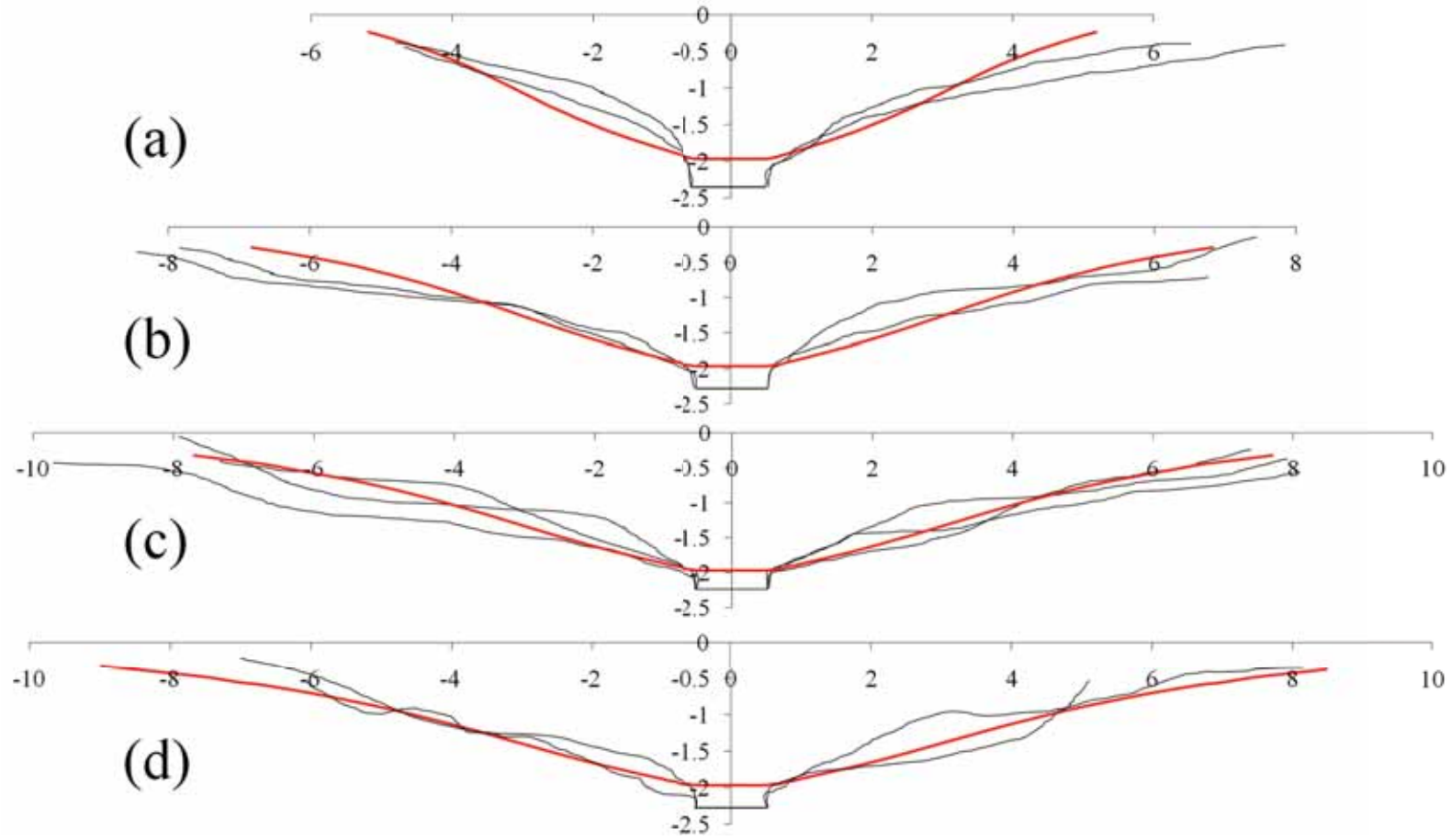

- **Crack profiles obtained from visual inspection;**
- **LEFM captures inclination and shape;**

Group anchors and anchors near free edges

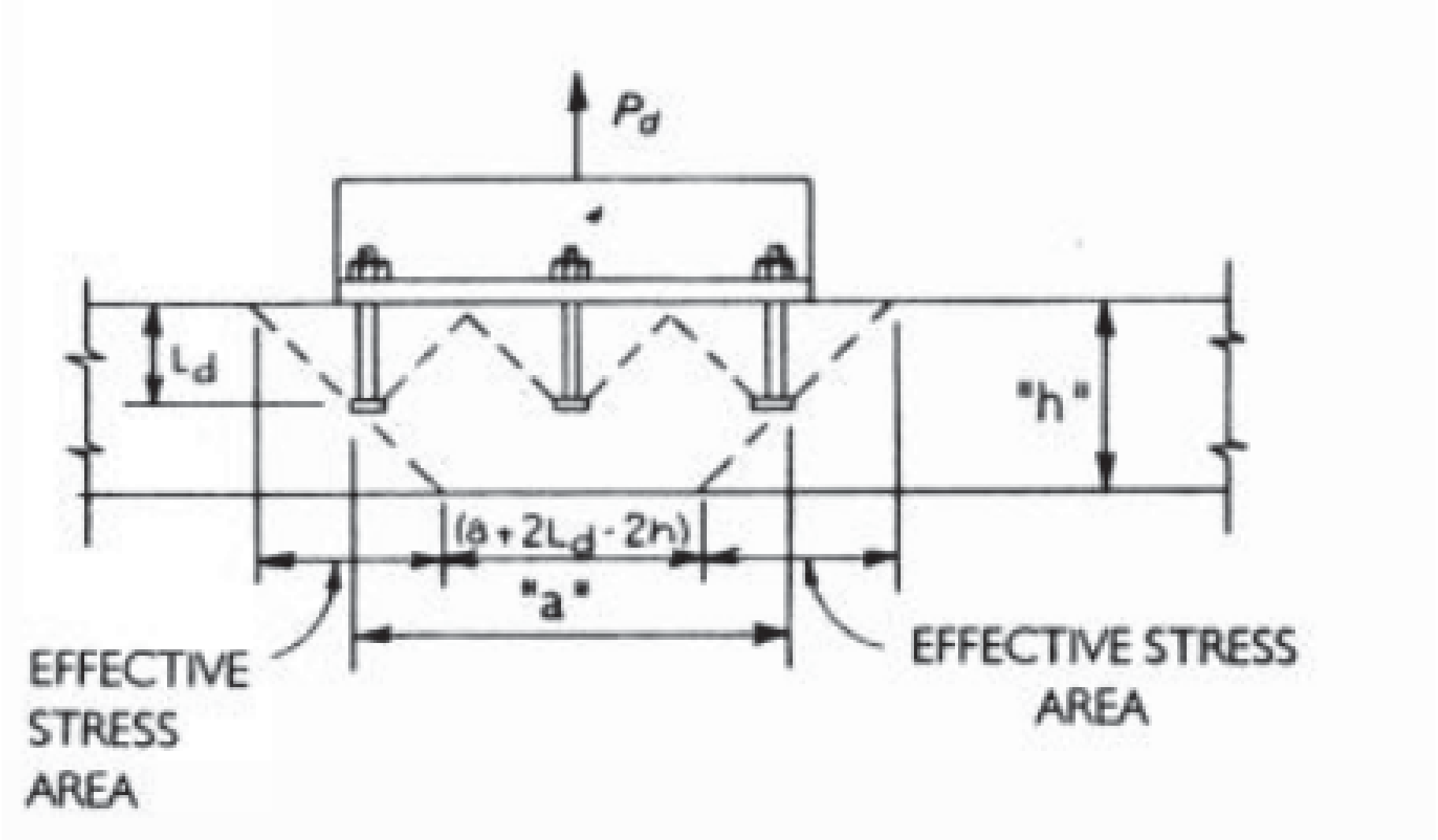

The codes still maintain some of the old approach: for a group, multiply the LEFM formula by:

$$\frac{A_{Nc}}{A_{Nco}}$$

The ratio of the projected areas of the break out cone associated with a group of *N* anchors and an isolated anchor, respectively does not correctly reflect the edge effects. It is overly conservative.

The Commentary then continues with modifications to the design formulas that reduce the conservatism in the design, with certain restrictions.

Toy problem showing this is incorrect

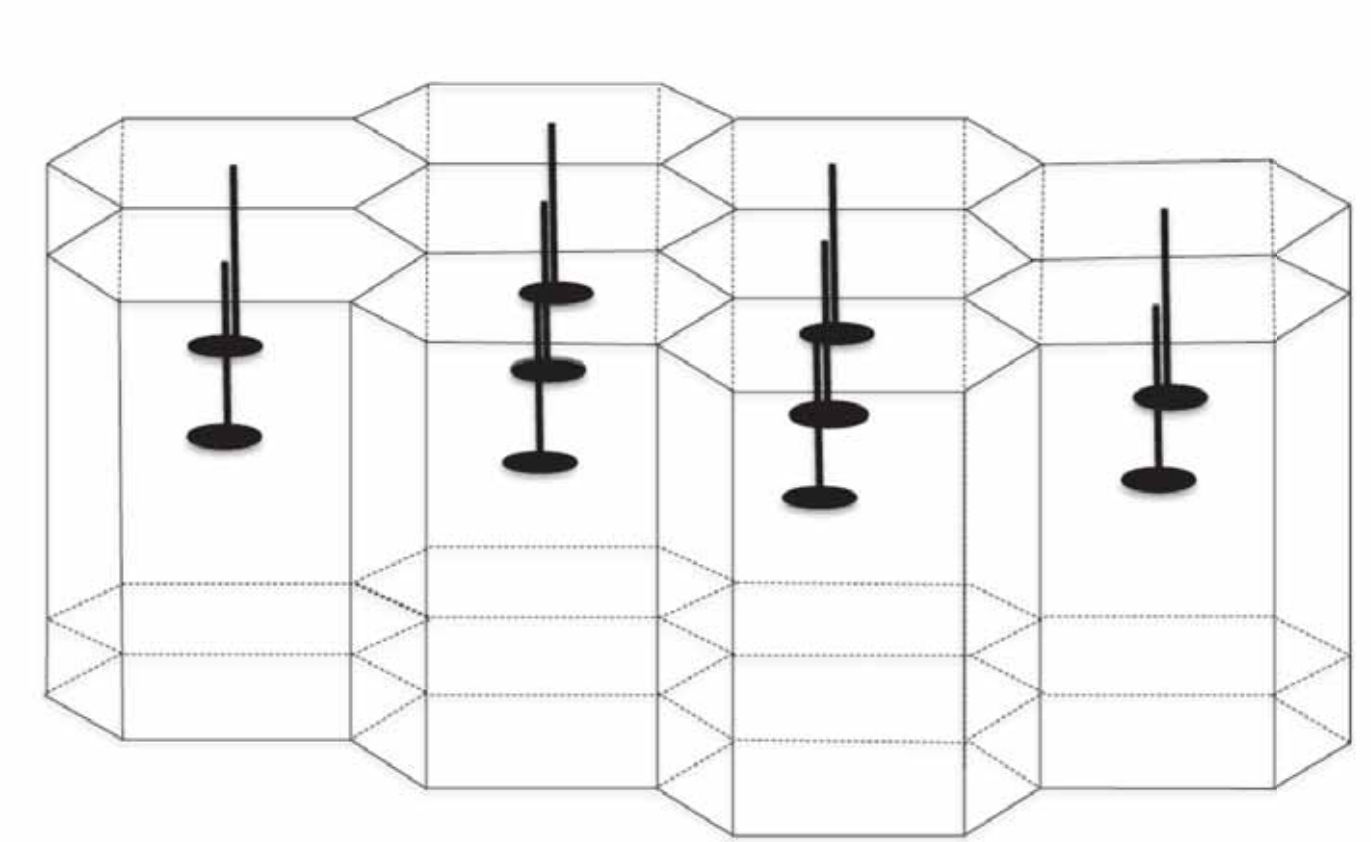

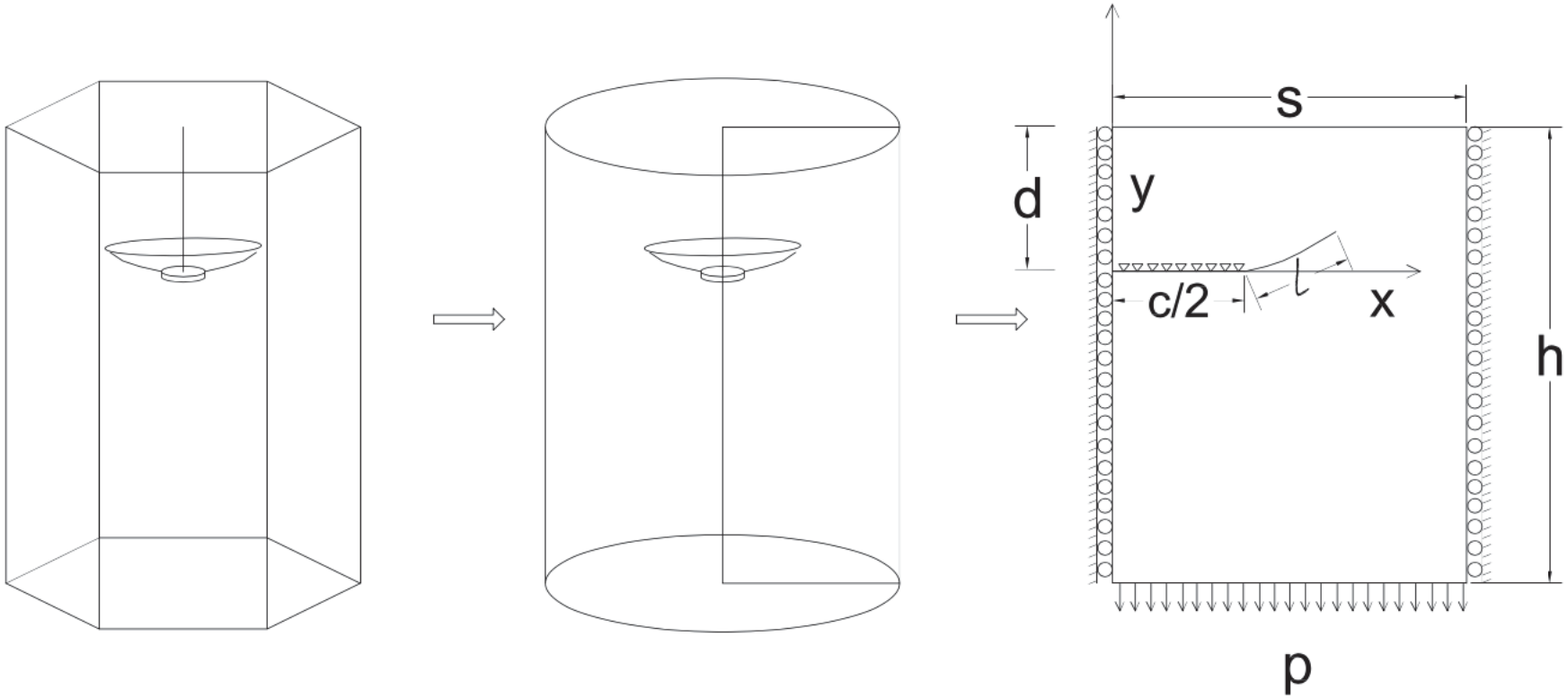
s
d
y
c/2
x
h
p

$$K_{Ic} = P_c d^{-3/2} f\left(\frac{l}{c}, \frac{d}{c}, \frac{s}{d}, \upsilon\right)$$

$$\frac{P_c}{K_{Ic} d^{3/2}} \equiv g = \min\left[1/f\right]$$

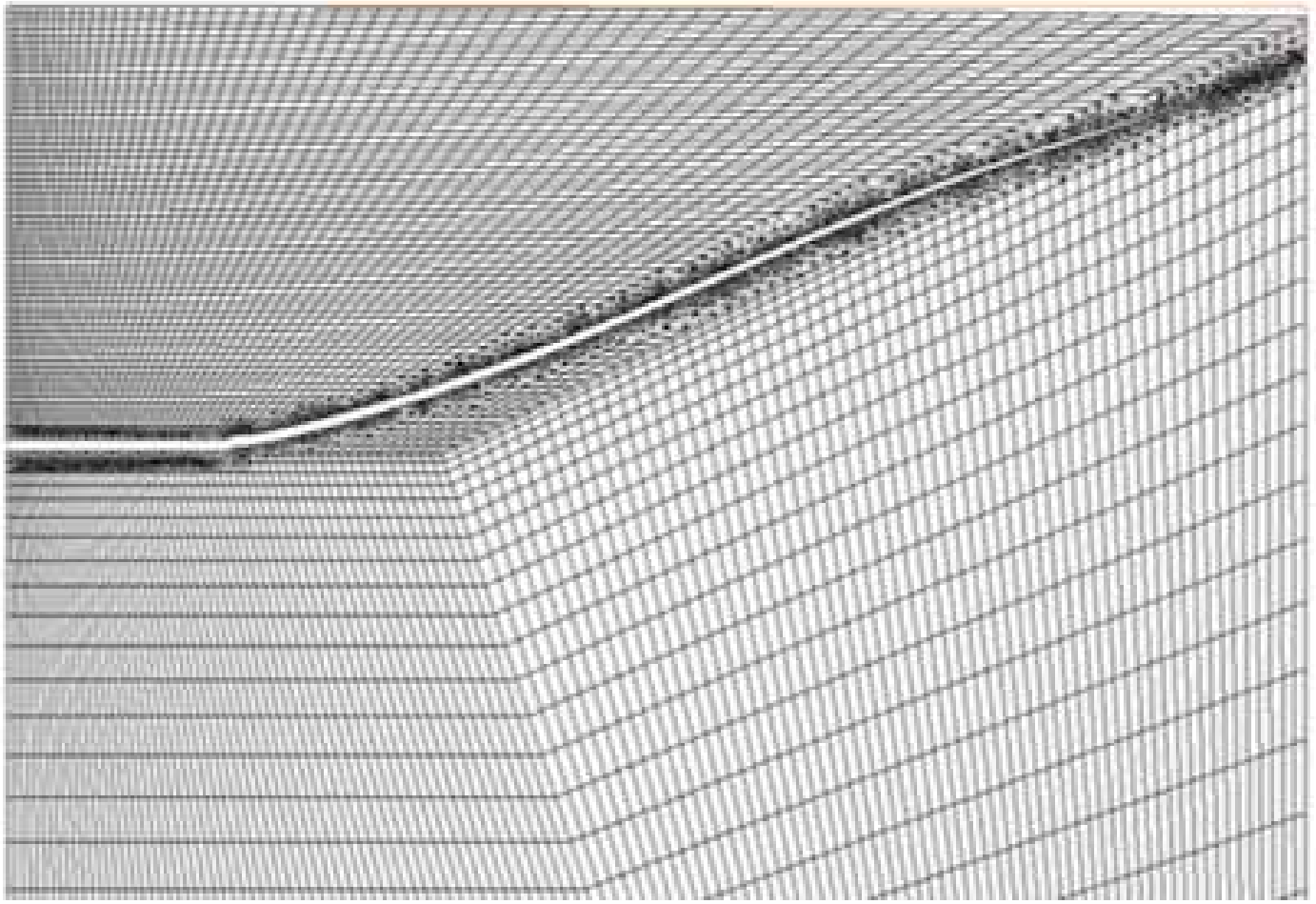

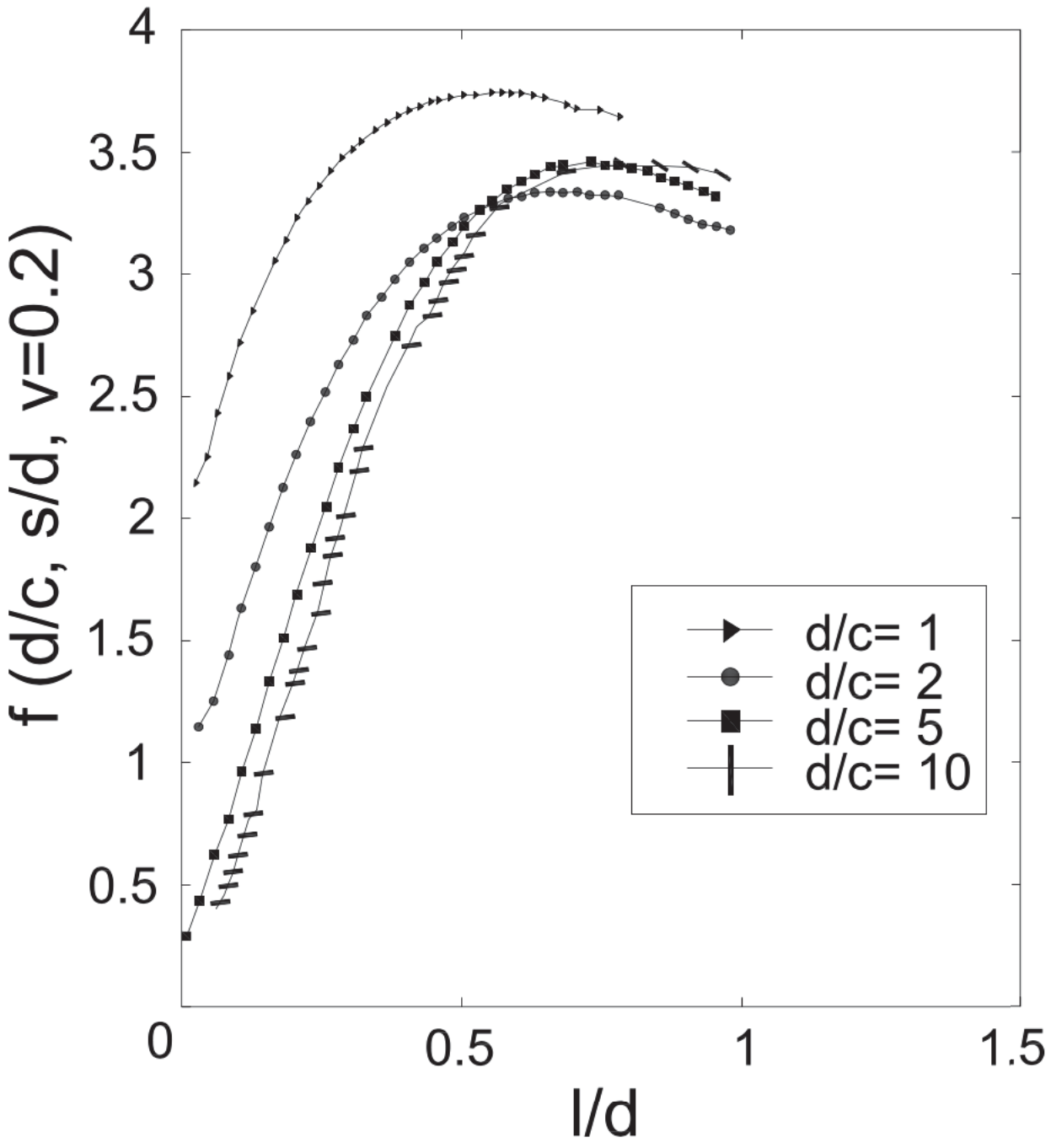
4
3.5
3
2.5
2
1.5
1
0.5
0
0.5
1
1.5
f (d/c, s/d, v=0.2)
l/d
d/c= 1
d/c= 2
d/c= 5
d/c= 10

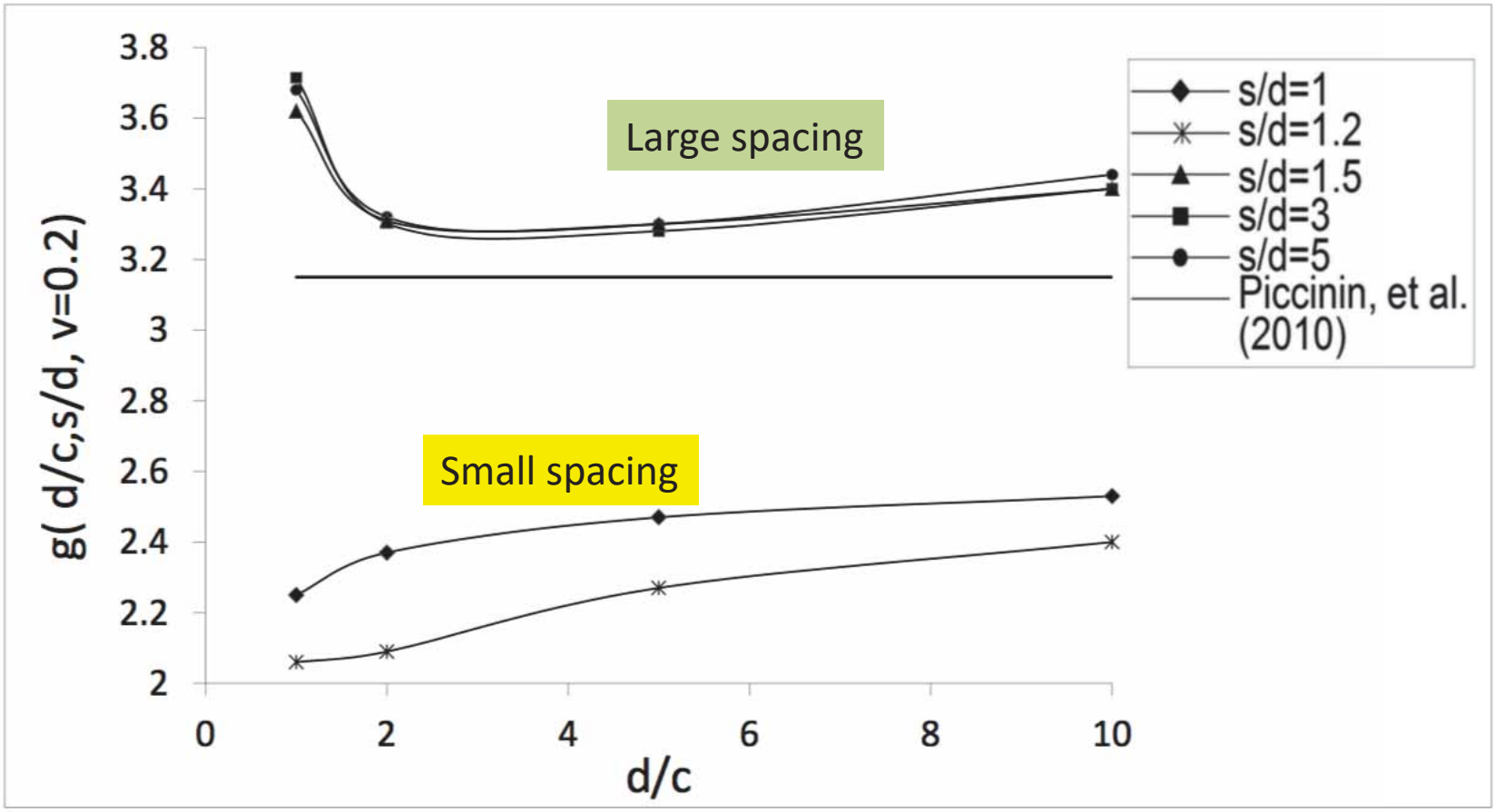
Large spacing
Small spacing
s/d=1
s/d=1.2
s/d=1.5
s/d=3
s/d=5
Piccinin, et al. (2010)
g(d/c,s/d, v=0.2)
d/c
3.8
3.6
3.4
3.2
3
2.8
2.6
2.4
2.2
2
0
2
4
6
8
10

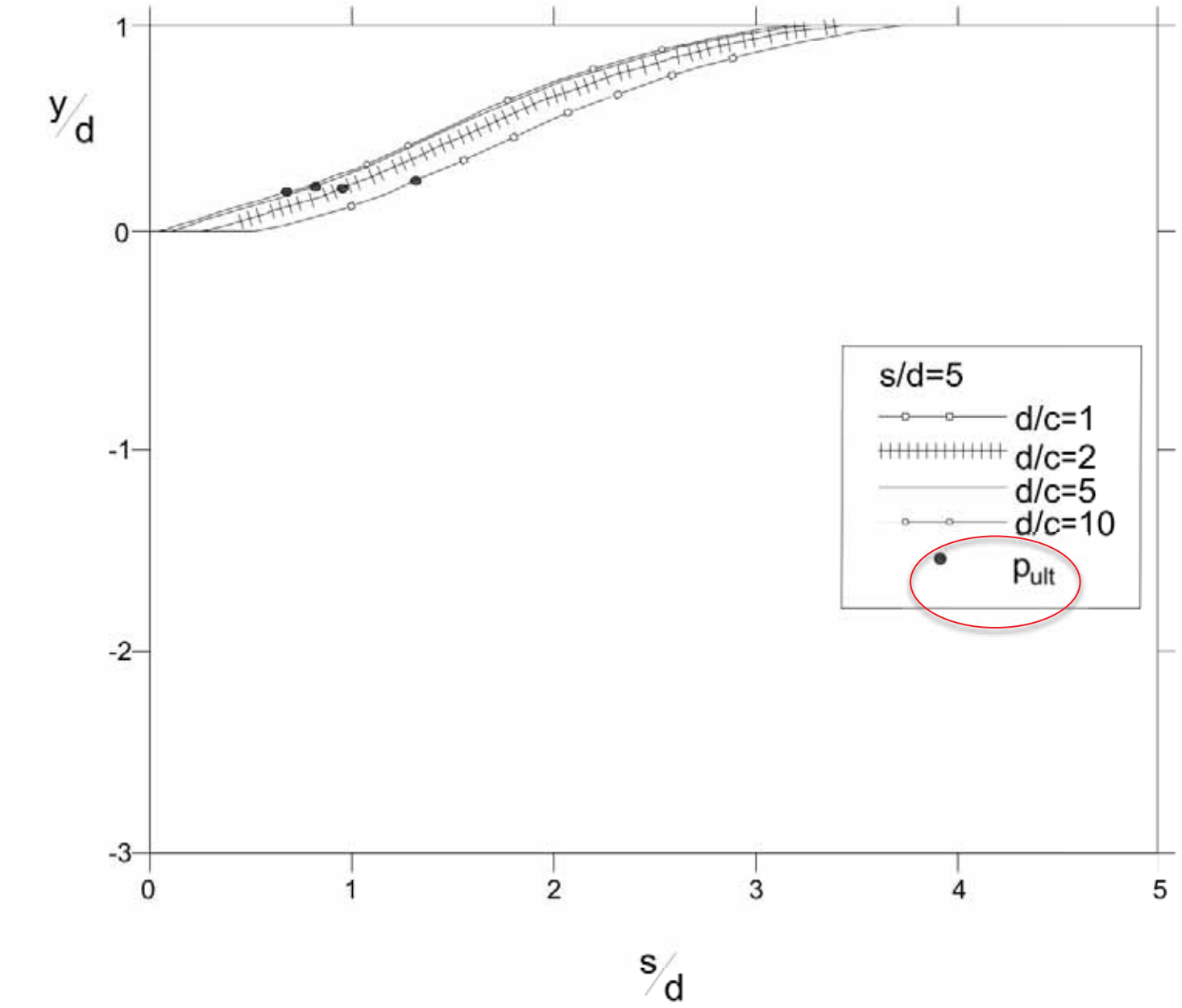
1
0
-1
-2
-3
y/d
0
1
2
3
4
5
s/d
s/d=5
d/c=1
d/c=2
d/c=5
d/c=10
p_ult

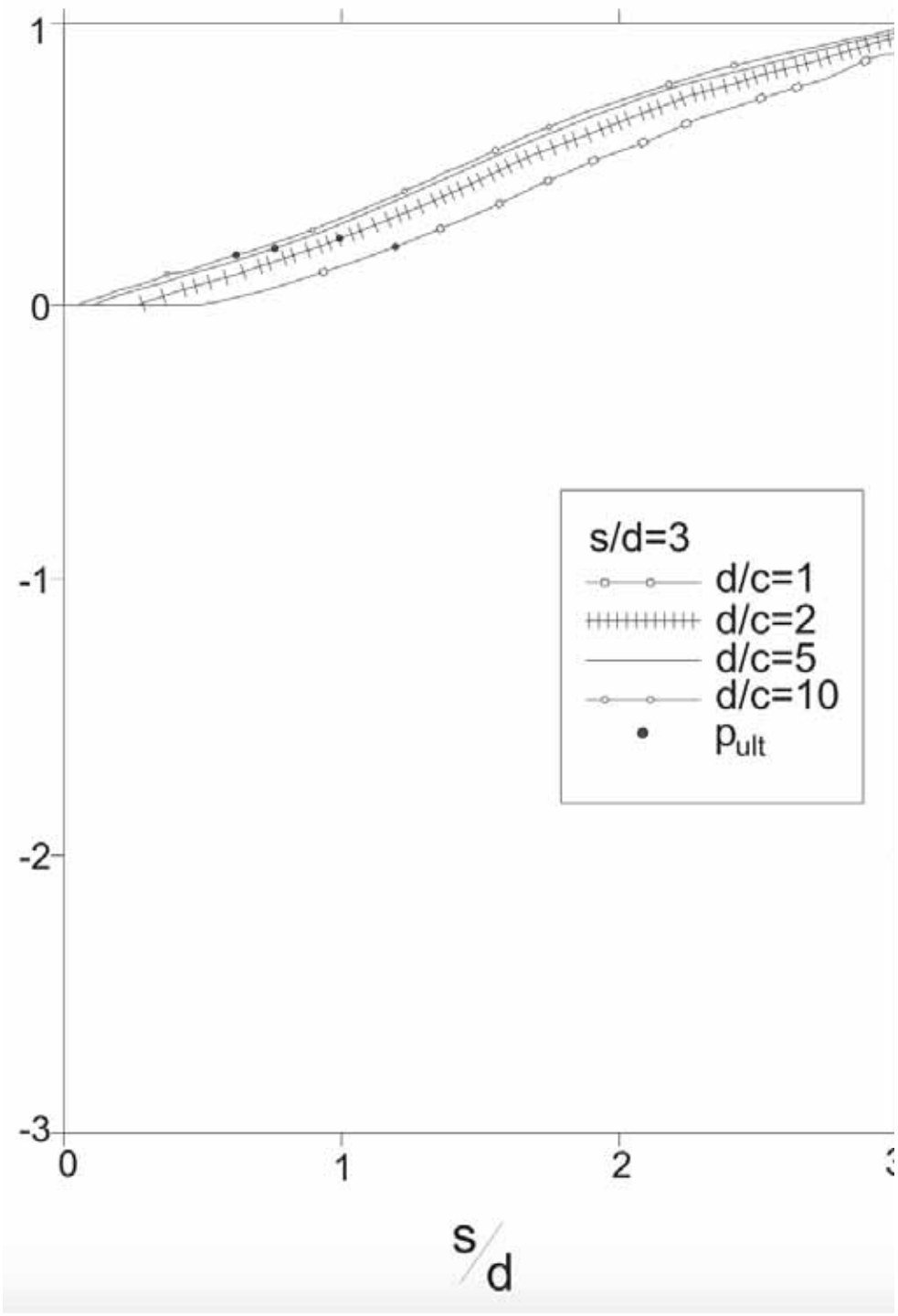
1
0
-1
-2
-3
0
1
2
s/d
s/d=3
d/c=1
d/c=2
d/c=5
d/c=10
p_ult

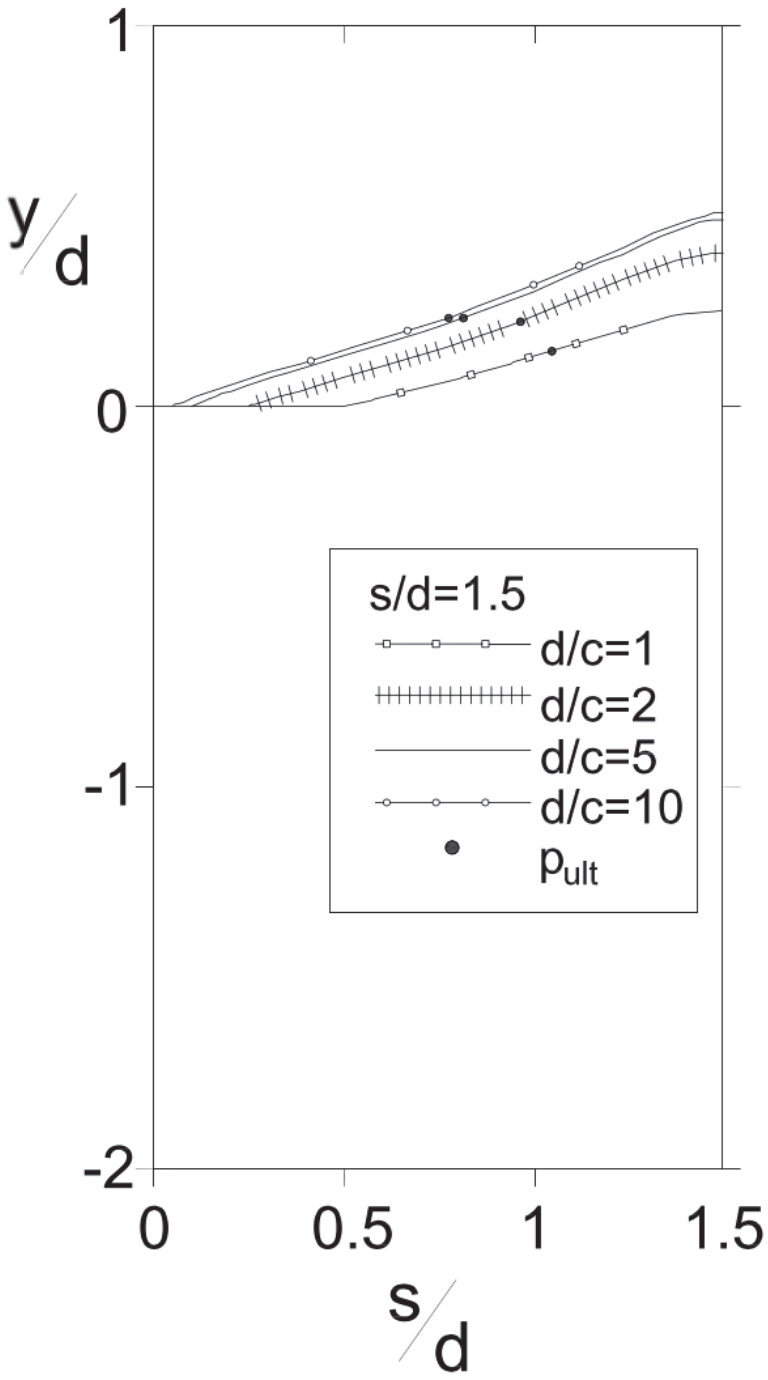
1
0
-1
-2
y/d
0
0.5
1
1.5
s/d
s/d=1.5
d/c=1
d/c=2
d/c=5
d/c=10
p_ult

$$A_{Nc} = \left[(\sqrt{N} - 1)s + 3h_{ef}\right]^2$$

$$\frac{P_{ult,N}}{NP_{ult,o}} = \frac{\left[(\sqrt{N-1})\,\frac{s}{3h_{ef}} + 1\right]^2}{N}$$

$$\text{setting } N = \infty$$

$$\frac{P_{ult,N=\infty}}{NP_{ult,o}} = \left(\frac{s}{3d}\right)^2$$

s/d=5,3,1.5,1.2,1.0 the capacity ratios are 1.0, 1.0, 0.25, 0.16 and 0.11, respectively (for *s/d=5* and *s/d*=1 the Code considers the anchors as non-interacting). The 75-90% range of the reduction prescribed by the Code is significantly larger than the ~20-30% reduction predicted by the simulations.

Suggestion

With the advent of powerful and sophisticated computational approaches to fracture simulation, derive capacity formulas through simulation.

Background

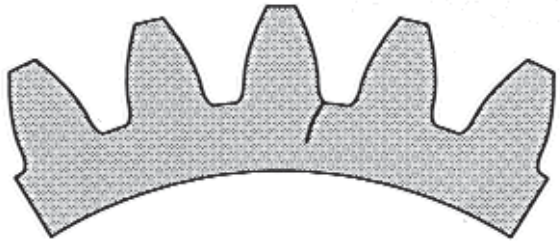

Thin rim -
catastrophic rim fracture

Thick rim -
“benign” tooth fracture

- Thin-rim gears desired for reduced weight.
- Stress fields and failure characteristics significantly different for thin-rim gears compared to conventional gears.
- Catastrophic failures have occurred in thin-rim gears.
- Safety and reliability can not be sacrificed.

Definition of Backup Ratio (m_B)

$$m_B = \frac{b}{h}$$

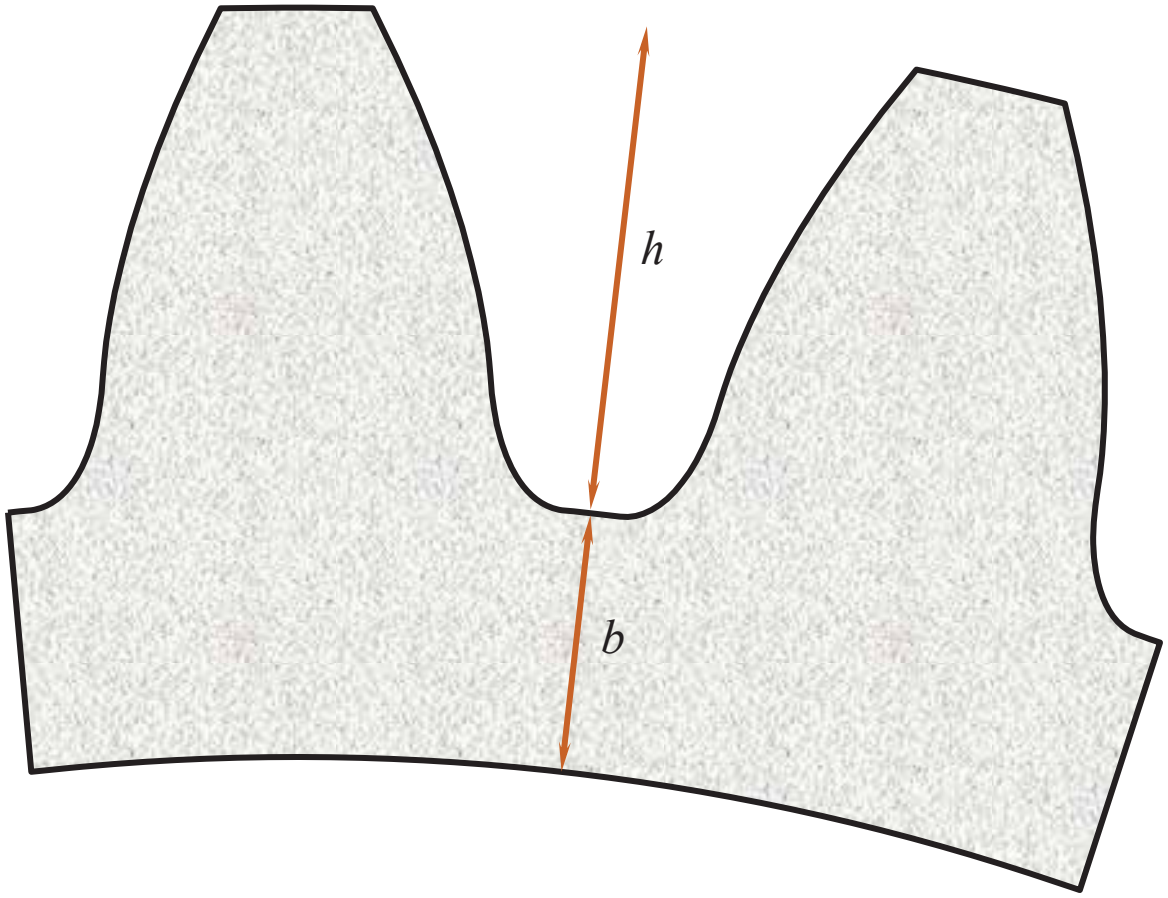

Bending stress index

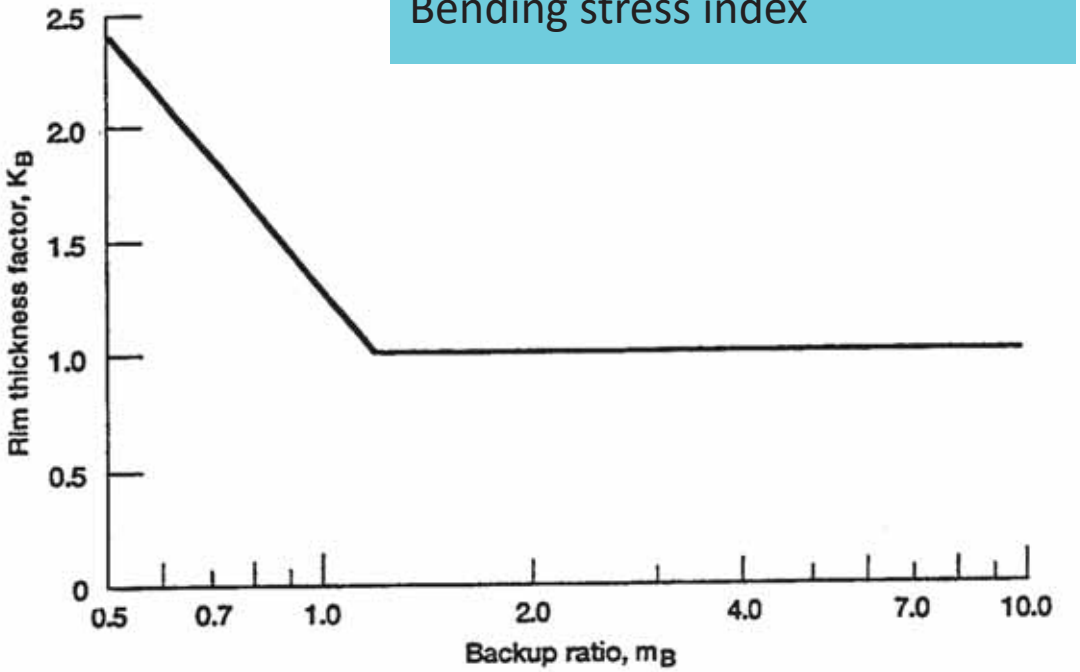

Figure 1.2.1.—Gear tooth bending stress index rim thickness correction factor (AGMA, 1990).

Objectives

Develop design guidelines to prevent rim fracture failure modes in gear tooth bending fatigue.

Crack Modeling Using Finite Element Method

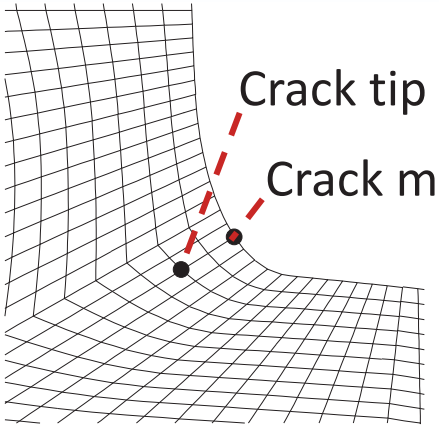

User-defined initial crack

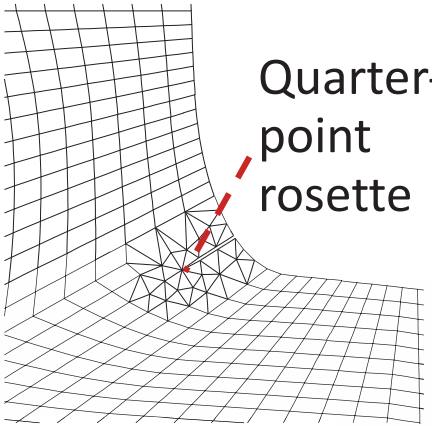

Final mesh of initial crack

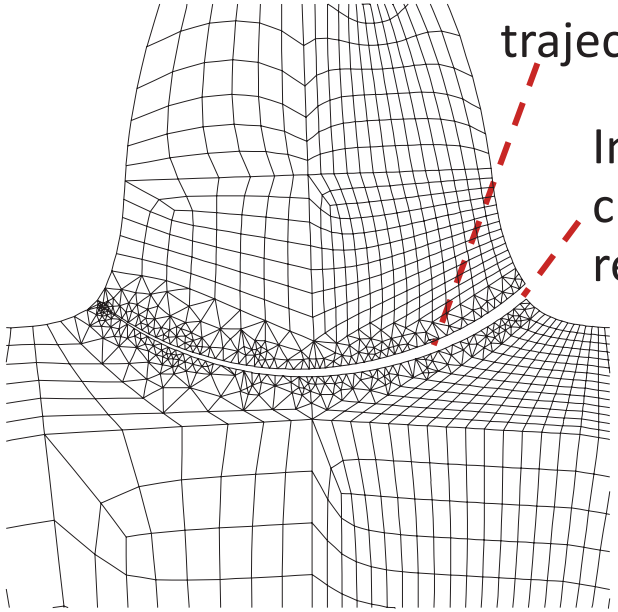

Predicted crack path

Crack Propagation Angle and Growth Rate

$$\theta_m = 2\tan^{-1}\left[\frac{\frac{K_I}{K_{II}} \pm \sqrt{\left(\frac{K_I}{K_{II}}\right)^2 + 8}}{4}\right]$$

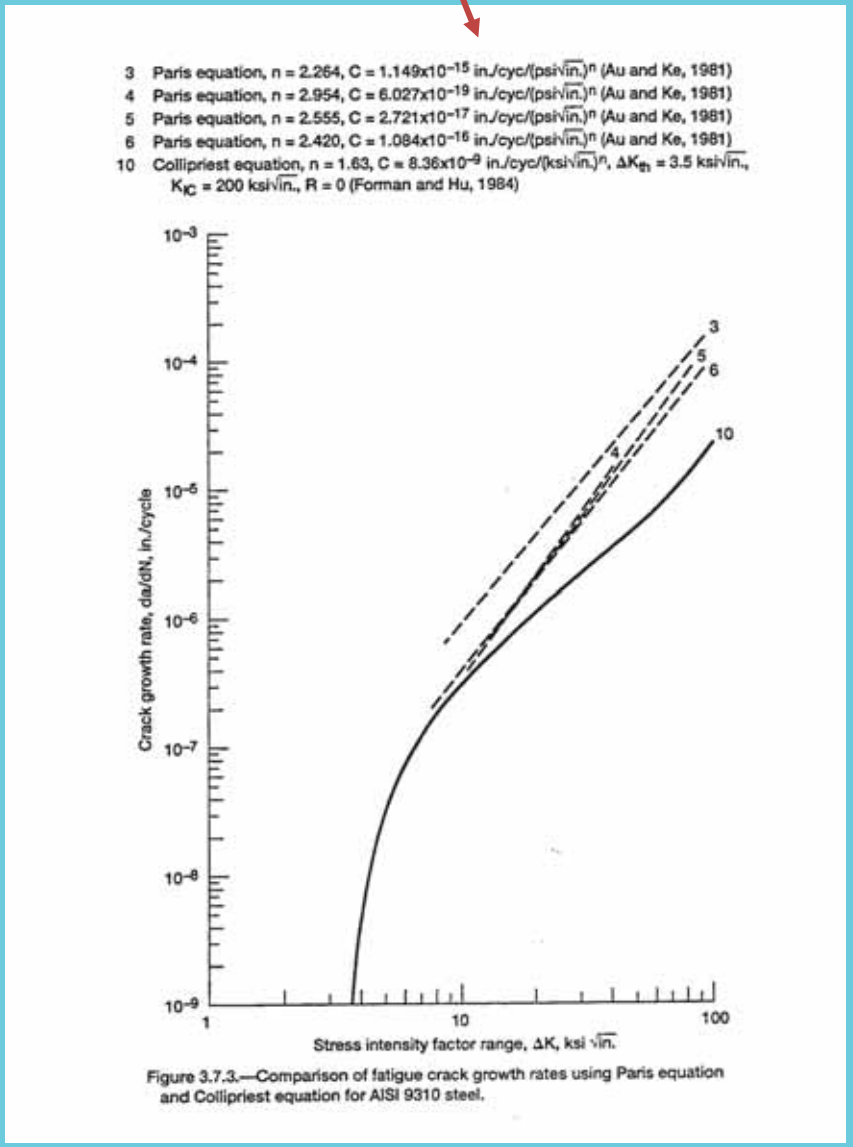

Figure 3.7.3.—Comparison of fatigue crack growth rates using Paris equation and Collipriest equation for AISI 9310 steel.

Analysis Procedure

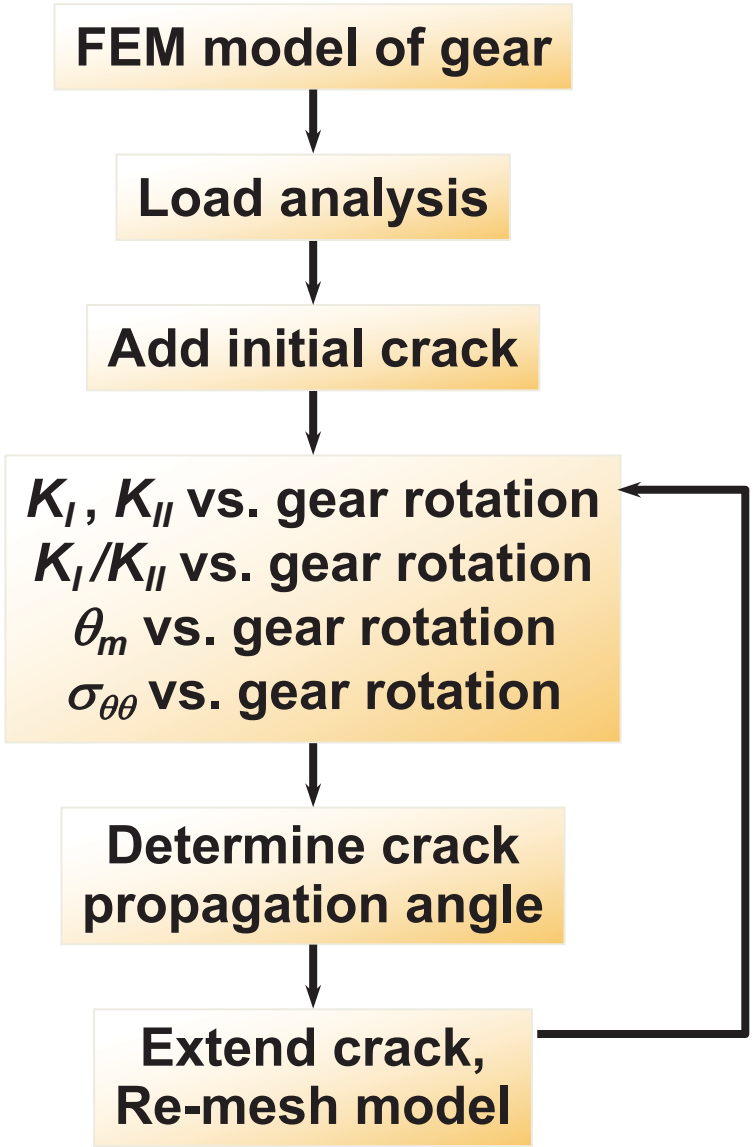

Typical Finite Element Gear Model

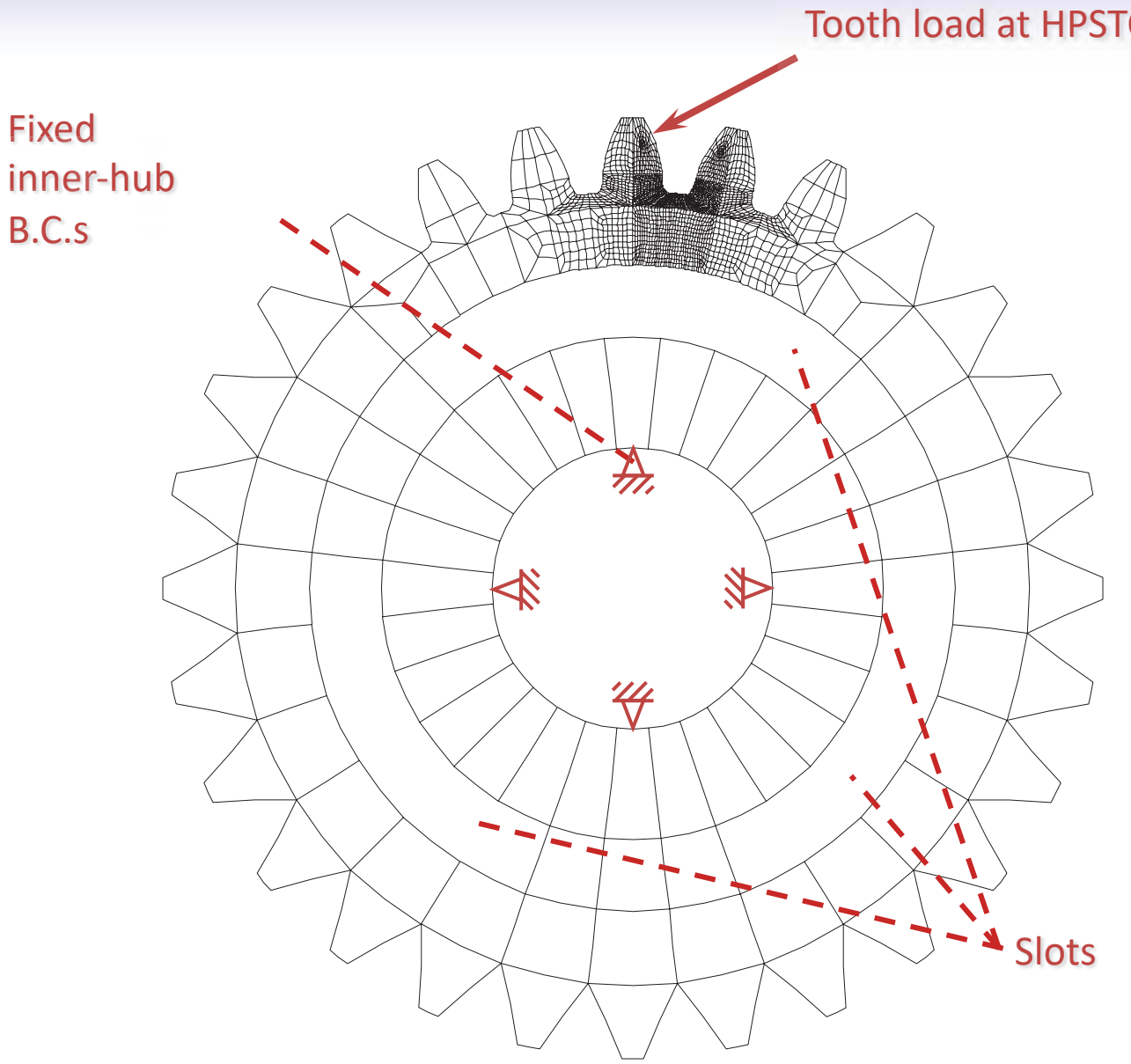

Load Case Locations for FEM

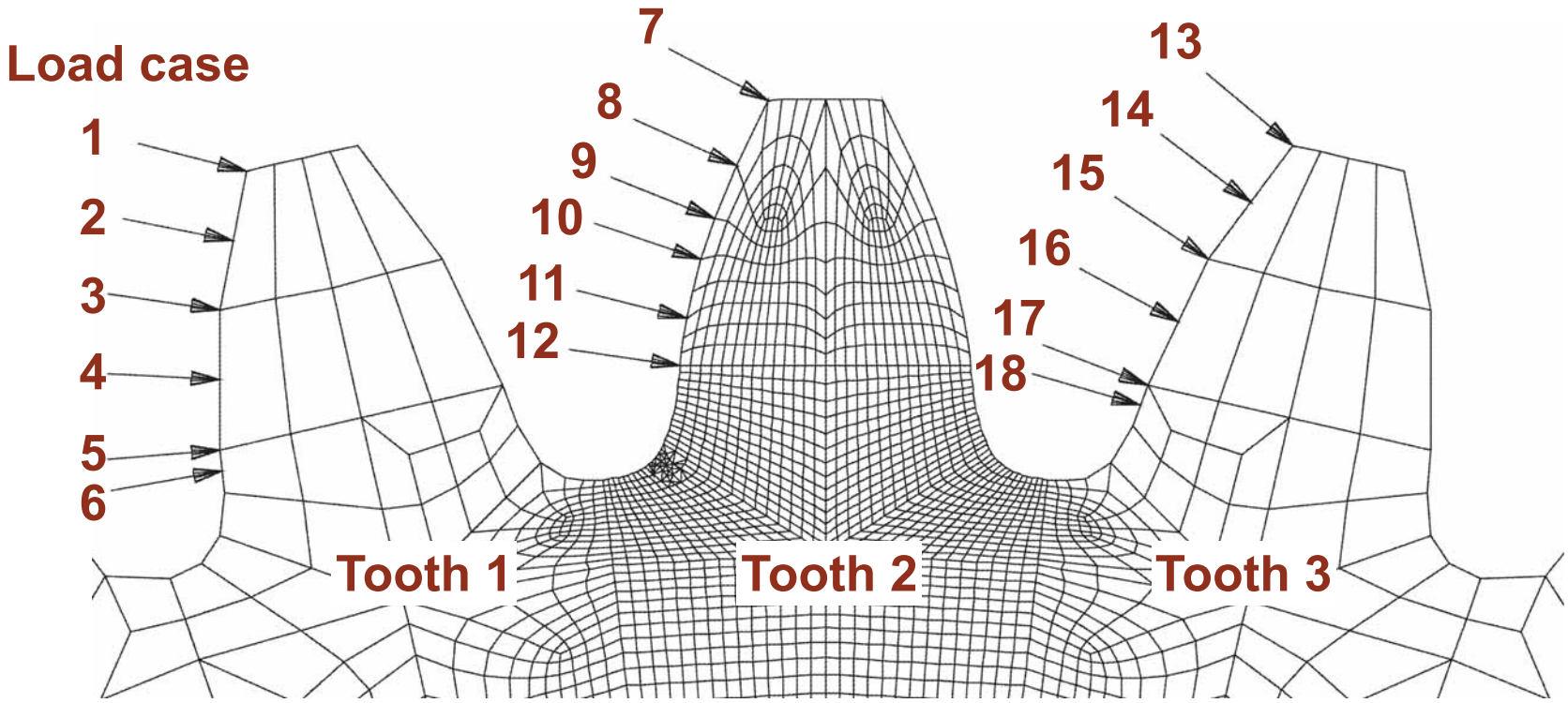

0.26-mm crack size, 68 N-m driver gear torque.

Test Gears

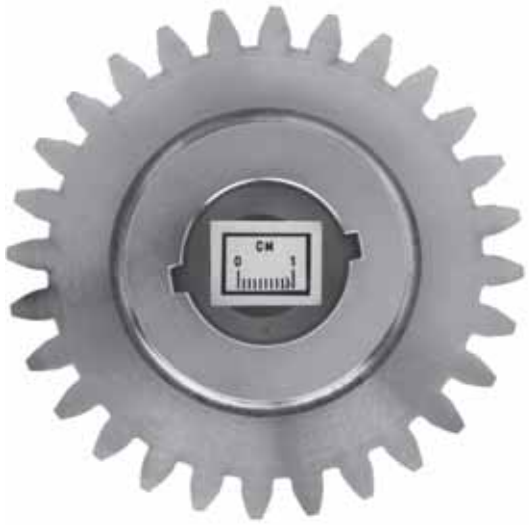

Backup ratio = 3.3

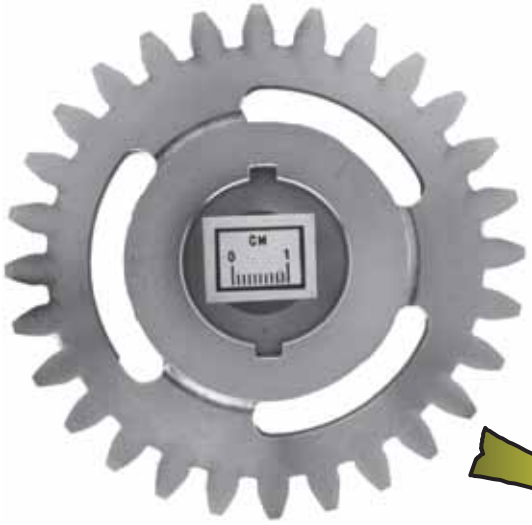

Backup ratio = 1.0

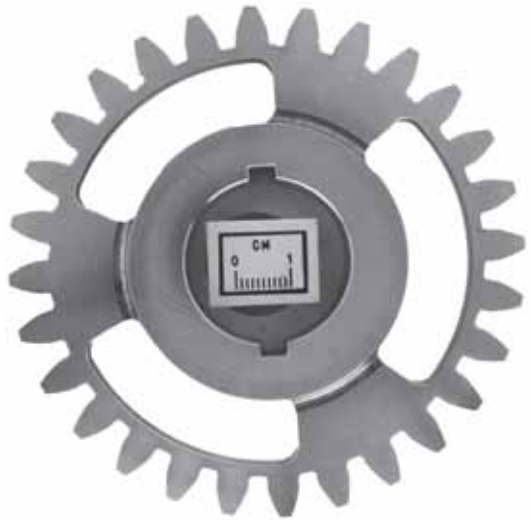

Backup ratio = 0.3

Notch inserted
in tooth fillet

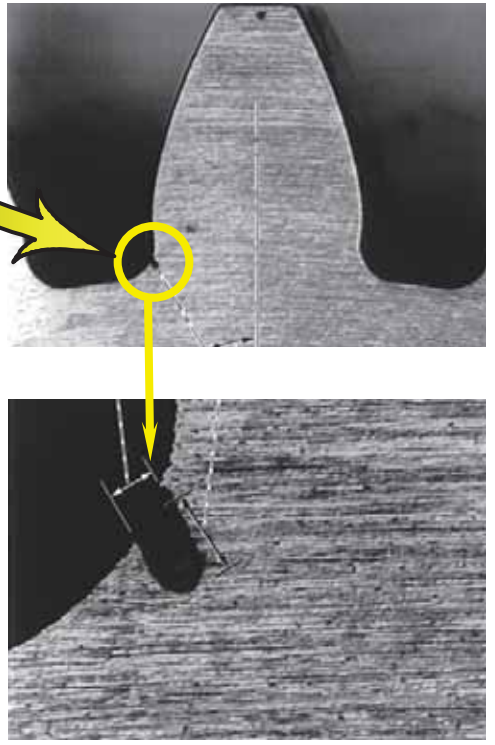

Definition of Backup Ratio (m_B)

$$m_B = \frac{b}{h}$$

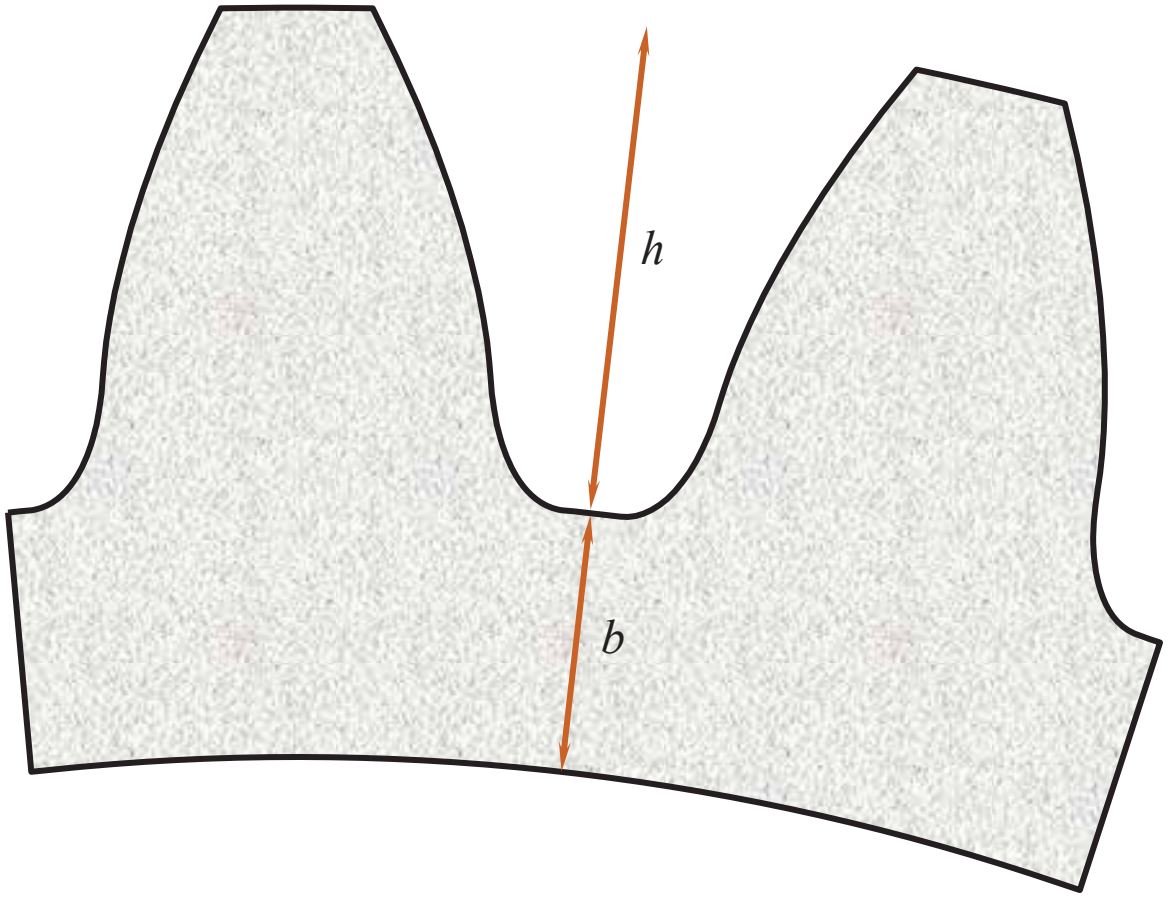

Definition of Initial Crack Location (θ_0)

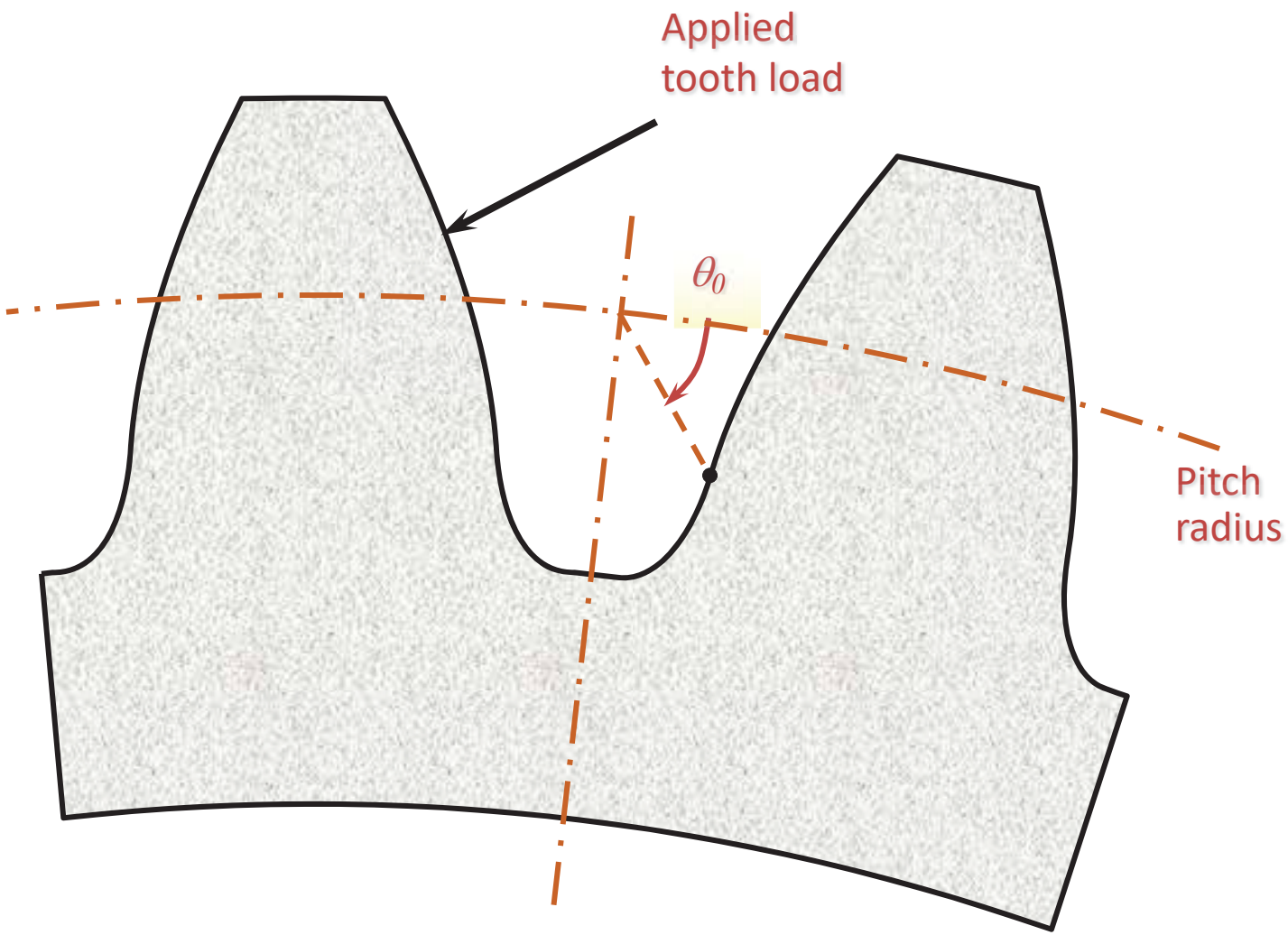

Effect of Initial Crack Location on Crack Path

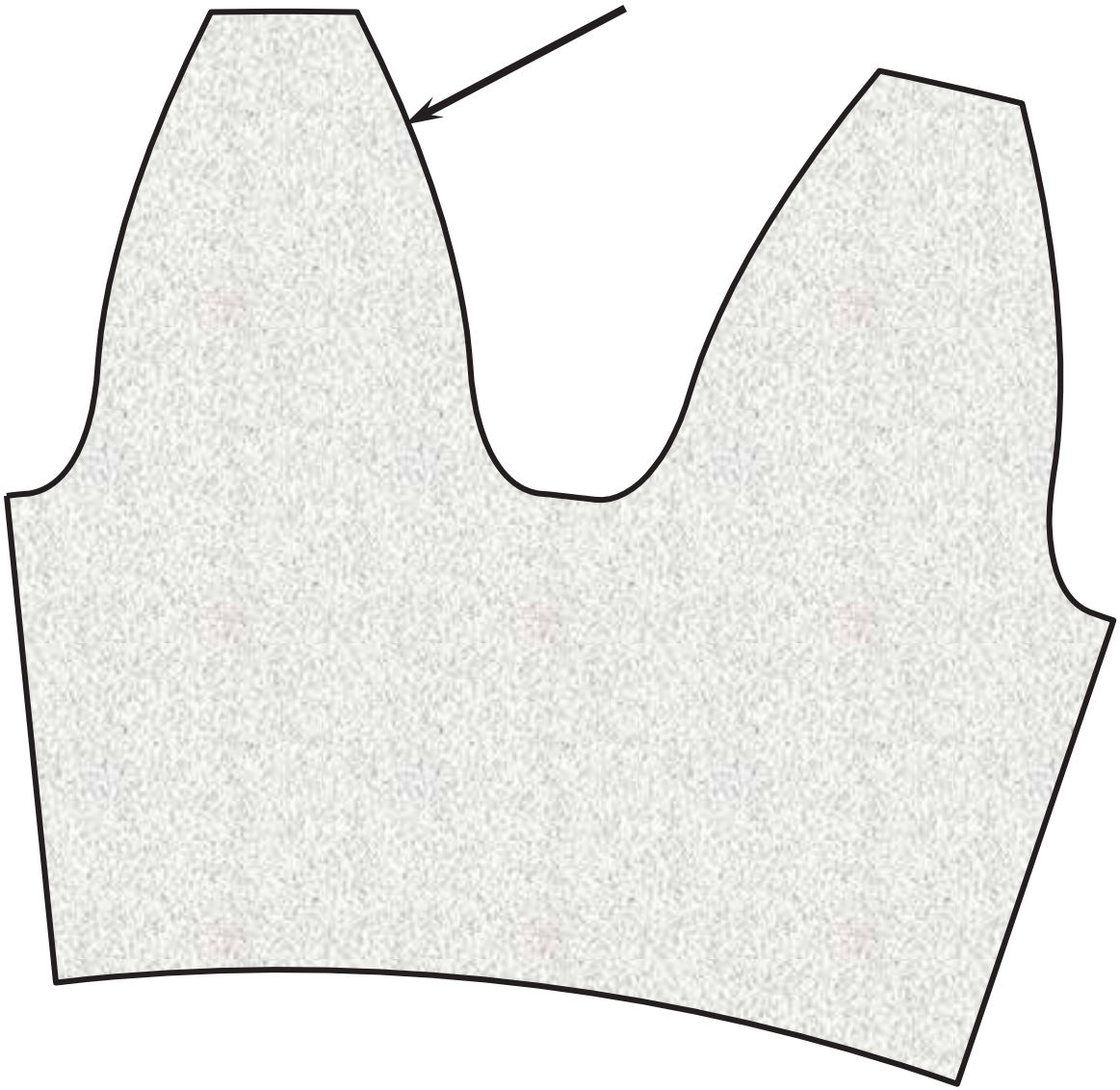

Gear Parameters:

- 28 teeth
- 8 pitch
- 1.75" pitch rad
- 20° press angle
- m_B = 1.0

Effect of Initial Crack Location on Crack Path

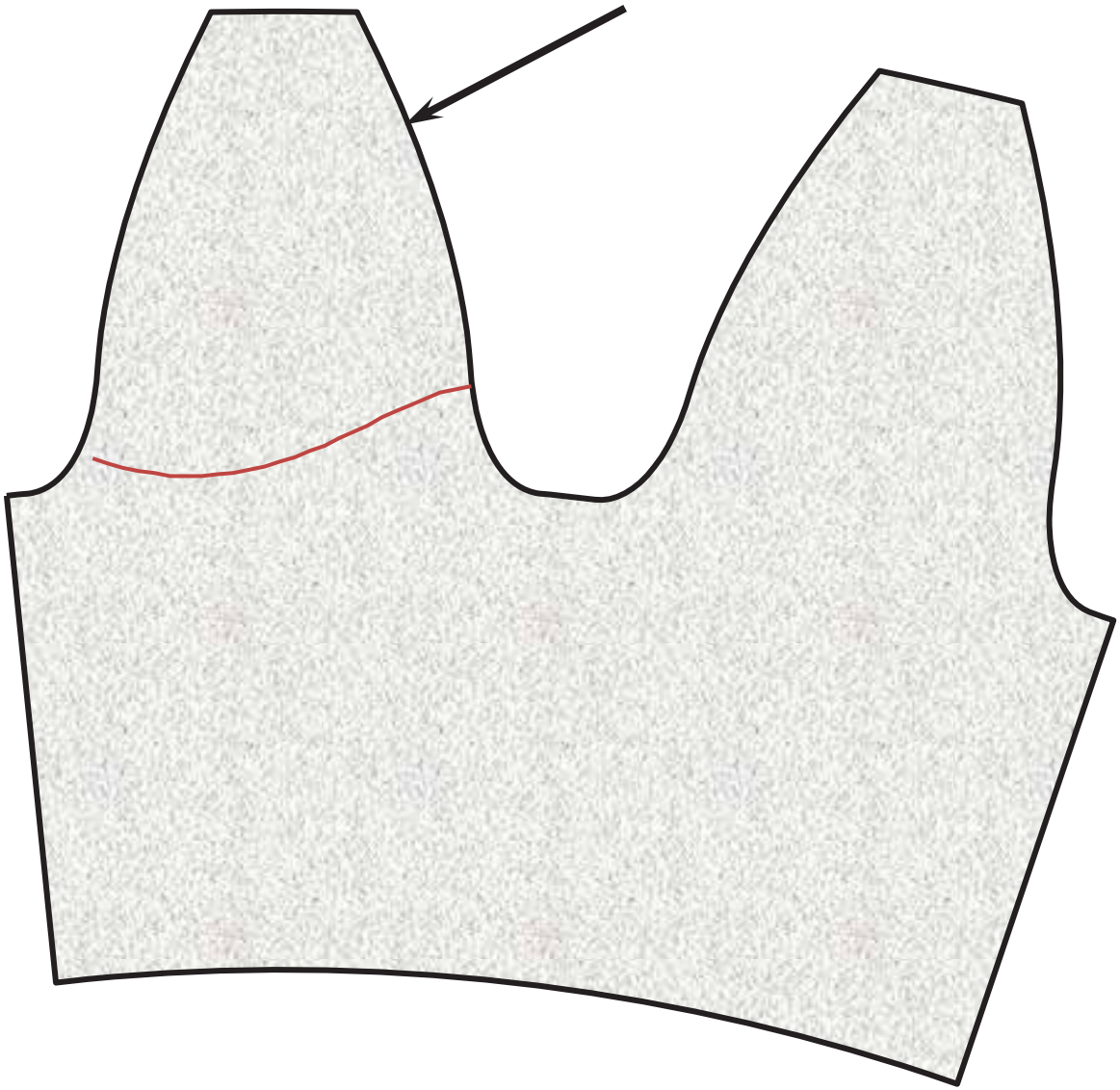

Initial crack location:

$\theta_0 = 120^\circ$

Failure mode:

Tooth fracture

Effect of Initial Crack Location on Crack Path

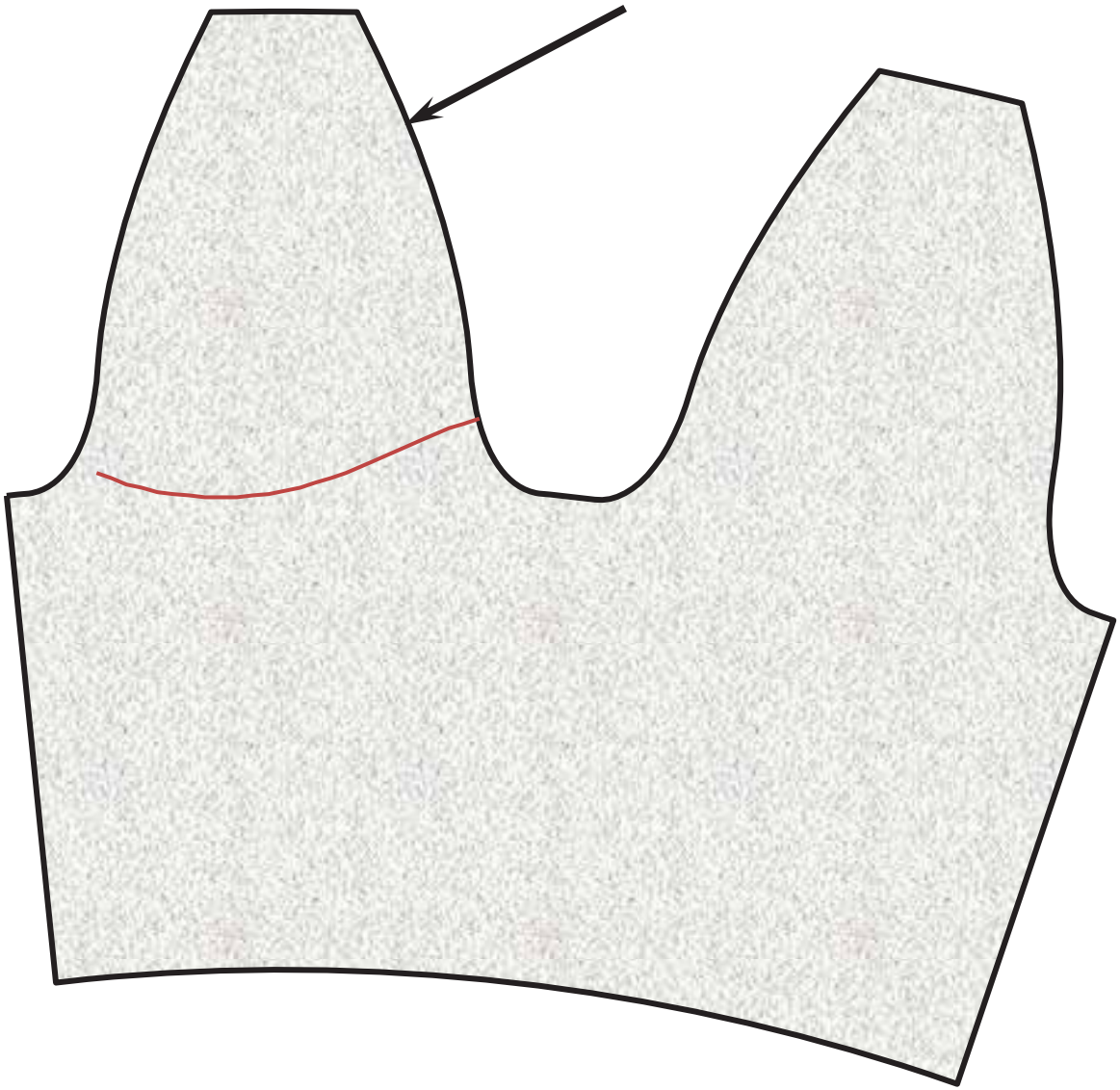

Initial crack location:

$\theta_0 = 114^\circ$

Failure mode:

Tooth fracture

Effect of Initial Crack Location on Crack Path

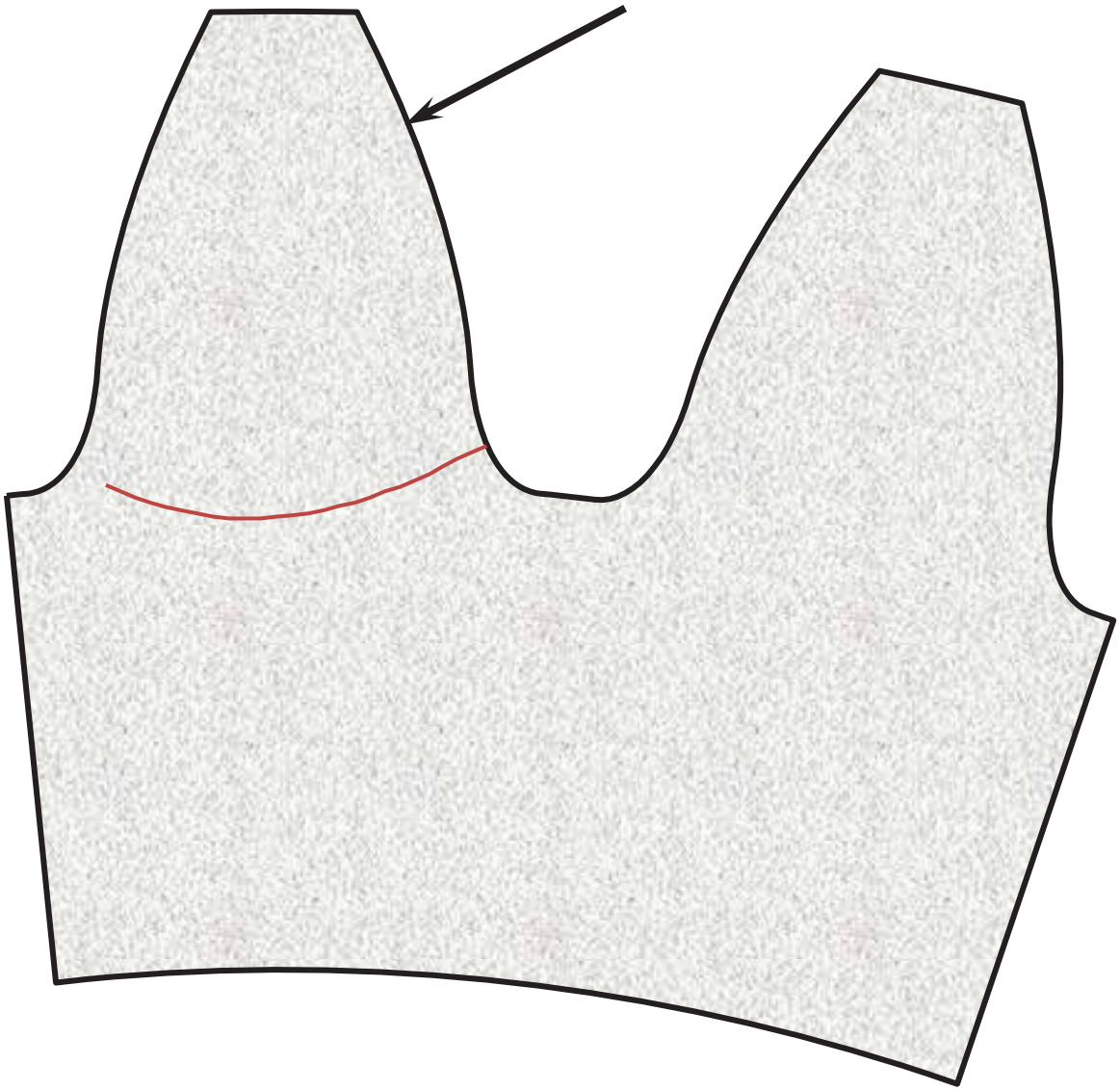

Initial crack location:

$\theta_0 = 109^\circ$

Failure mode:

Tooth fracture

Effect of Initial Crack Location on Crack Path

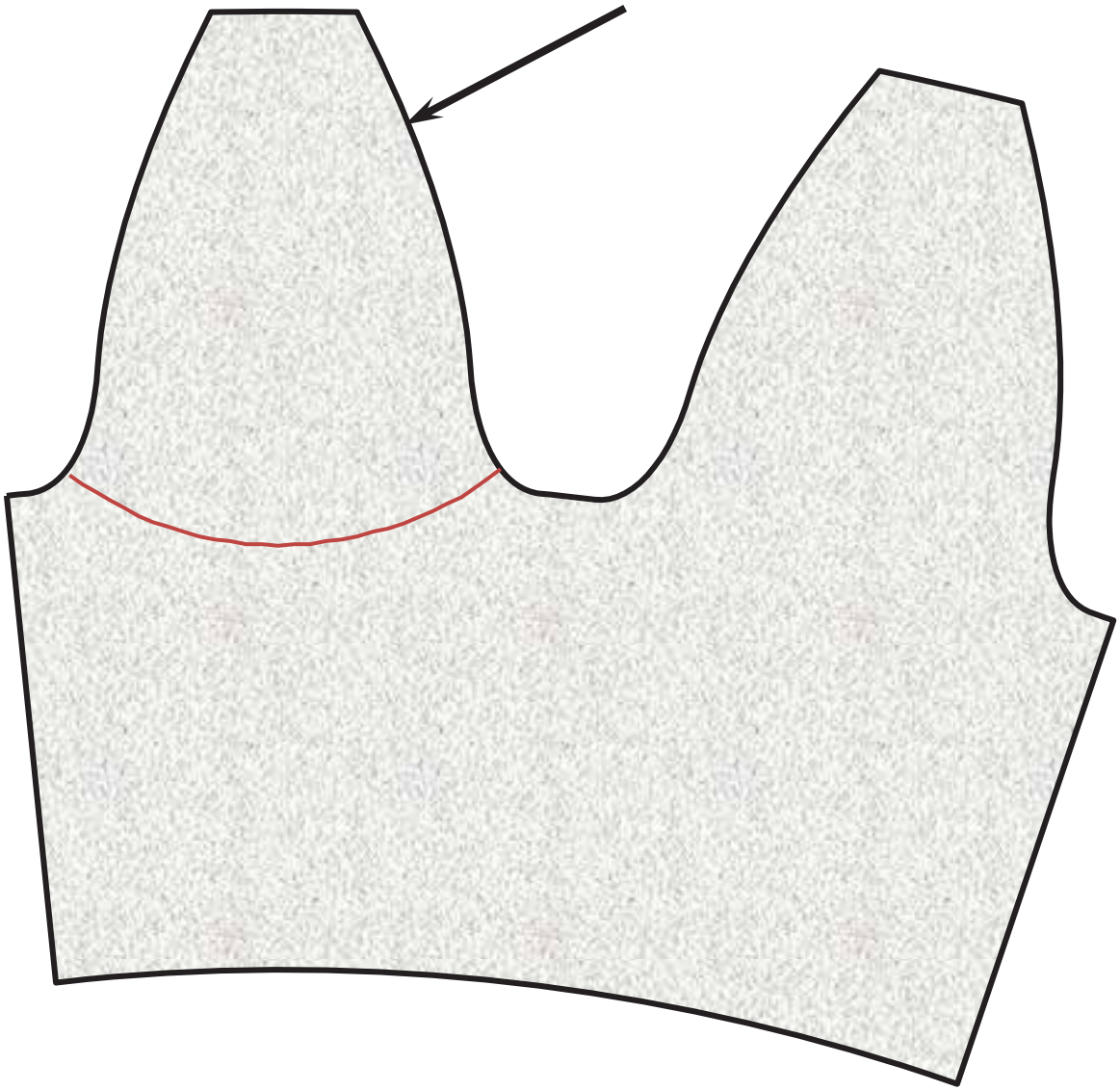

Initial crack location:

θ_0 = 104°

(max tensile)

Failure mode:

Tooth fracture

Effect of Initial Crack Location on Crack Path

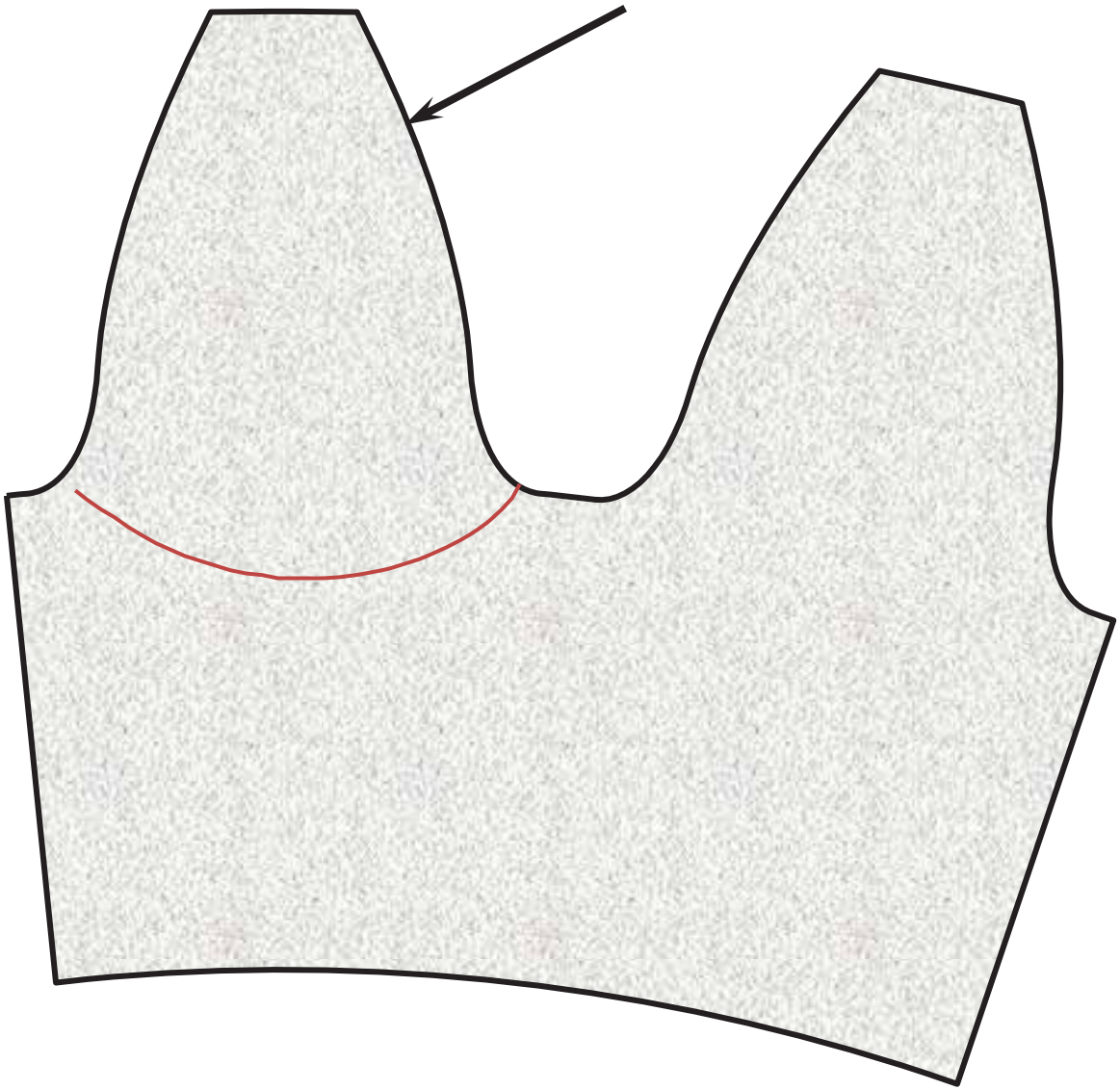

Initial crack location:

$\theta_0 = 99°$

Failure mode:

Tooth fracture

Effect of Initial Crack Location on Crack Path

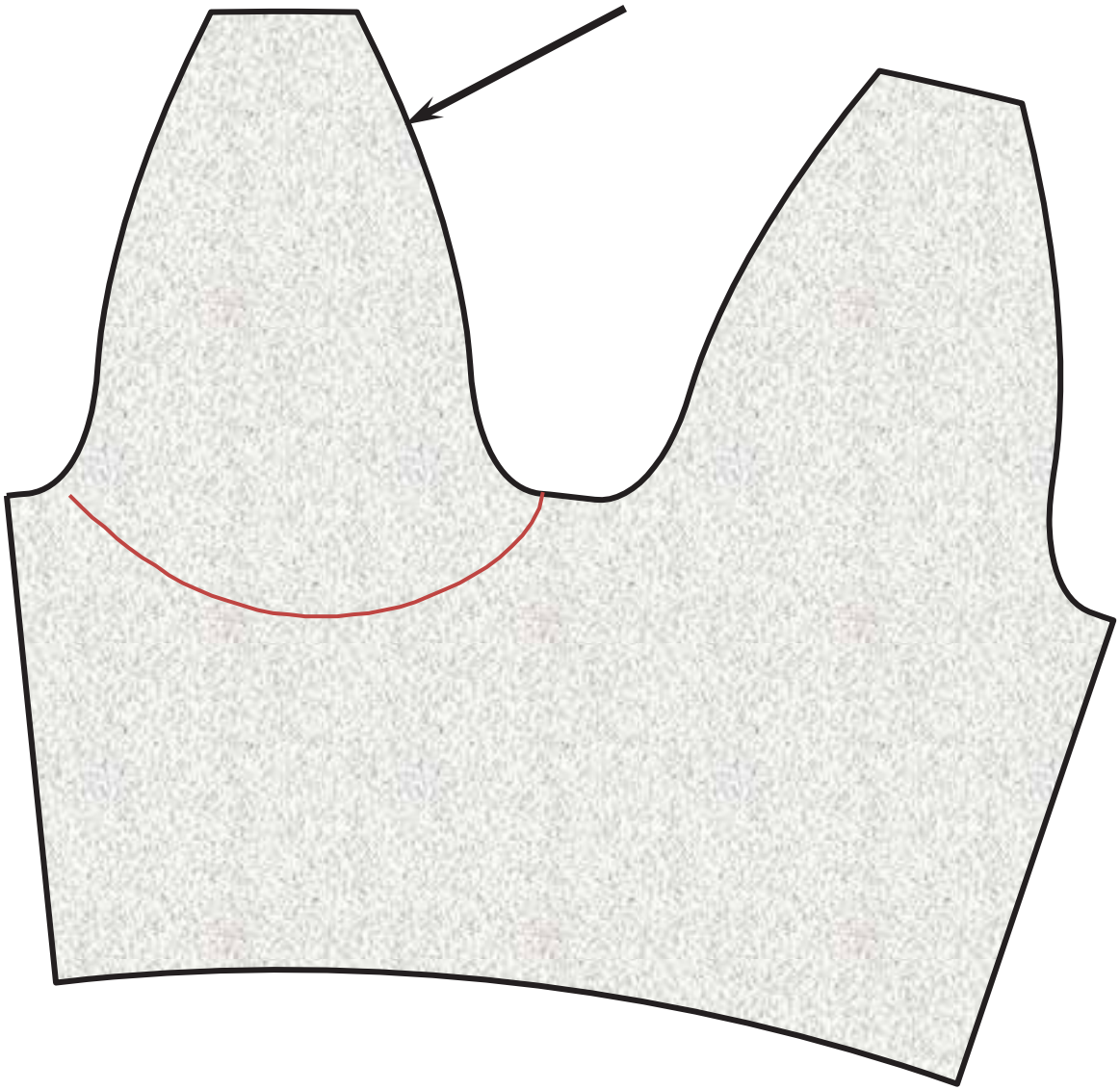

Initial crack location:

$\theta_0 = 94°$

Failure mode:

Tooth fracture

Effect of Initial Crack Location on Crack Path

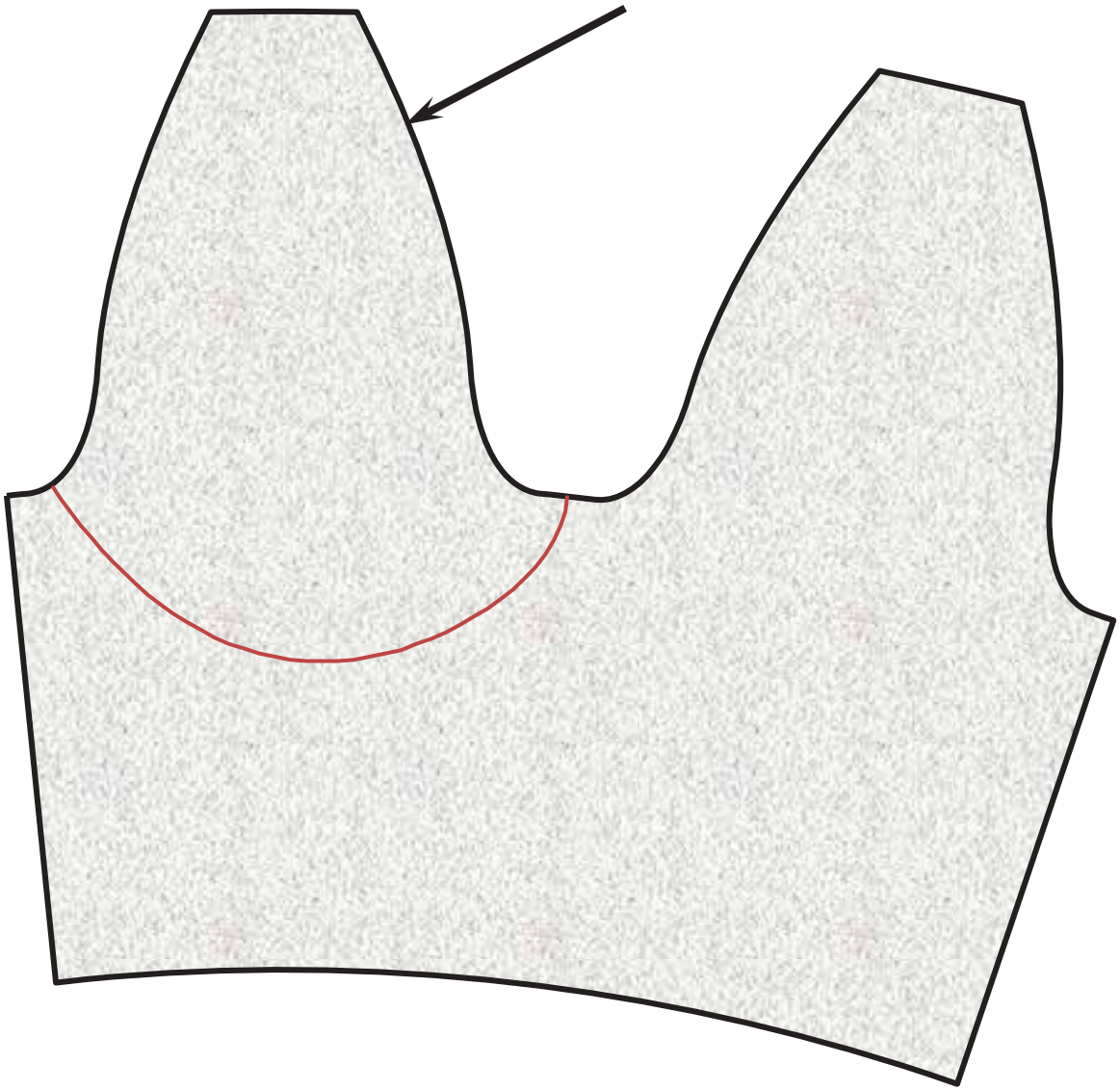

Initial crack location:

$\theta_0 = 88^\circ$

(root centerline)

Failure mode:

Tooth fracture

Effect of Initial Crack Location on Crack Path

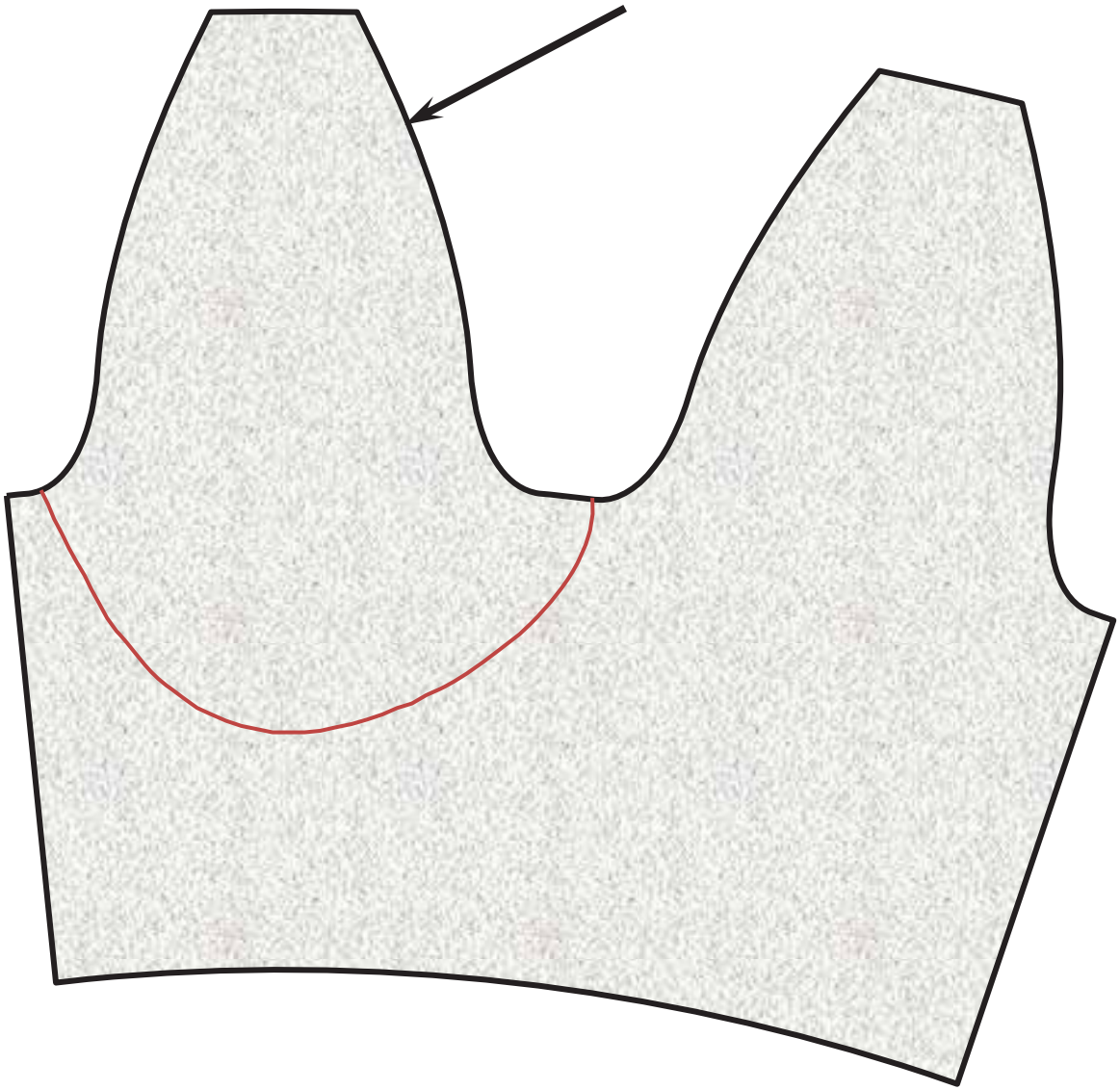

Initial crack location:

$\theta_0 = 83^\circ$

Failure mode:

Tooth fracture

Effect of Initial Crack Location on Crack Path

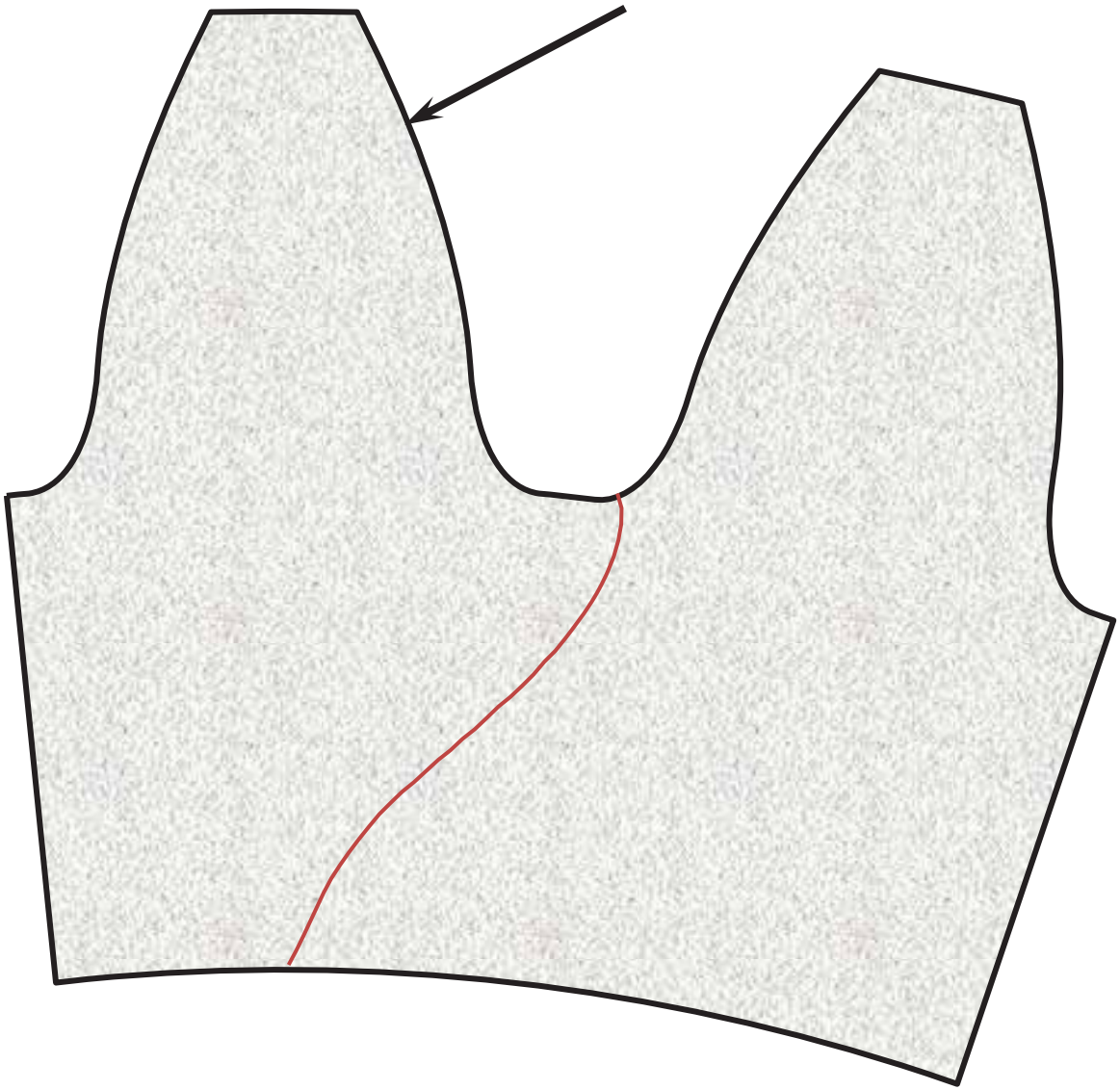

Initial crack location:

$\theta_0 = 78^\circ$

Failure mode:

Rim fracture

Effect of Initial Crack Location on Crack Path

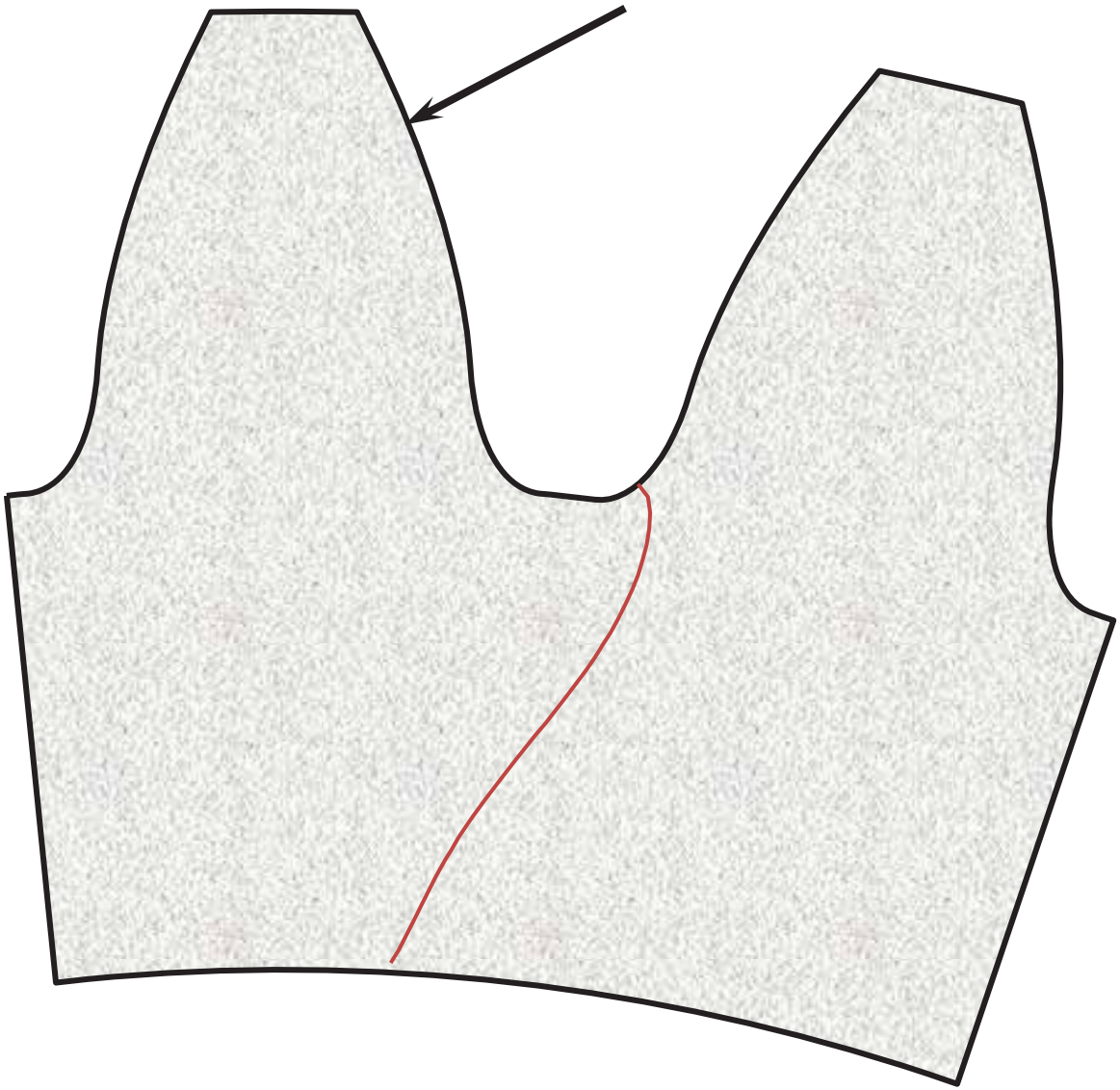

Initial crack location:

$\theta_0 = 73^\circ$

Failure mode:

Rim fracture

Effect of Initial Crack Location on Crack Path

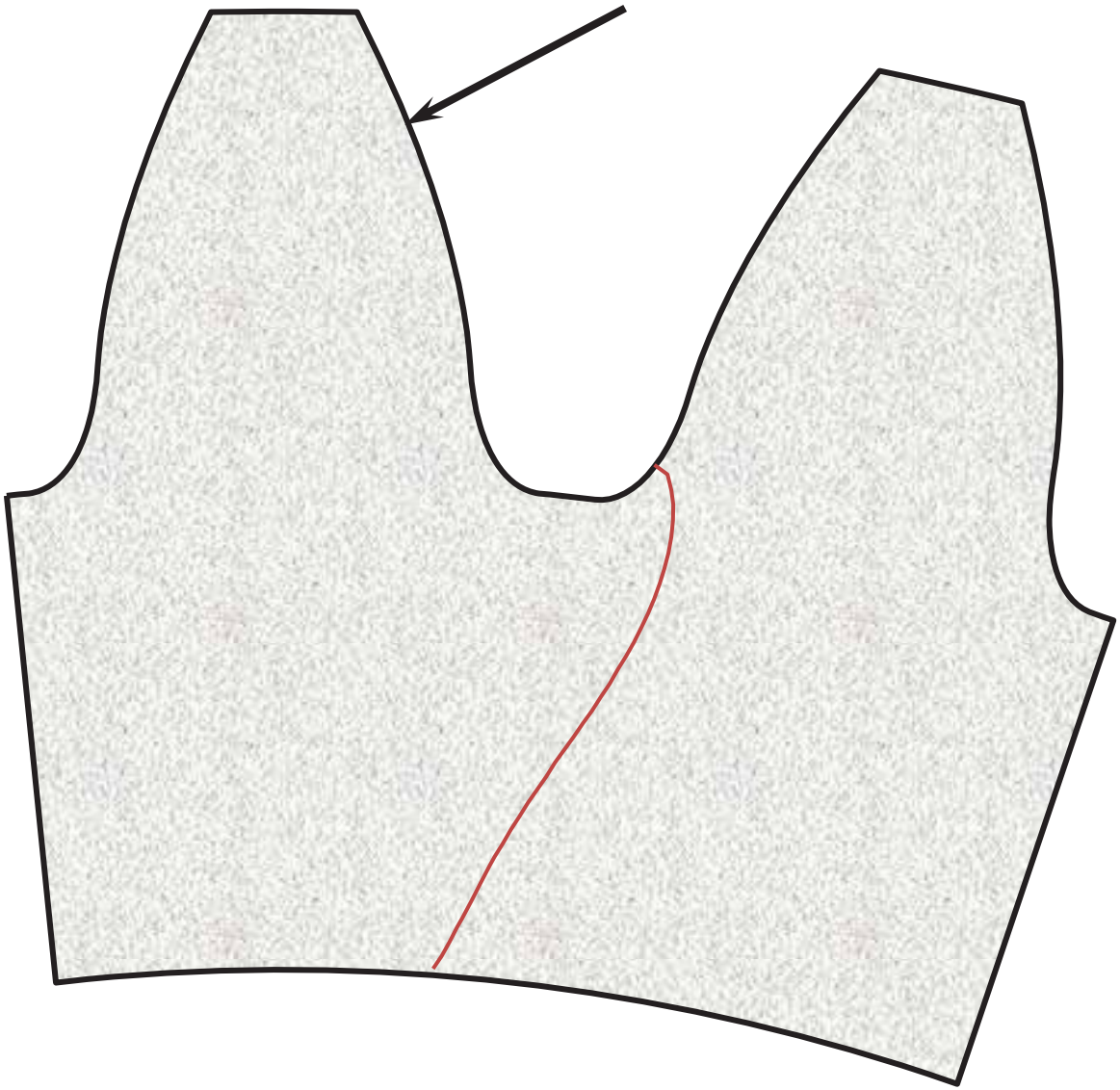

Initial crack location:

$\theta_0 = 68^\circ$

Failure mode:

Rim fracture

Effect of Initial Crack Location on Crack Path

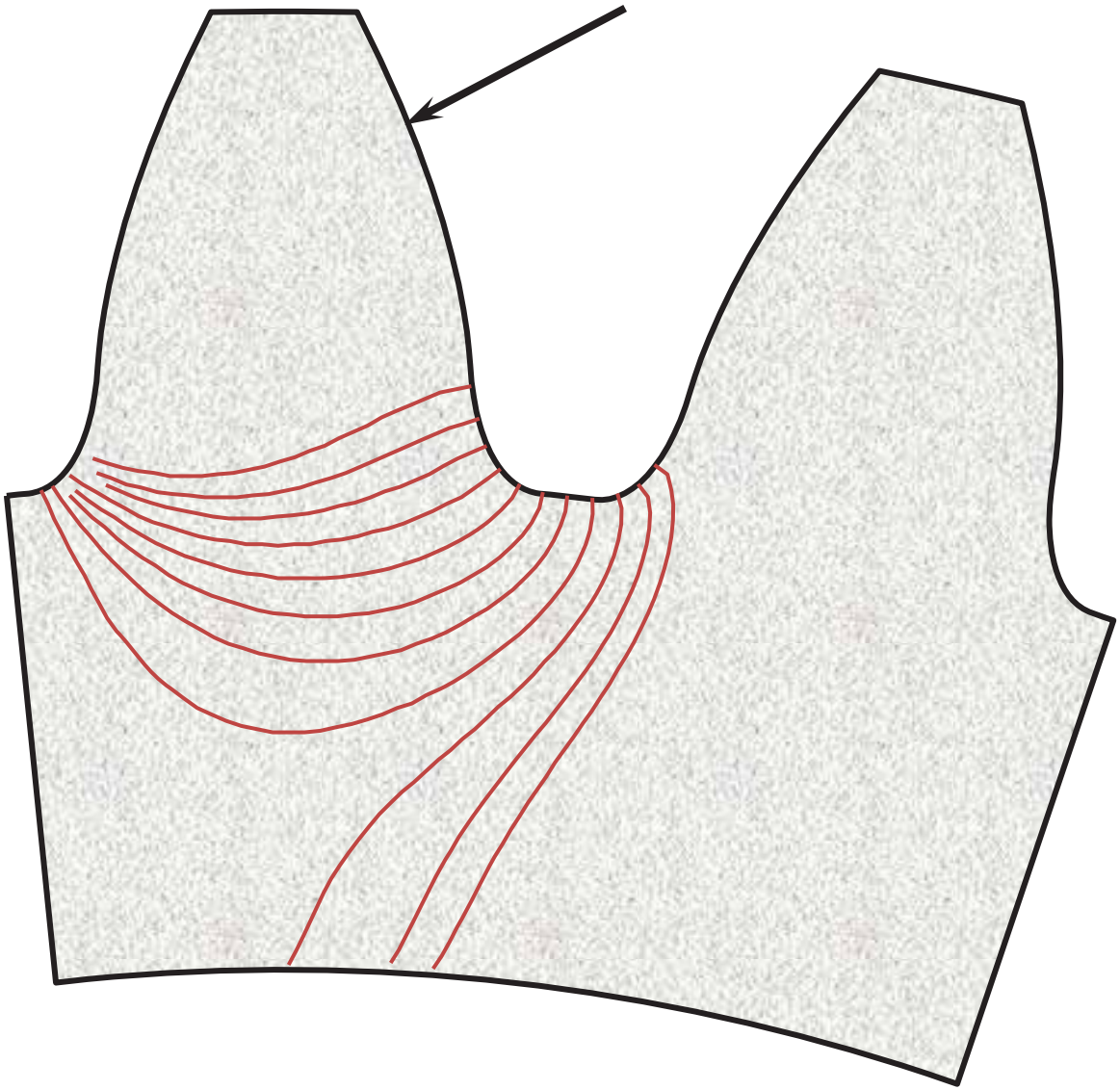

Stress Intensity Factors

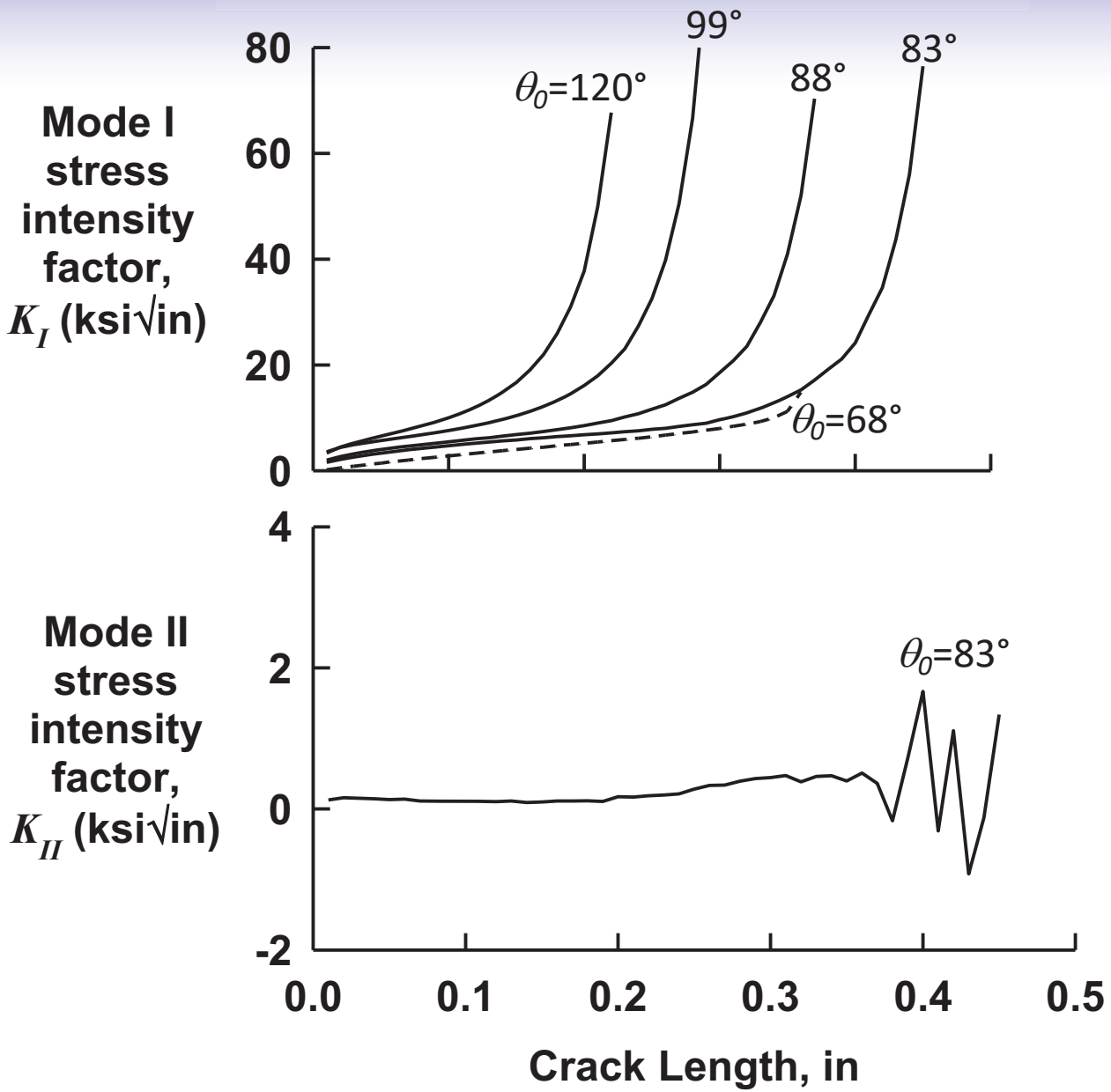

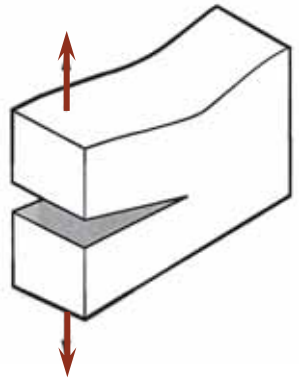

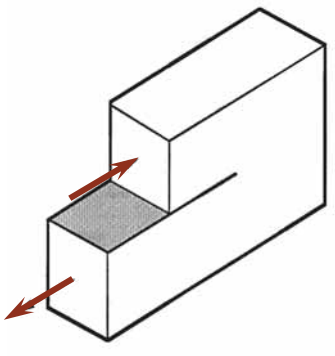

Effect of Backup Ratio on Crack Path

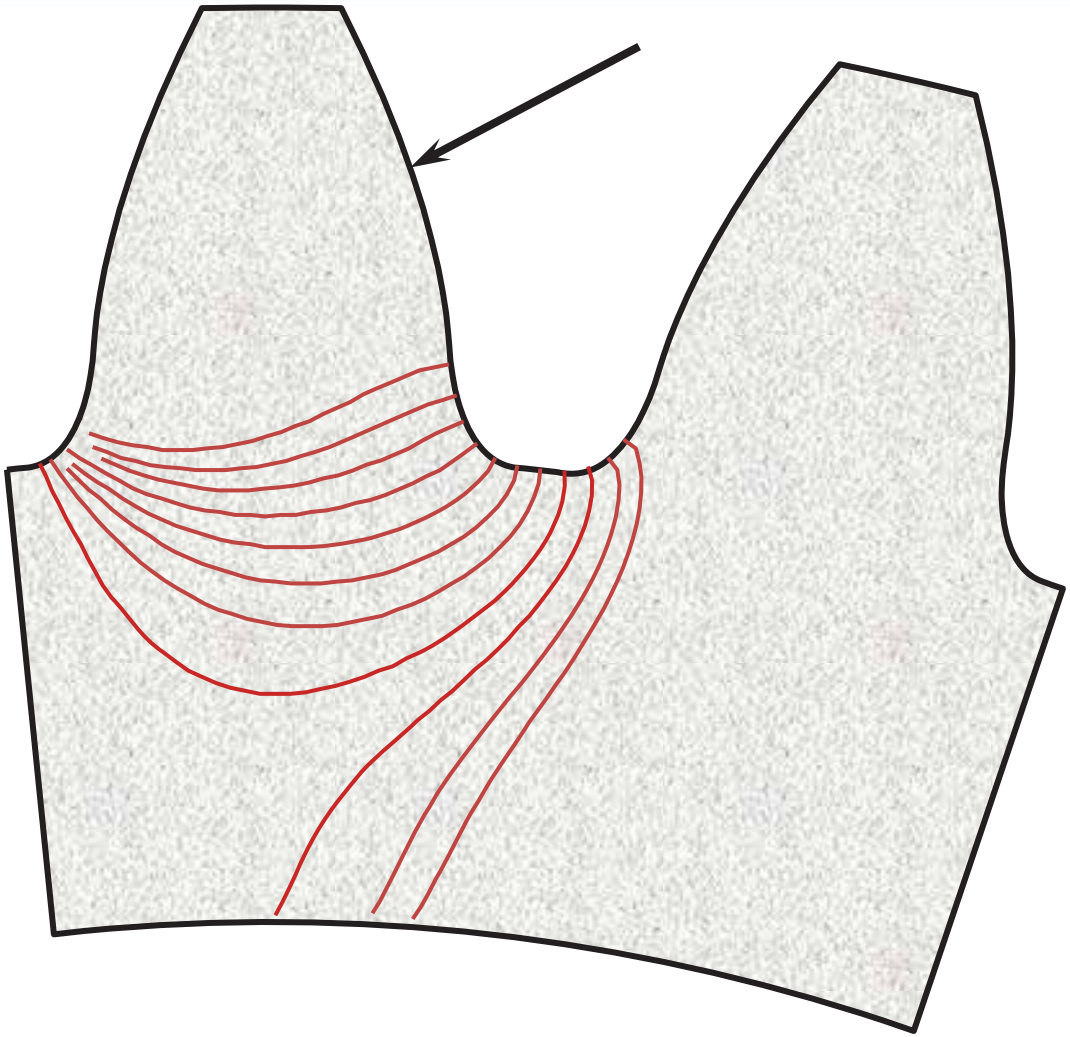

Backup ratio:

m_B = 1.0

Tooth/rim fracture transition:

θ_0 = 81°

Effect of Backup Ratio on Crack Path

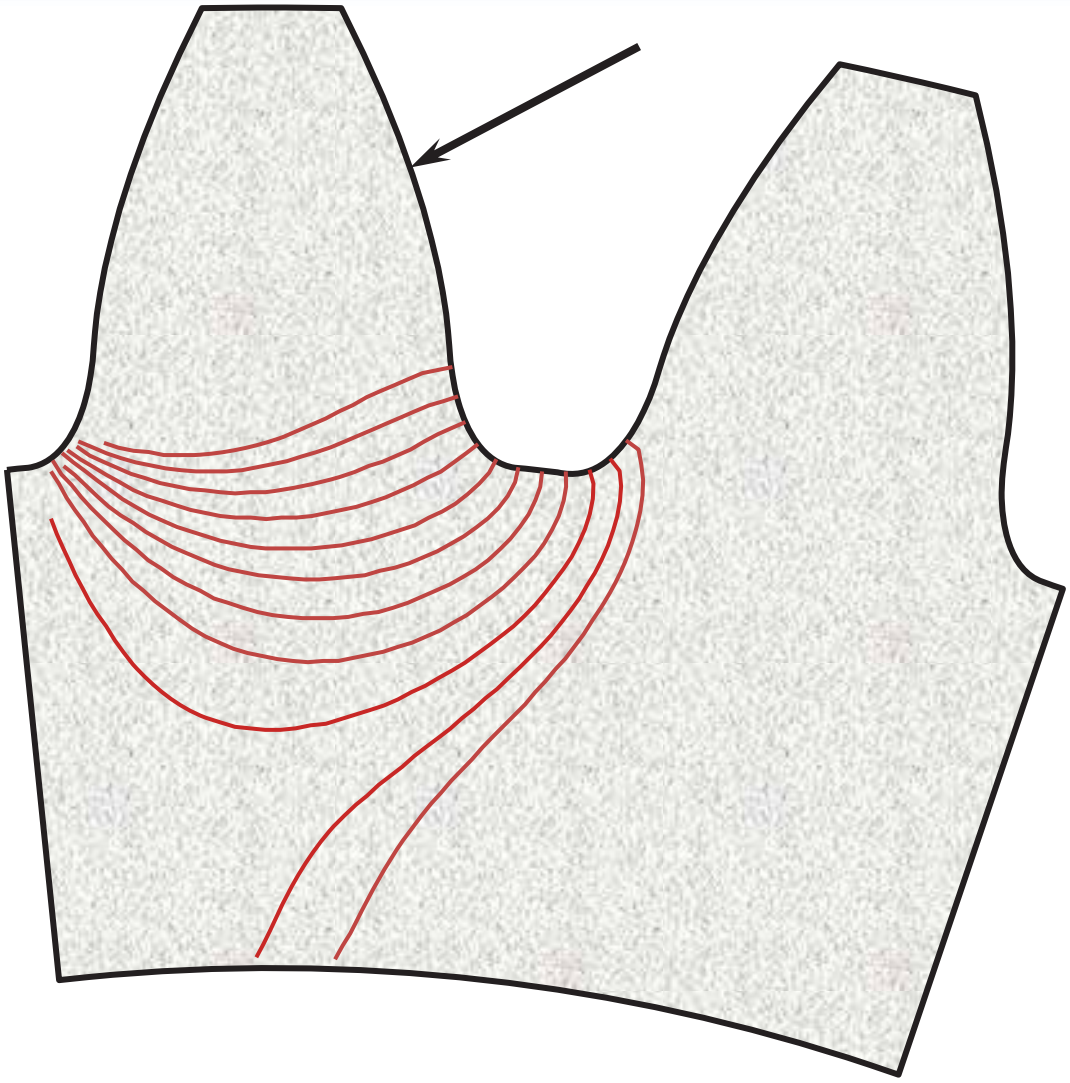

Backup ratio:

m_B = 1.1

Tooth/rim fracture transition:

θ_0 = 76°

Effect of Backup Ratio on Crack Path

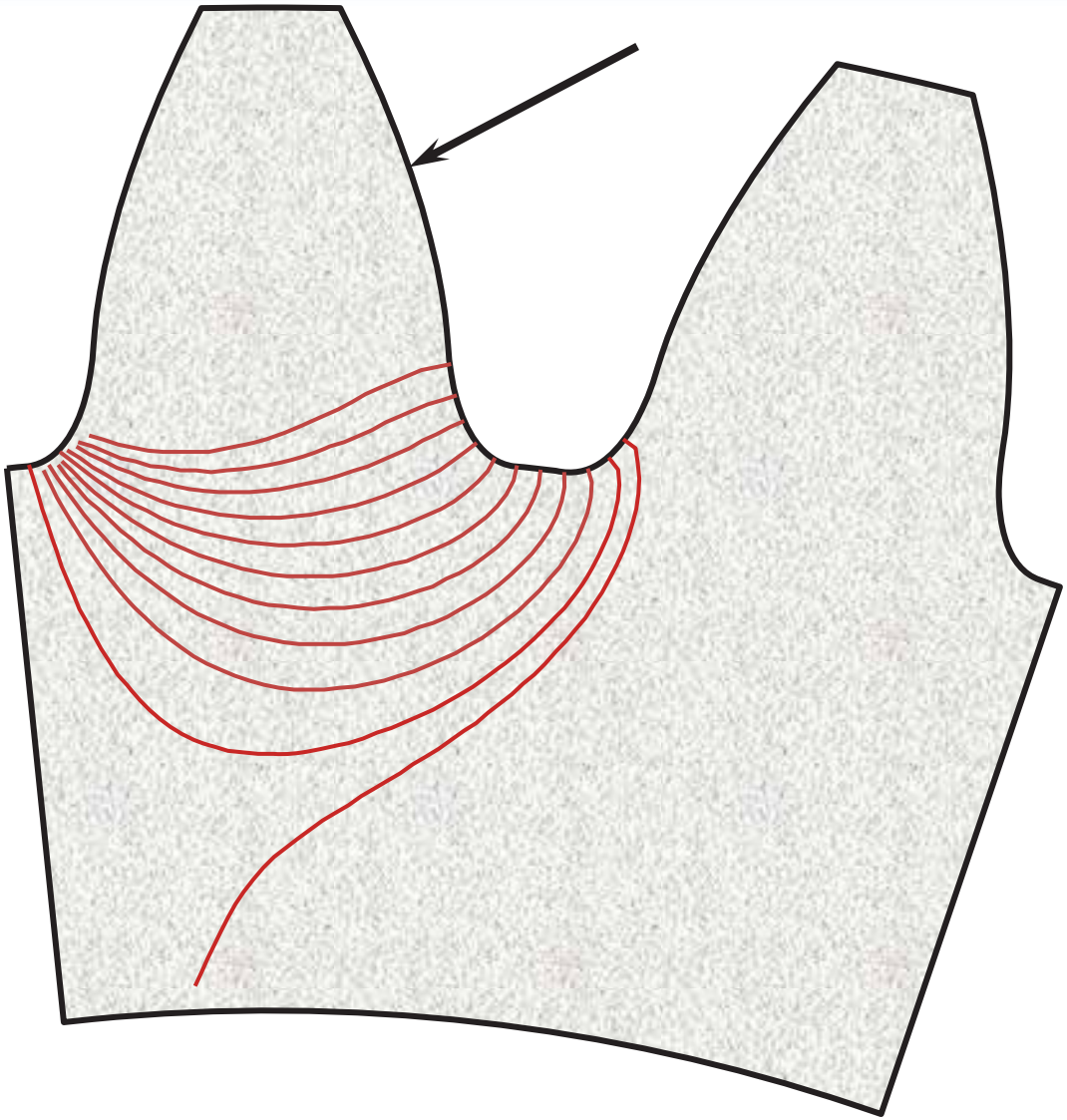

Backup ratio:

m_B = 1.2

Tooth/rim fracture transition:

θ_0 = 71°

Effect of Backup Ratio on Crack Path

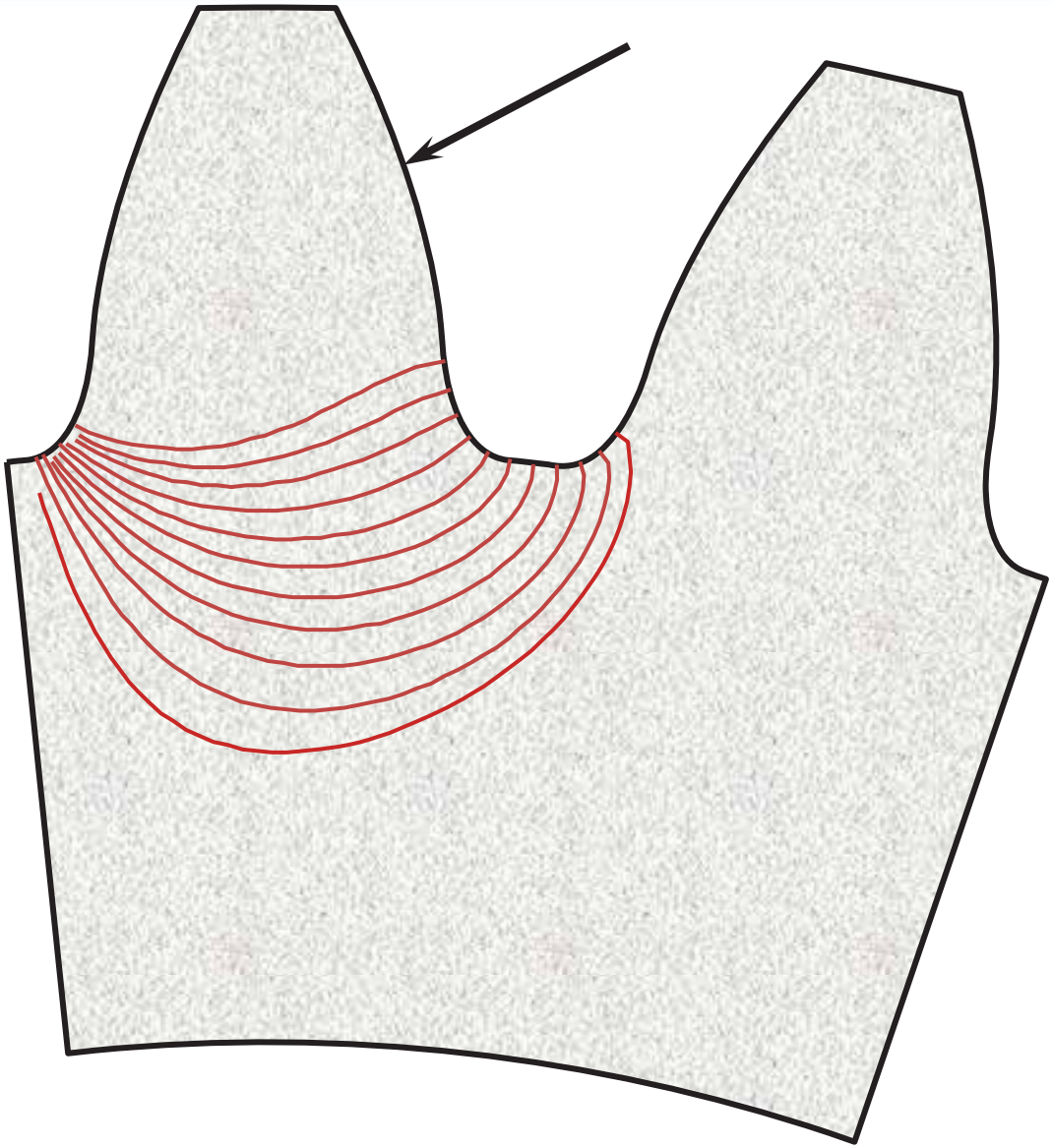

Backup ratio:

m_B = 1.3

Tooth/rim fracture transition:

All tooth fractures

Effect of Backup Ratio on Crack Path

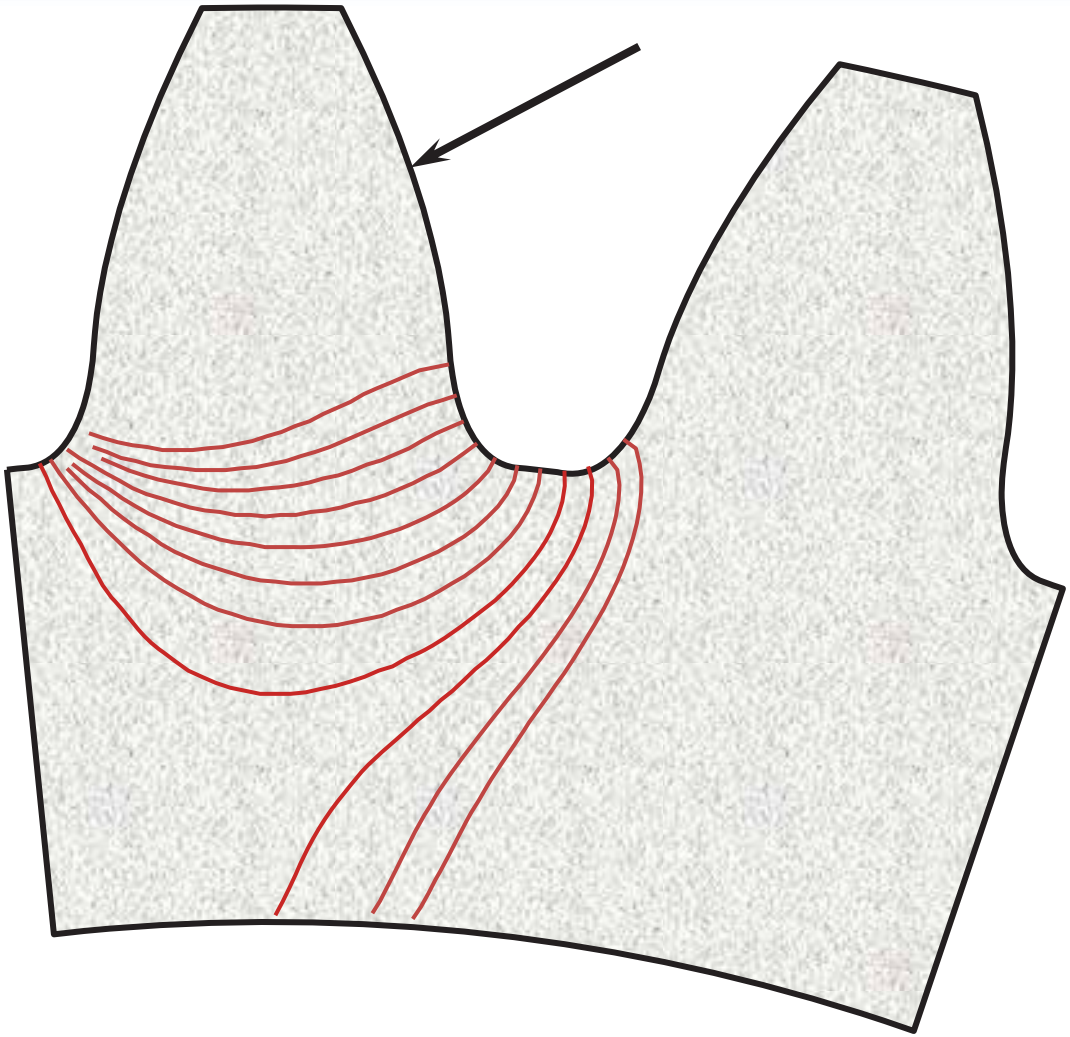

Backup ratio:

m_B = 1.0

Tooth/rim fracture transition:

θ_0 = 81°

Effect of Backup Ratio on Crack Path

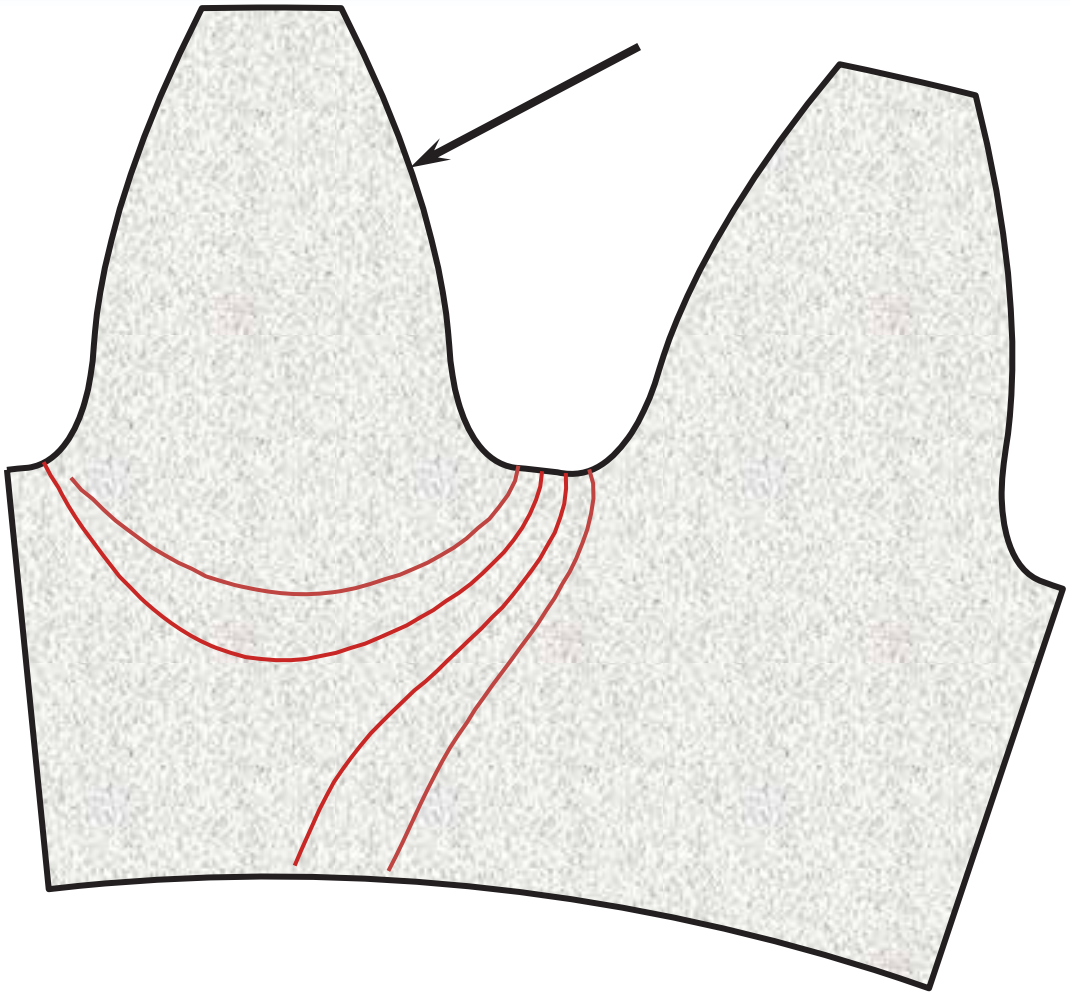

Backup ratio:

m_B = 0.9

Tooth/rim fracture transition:

θ_0 = 86°

Effect of Backup Ratio on Crack Path

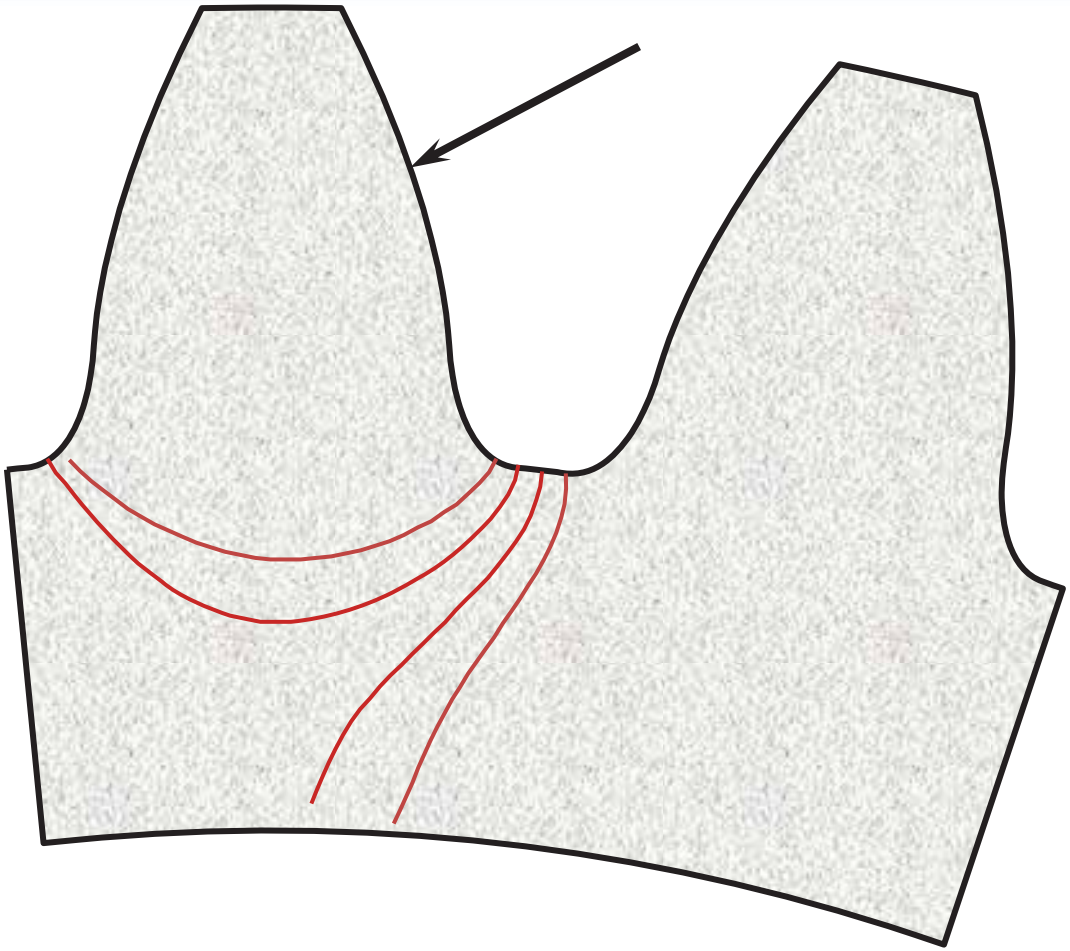

Backup ratio:

m_B = 0.8

Tooth/rim fracture transition:

θ_0 = 91°

Effect of Backup Ratio on Crack Path

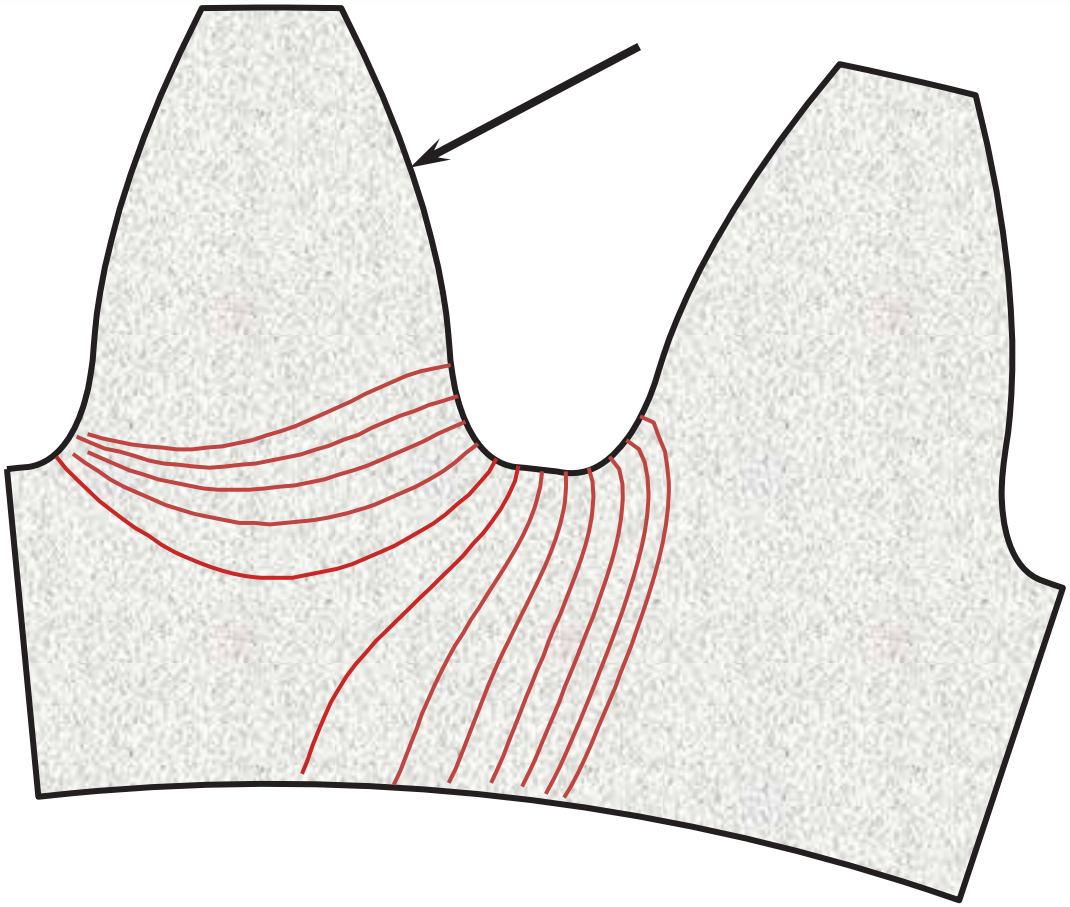

Backup ratio:

m_B = 0.7

Tooth/rim fracture transition:

θ_0 = 97°

Effect of Backup Ratio on Crack Path

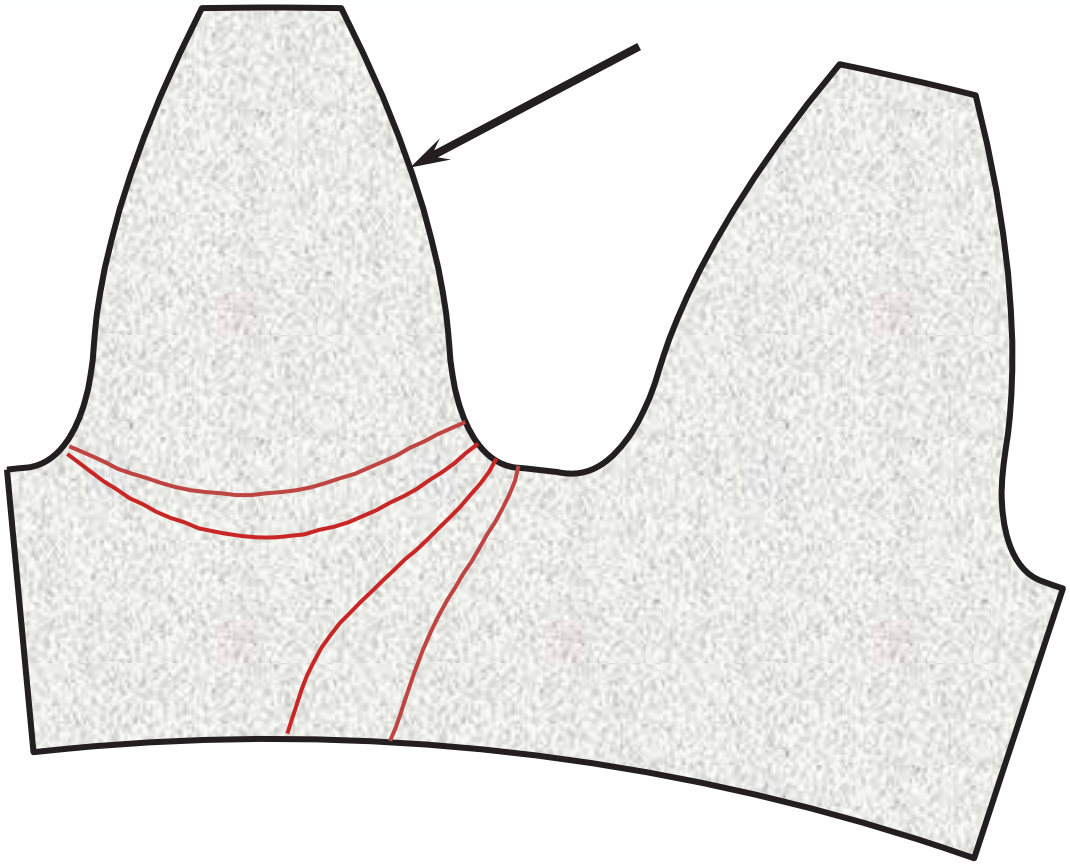

Backup ratio:

m_B = 0.6

Tooth/rim fracture transition:

θ_0 = 102°

Effect of Backup Ratio on Crack Path

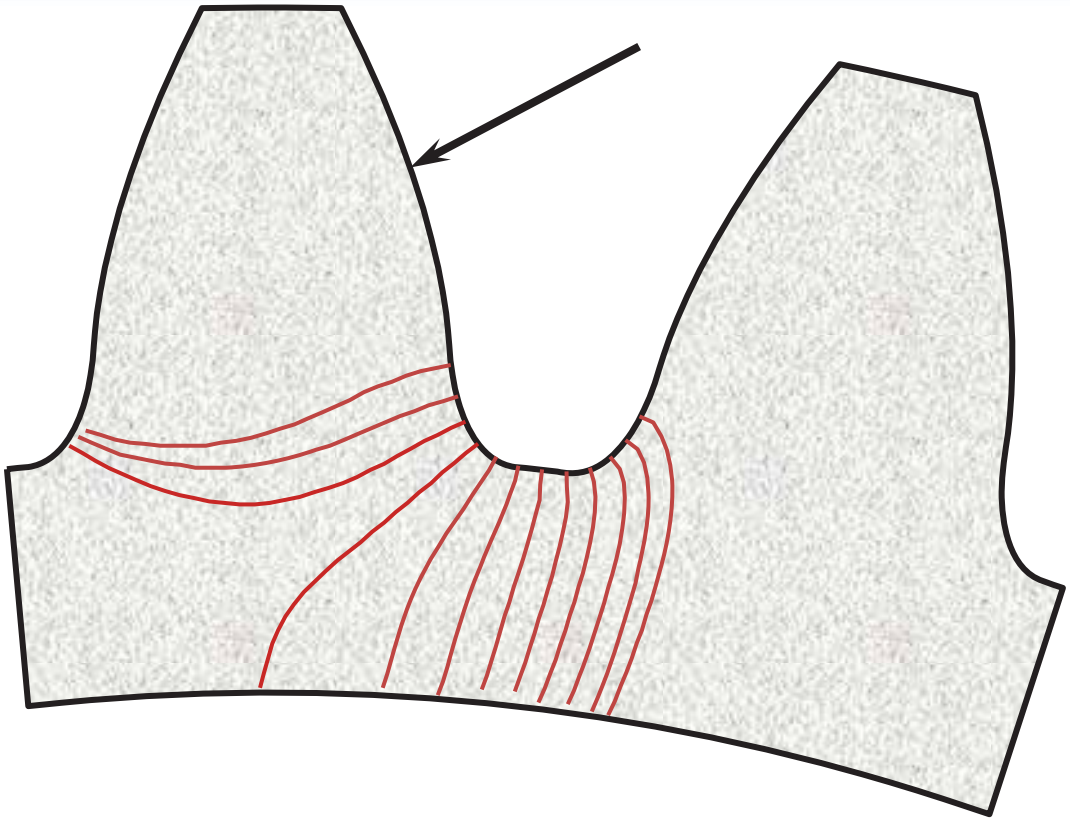

Backup ratio:

m_B = 0.5

Tooth/rim fracture transition:

θ_0 = 107°

Validation of Finite Element Modeling

Backup ratio = 3.3

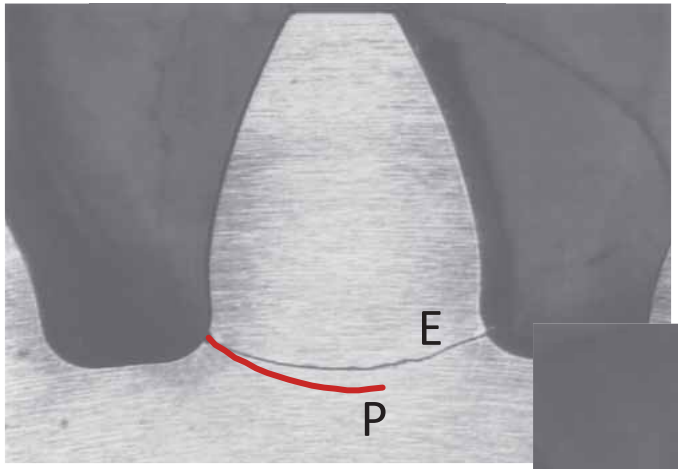

E = Experiment
P = Predicted

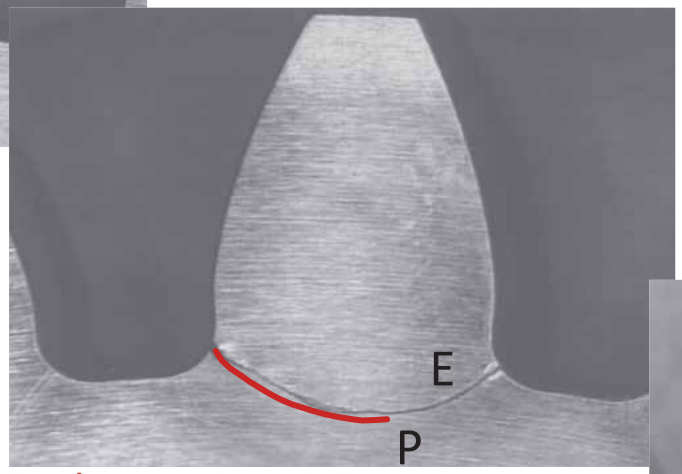

Backup ratio = 1.0

Backup ratio = 0.5

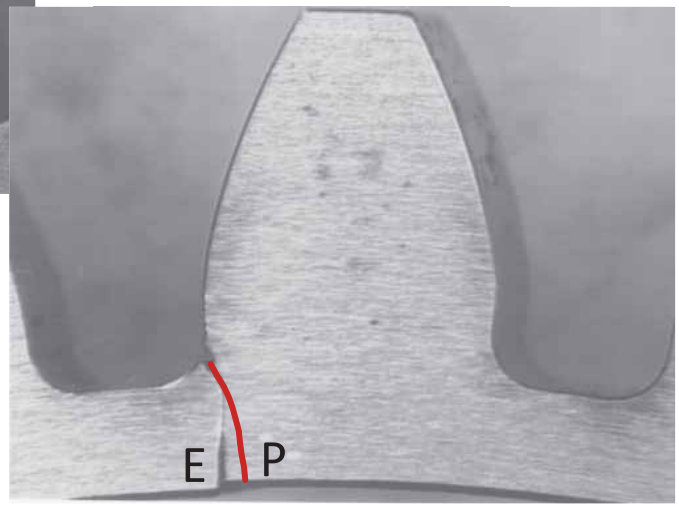

Design Map

T = tooth fractures
R = rim fractures
C = compression

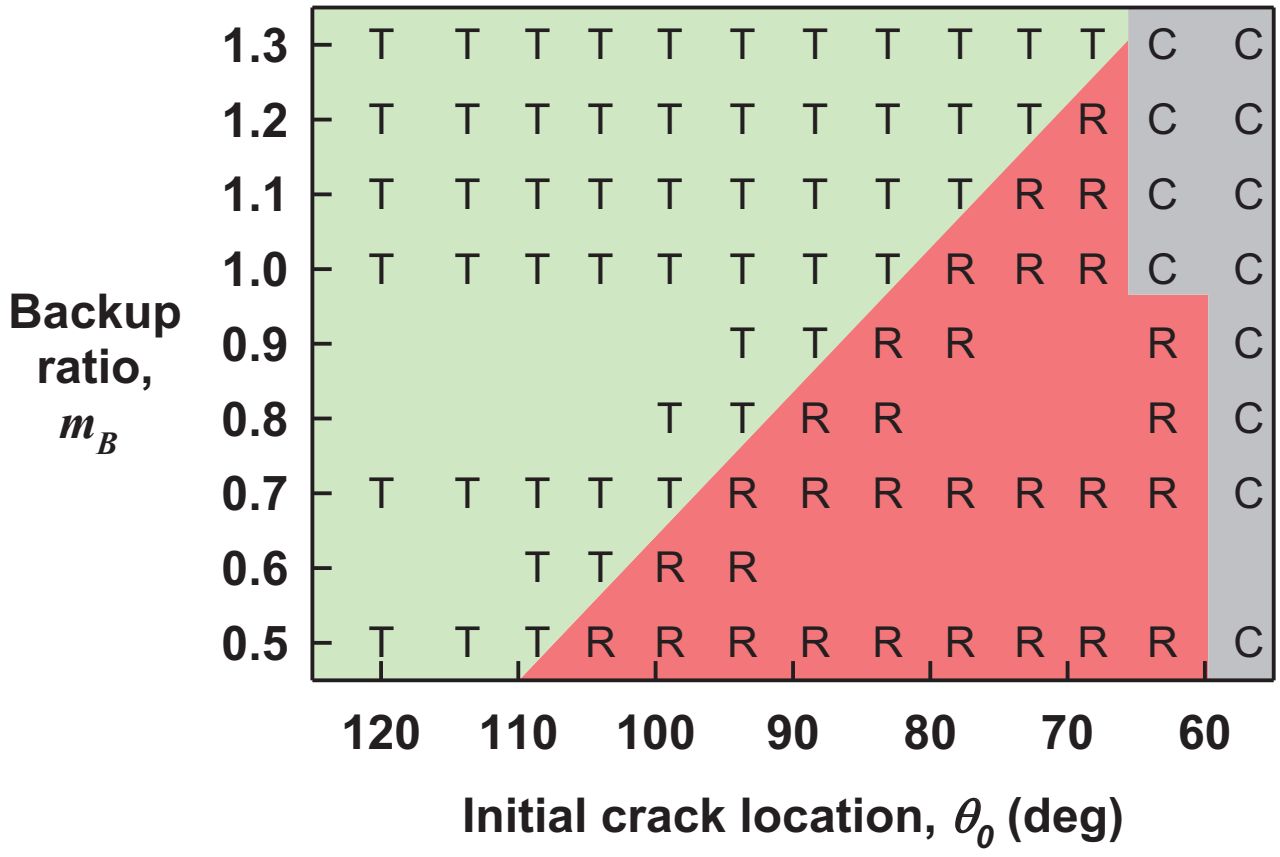

Mode I Stress Intensity Factors

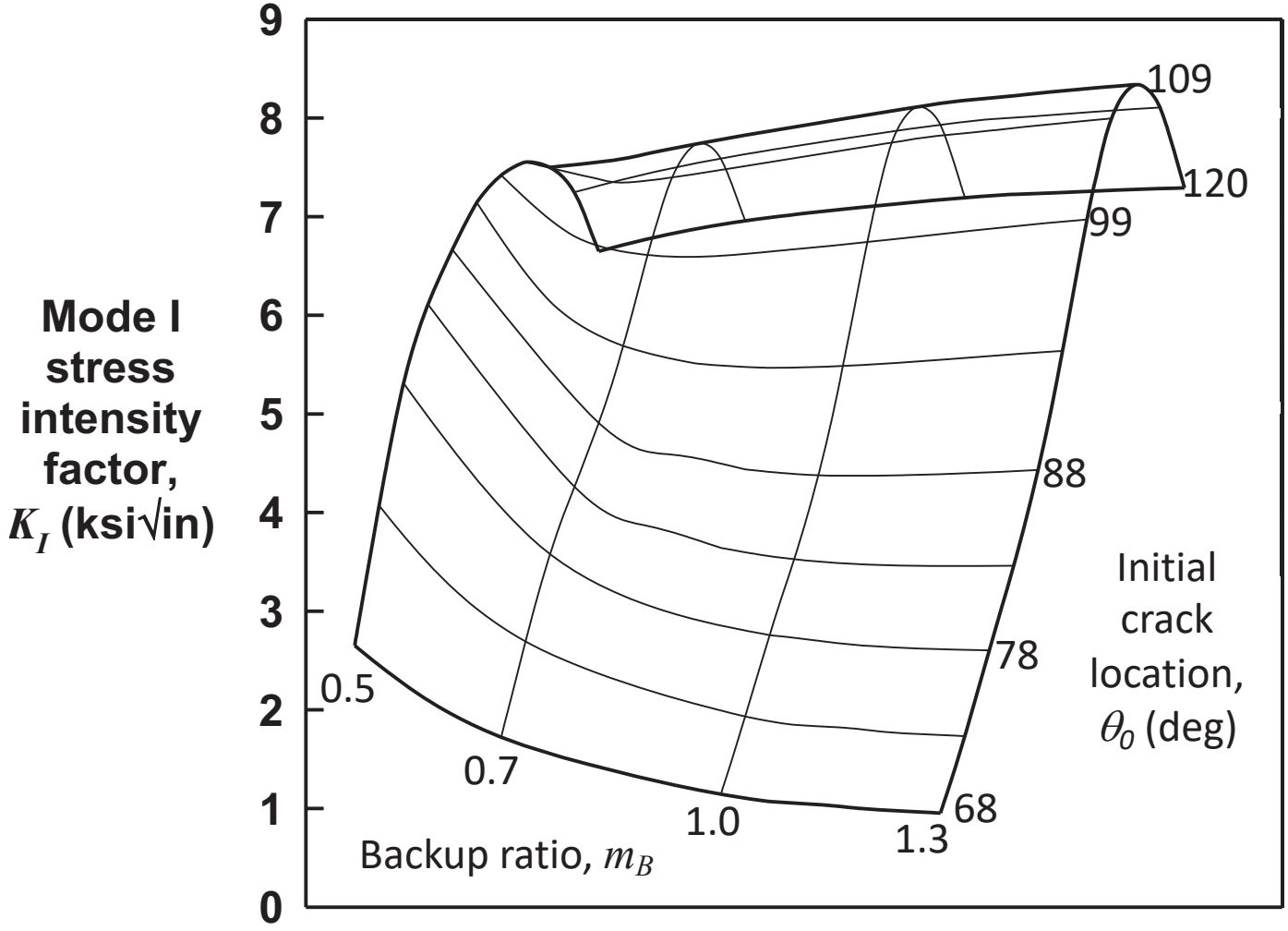

Gear Parameters:

- 28 teeth
- 8 pitch
- 1.75" pitch rad
- 20° press angle

- 500 lb tooth load
- 0.030" crack size

Mode I Stress Intensity Factors

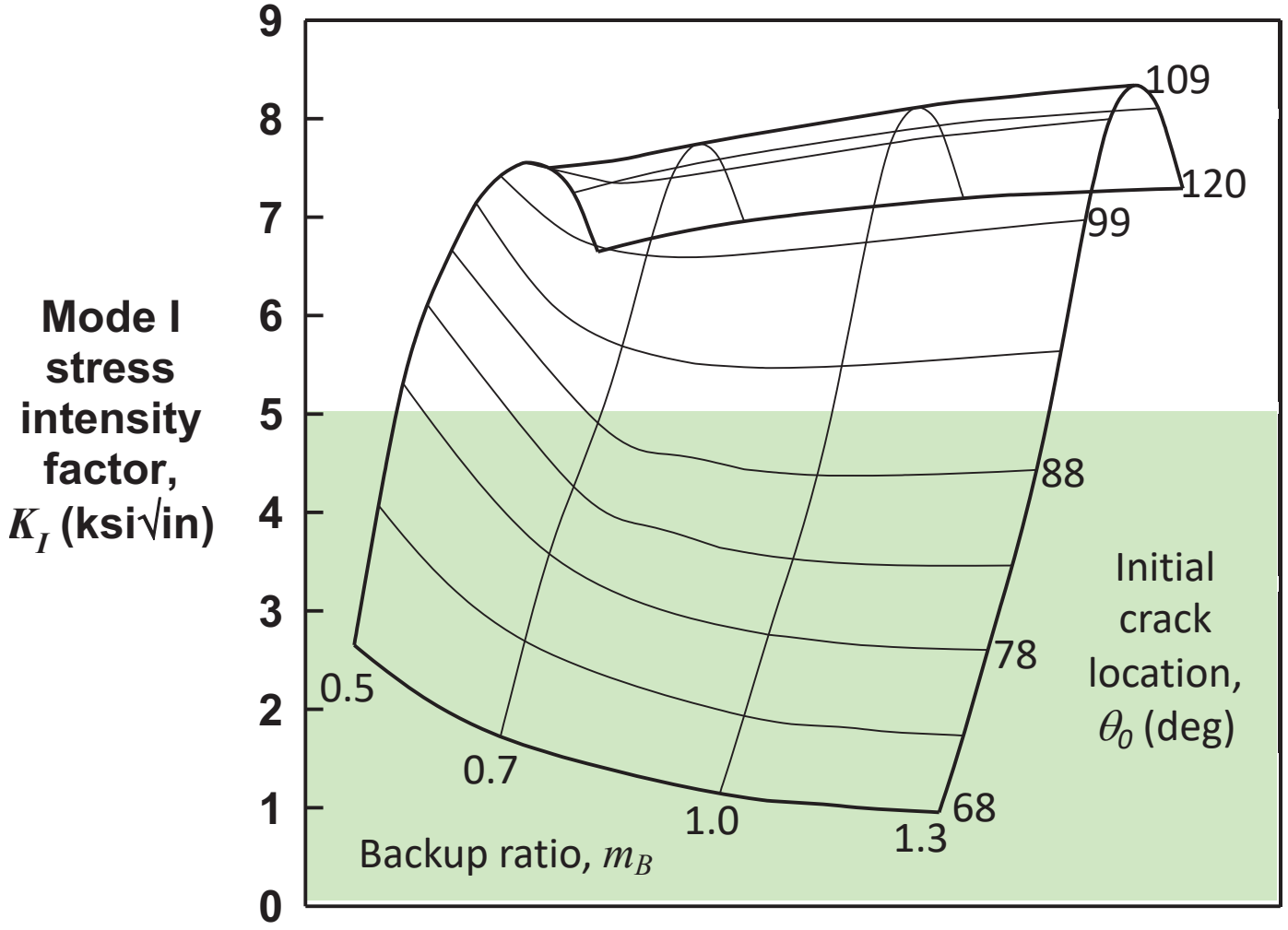

Gear Parameters:

- 28 teeth
- 8 pitch
- 1.75" pitch rad
- 20° press angle

- 500 lb tooth load
- 0.030" crack size

- AISI 9310 steel
- ΔK_{th} = 5 ksi√in

Crack Propagation Angle and Growth Rate

$$\theta_m = 2\tan^{-1}\left[\frac{\frac{K_I}{K_{II}} \pm \sqrt{\left(\frac{K_I}{K_{II}}\right)^2 + 8}}{4}\right]$$

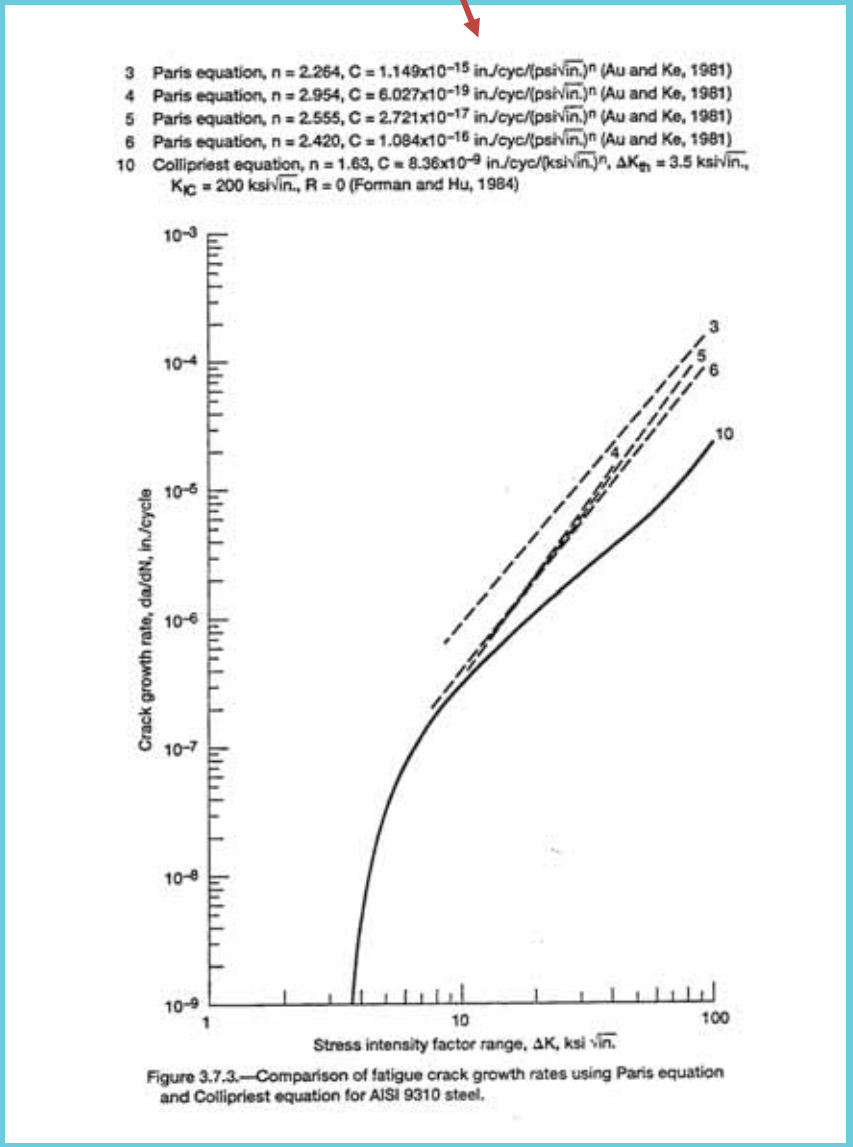

Figure 3.7.3.—Comparison of fatigue crack growth rates using Paris equation and Collipriest equation for AISI 9310 steel.

Design Map

T = tooth fractures
R = rim fractures
N = no fracture